Probing the structure, Dynamics & Function of Proteins by NMR

1. *E. coli* thioesterase/protease.
2. Hepatoma-derived growth factor (hHDGF)
3. SARS CoV nucleocapsid protein

Tai-huang Huang (黃太煌)
Institute of Biomedical Sciences
Academia Sinica
Taipei, Taiwan
(bmthh@gate.sinica.edu.tw)

Basic Nuclear Spin Interactions

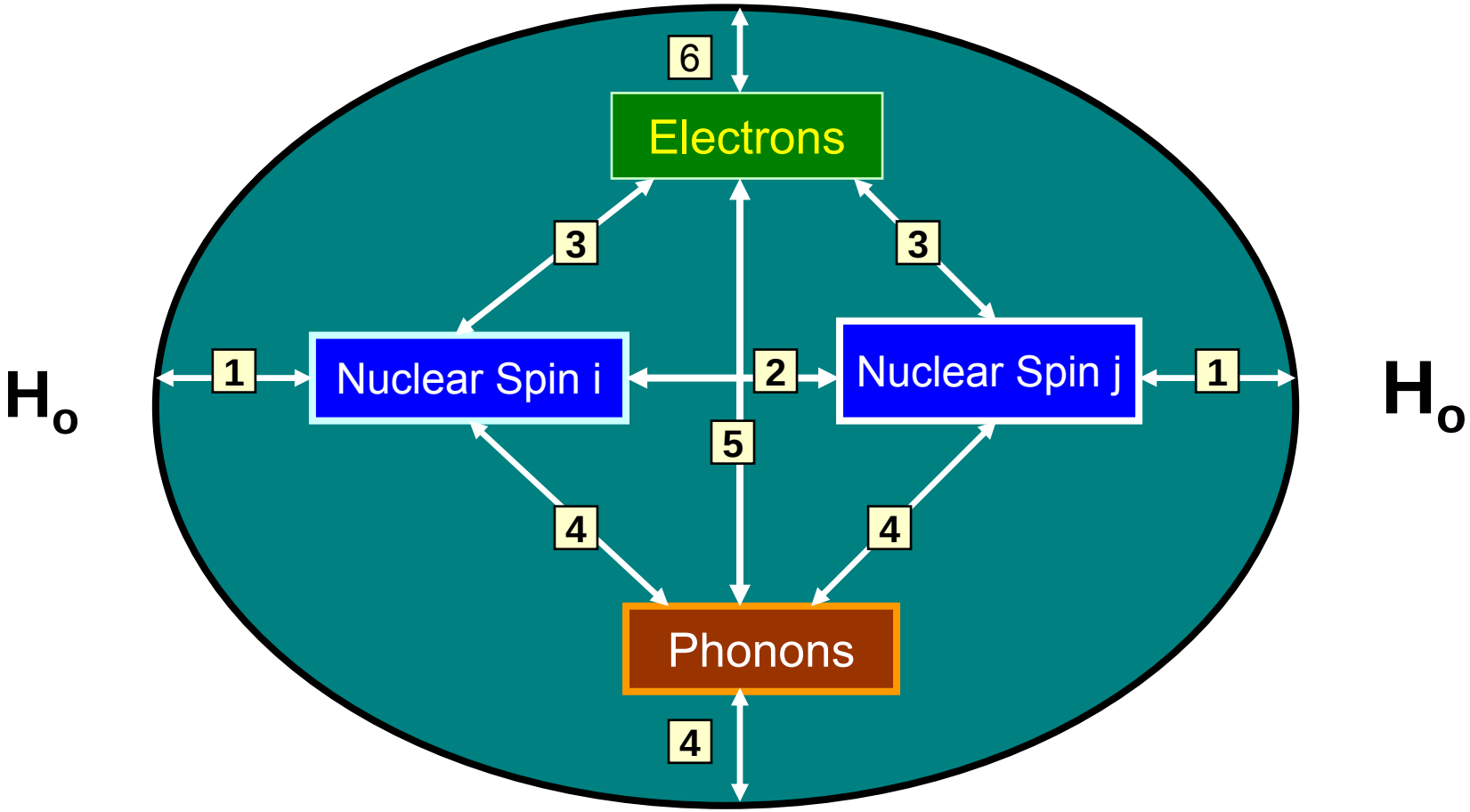

Dominant interactions: $H = H_Z + H_D + H_S + H_Q + H_J + \cdots$

H_Z = Zeeman Interaction; H_J: J-coupling; H_D = Dipolar Interactions

H_S = Chemical Shielding Interaction. H_Q = Quadrupolar Interaction

Protein target: ***E. coli*** **thioesterase/protease I**
(thioesterase, esterase, protease, arylesterase, and lysophopholipase)

Biological significance:

TEP-I is an ubiquitous protein involved in:

- Fatty acid synthesis
- Synthesis of polyketides, immunosupressants & peptide antibiotics
- Removal of acyl-chains from post-translational modified proteins such as Ras
- Bioluminescence
- Important industrial protein for synthesizing stereospecific acids, alcohols & esters etc

Why Study this enzyme ?

- A member of a new subclass of lipolytic enzymes, of which no structure is known.

→ New structure or new fold ?

- A excellent model system for studying the molecular events involved in enzyme catalysis.

Goals

I. Structure : A new structure or a new fold ?

Lin, T.H., Chen, C.P., Huang, R.F., Lee, Y.L., Shaw, J.F. and Huang, T.h. (1998) J. Biomol. NMR **11**, 363-380. "Multinuclear NMR resonance Assignments and The Secondary Structure of *E. coi* Thioesterase/ Protease I, a member of a New Subclass of Lipolytic Enzymes ".

II. Dynamics. Functional roles of protein dynamics?

Huang, Y.T., Liaw, Y.C., Gorbatyuk, V. and Huang, T.-h. (2001) "The backbone dynamics of *E. coli* thioesterase/protease I –Evidence of a flexible active site environment of a serine protease" J. Mol. Biol. **307**, 1075-1090.

III. Structure – functional relationship

Molecular mechanism of enzyme catalysis

1. Tyukhtenko, S.I., Livinchyuk, A.V., Huang, Y.T., Chang, C.F., Shaw, J.F., and Huang, T.-h. (2002) "NMR Studies of the Hydrogen Bonds Involving the Catalytic Triad of *E. coli* Thioesterase/Protease I" FEBS Lett. **528**, 203-206.
2. Tyukhtenko, S.I., Livinchyuk, A.V., Huang, Y.T., Chang, C.F., Shaw, J.F., and **Huang, T.-h.*** (2003) "Sequential structural changes of *E.* coli thioestease/protease-I in forming Michaelis and Transition state complexes with diethyl p-nitrophenyl phosphate" Biochemistry, **42**(27) 8289 – 8297.

I. Structure

- TEP-I is a 182 a.a. protein of molecular weight 21 kDa.
- Standard heteronuclear multi-dimensional NMR techniques.

Determining Macromolecular Structures

(1)
Prepare
NMR samples
^{2}H, ^{13}C and/or ^{15}N-Labeled

(2)
Obtain
NMR spectra -
(1D, 2D, 3D & 4D)

(3)
Assign
NMR
resonances

(4)
Obtain
NMR restraints
distances,
dihedral angles
bond orientations

(5)
Structure
Calculation
and
refinement

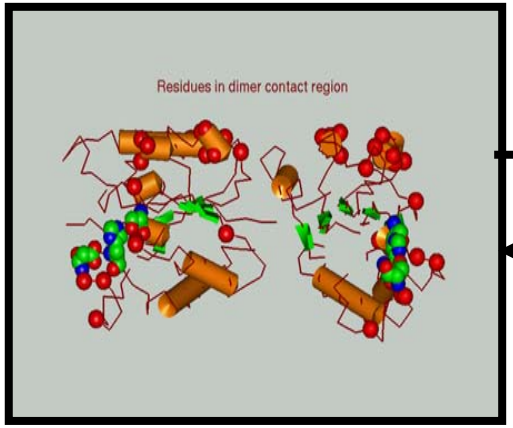

Determining protein structure by NMR:

1. Determine secondary structure.
2. Determine tertiary structure.
3. Structure refinement.
4. Dynamics, Function, Drug design.

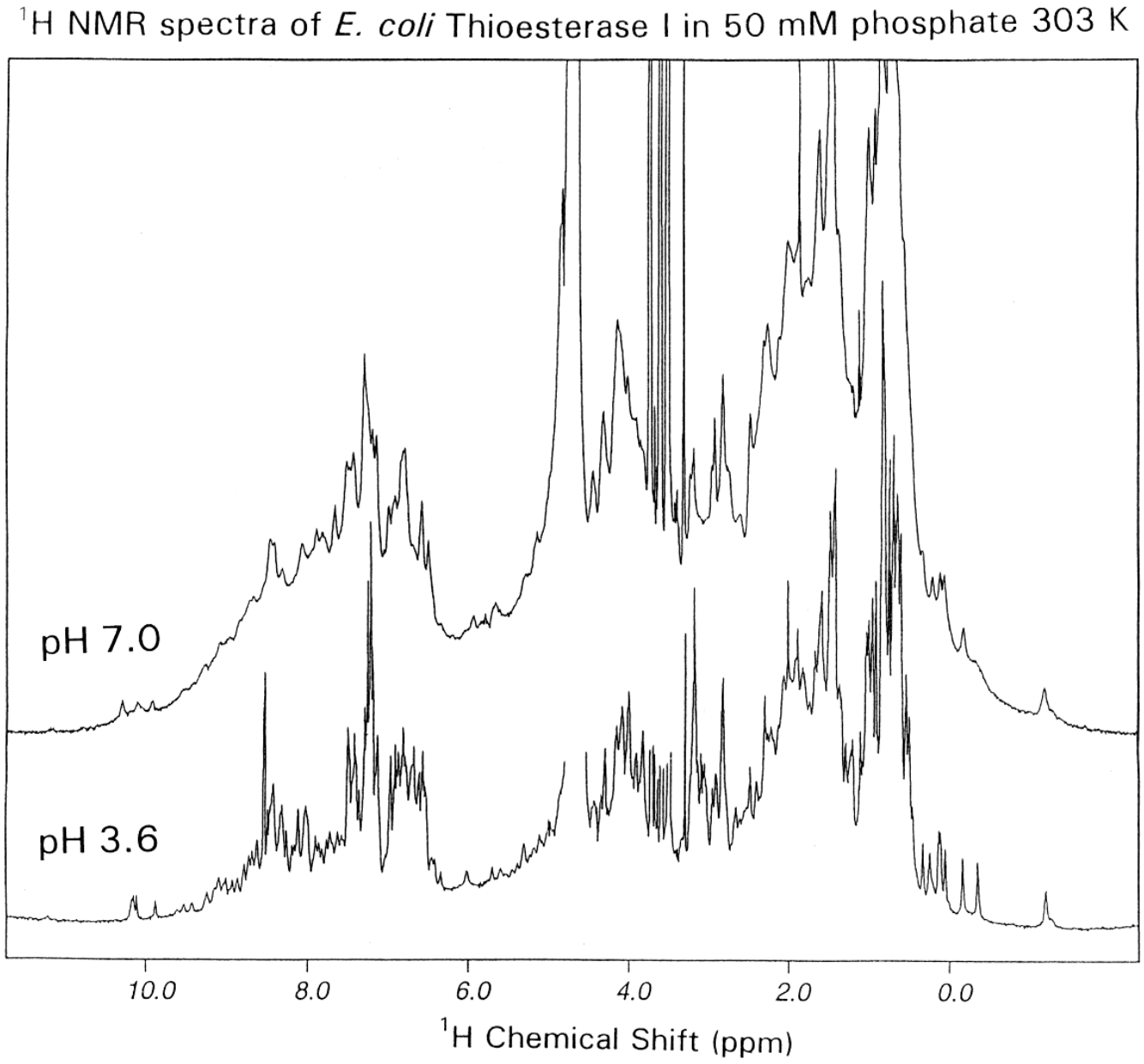
^{1}H NMR spectra of *E. coli* Thioesterase I in 50 mM phosphate 303 K
pH 7.0
pH 3.6
10.0
8.0
6.0
4.0
2.0
0.0
^{1}H Chemical Shift (ppm)

Chemical shift referencing

References:

1. Wishart, D. and Case, D.A. (2001) Method Enzymology 338, 3-34.
2. Wishart, D. and Sykes, B.D. (1994) Method Enzymol. 239, 363-392.
3. Markley, J.L. et al. (1998) J. Biomol. NMR 12, 1.

IUPAC/IUBMB recommended Ξ ratios for indirect chemical shift referencing in biomolecular NMR (relative to DSS)

Nucleus	Compound	Ξ ratio
^{1}H	DSS (Internal)	1.000,000,000
^{13}C	DSS (Internal)	0.251,449,530
^{15}N	100% Liquid NH_3 (External)	0.101,329,118
^{19}F	100% CF_3COOH (External)	0.940,867,196
^{31}P	10% $(CH_3)_3PO_4$ (Internal)	0.404,808,636

DSS: 2,2-dimethyl-2-silapantane-5-sulfonic acid.

^{15}N-HSQC spectrum

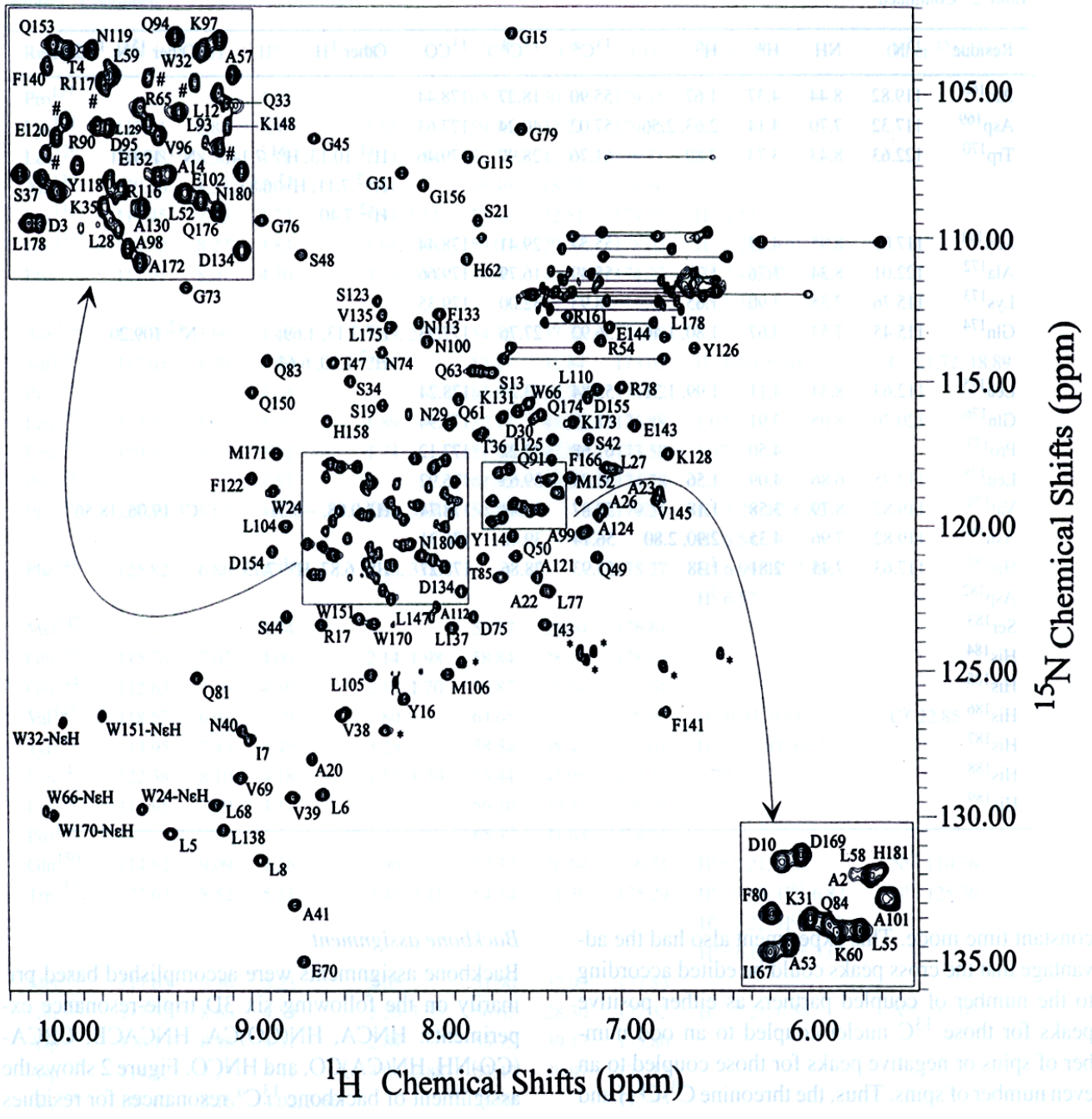

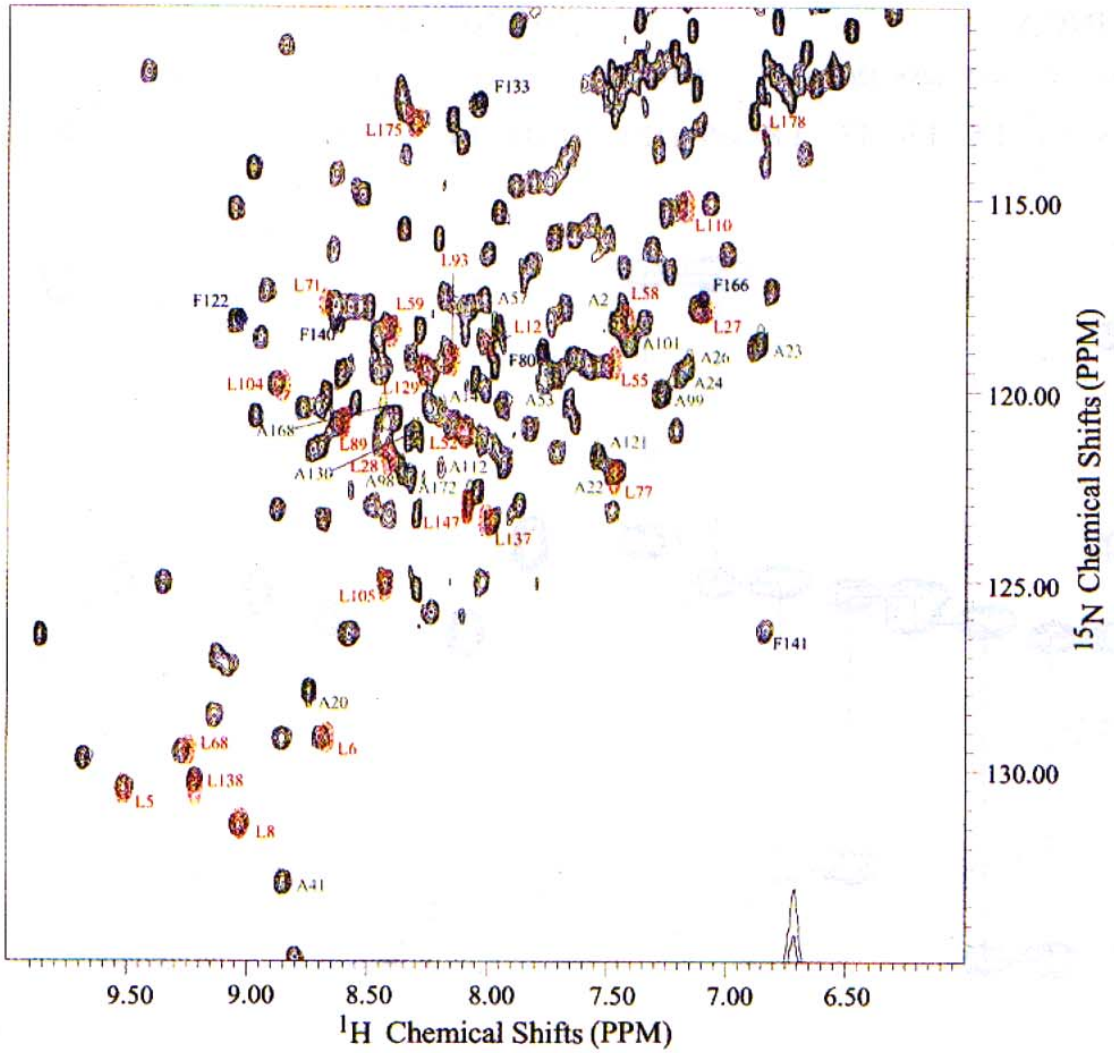

Figure 3. Overlay of four 2D ^{15}N-HSQC spectra acquired with four different *E. coli* thioesterase/protease I samples differing in ^{15}N-labeling positions, but in the same solvent (pH 3.5 in 90% H_2O) and under similar NMR conditions (310 K). Samples employed were: black – uniformly ^{15}N-labeled; blue – [^{15}N]-Phe-labeled; red – [^{15}N]-Leu-labeled; green – [^{15}N]-Ala-labeled.

Heteronuclear multidimensional NMR experiments for resonance assignments

Magnetization transfer pathway:

$^{1}H \rightarrow {}^{15}N \rightarrow {}^{13}C \rightarrow {}^{15}N$

$\rightarrow {}^{1}H \rightarrow {}^{1}H$ Detection

➔ Detect ^{1}H, ^{13}C, ^{15}N resonances

➔Permit sequential correlation of backbone ^{1}H-^{13}C-^{15}N resonances !!!

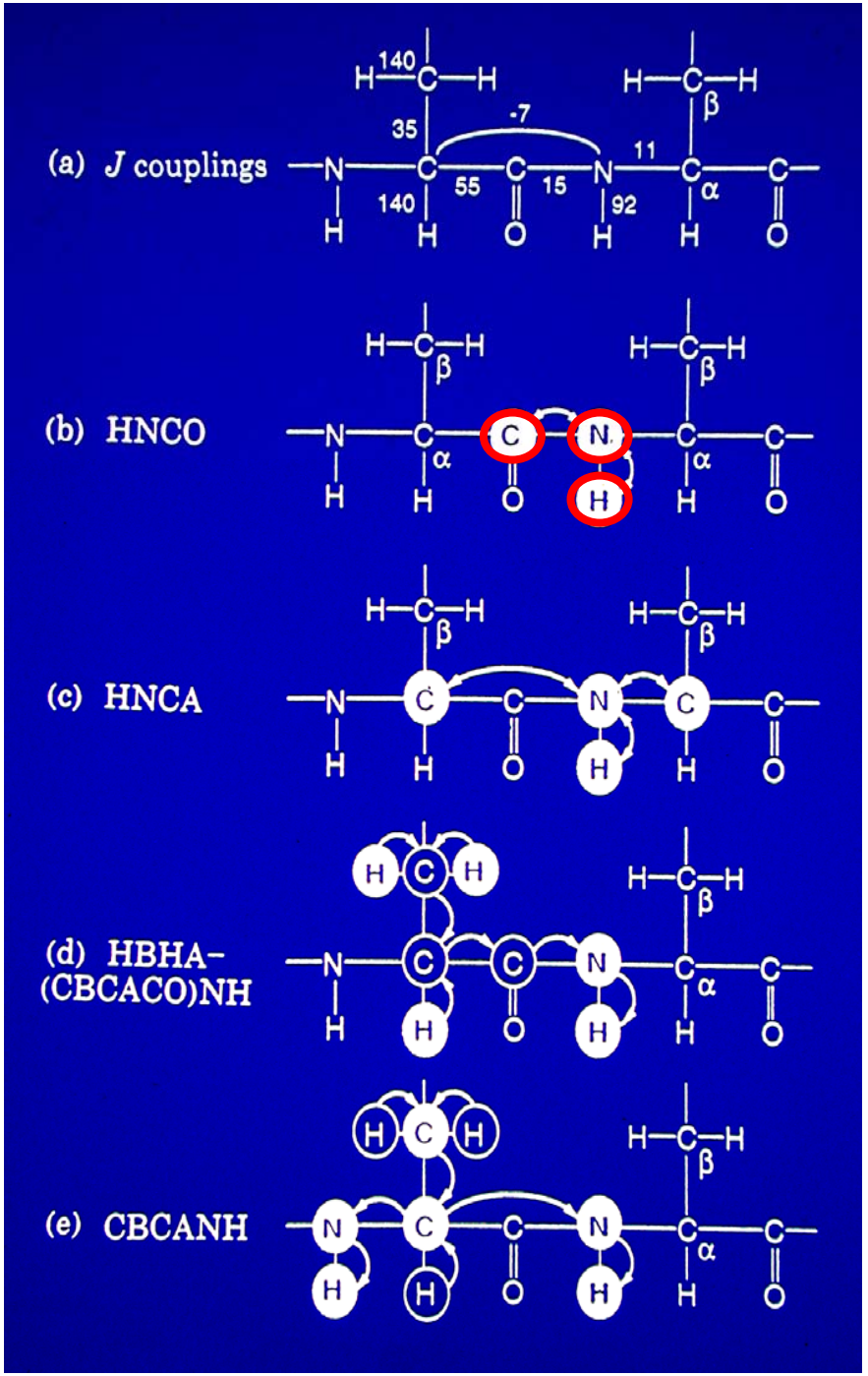

Table 1. Acquisition parameters for experiments

Experiment	Nucleus			No. of complex points			SW (Hz)			Scans	Total time (h)
	F1	F2	F3	F1	F2	F3	F1	F2	F3		
HNCO	^{15}N	^{13}CO	$^{1}H^{N}$	32	40	512	2432	1962	4237	8	14
HNCA	^{15}N	$^{13}C^{\alpha}$	$^{1}H^{N}$	52	105	512	2432	9054	4237	16	120
HN(CA)CO	^{15}N	^{13}CO	$^{1}H^{N}$	32	40	512	2432	1962	4237	48	87
HN(CO)CA	^{15}N	$^{13}C^{\alpha}$	$^{1}H^{N}$	32	32	512	2432	5282	4237	8	12
CBCA(CO)NH	^{15}N	$^{13}C^{\alpha/\beta}$	$^{1}H^{N}$	32	64	512	2432	12072	4237	32	91
HNCACB	^{15}N	$^{13}C^{\alpha/\beta}$	$^{1}H^{N}$	32	64	512	2432	12072	4237	32	94
TOCSY-HSQC	^{1}H	^{15}N	$^{1}H^{N}$	128	64	512	7801	2432	4237	8	92
NOESY-HSQC	^{1}H	^{15}N	$^{1}H^{N}$	128	64	512	7801	2432	4237	8	133
HCCH-TOCSY	^{1}H	^{13}C	^{1}H	128	105	512	6849	10563	6849	8	141
C(CO)NH	^{15}N	^{13}C	$^{1}H^{N}$	32	70	512	2432	12072	4237	32	95
CT-HSQC	^{13}C	^{1}H		160	1024		10563	6849		48	5
HSQC	^{15}N	$^{1}H^{N}$		128	1024		2432	4237		16	0.66

Average secondary shift for various nuclei relative to random coil values (ppm)

Nucleus	Helix	β-strand
$^{1}H^{\alpha}$	-0.38	0.38
N-^{1}H	-0.19	0.29
2-^{13}C ($^{13}C^{\alpha}$)	2.6	-1.4
1-^{13}C(CO)	1.7	-1.4
^{15}N	-1.7	1.2

Usually only $^{1}H^{\alpha}$, $^{13}C^{\alpha}$, ^{13}CO are used for identifying secondary structures.

$^1H^{\alpha}$ Chemical shift and secondary structure

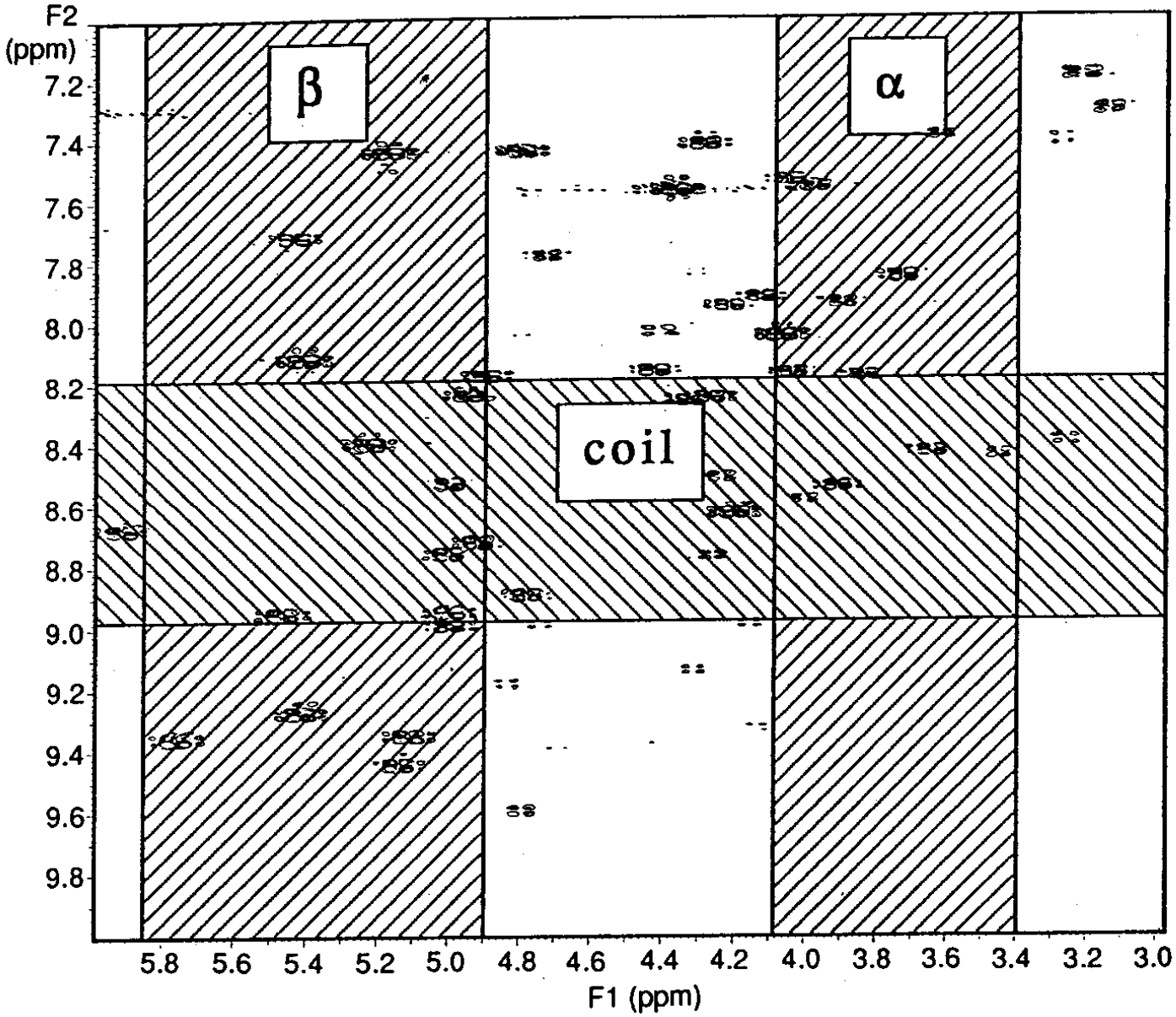

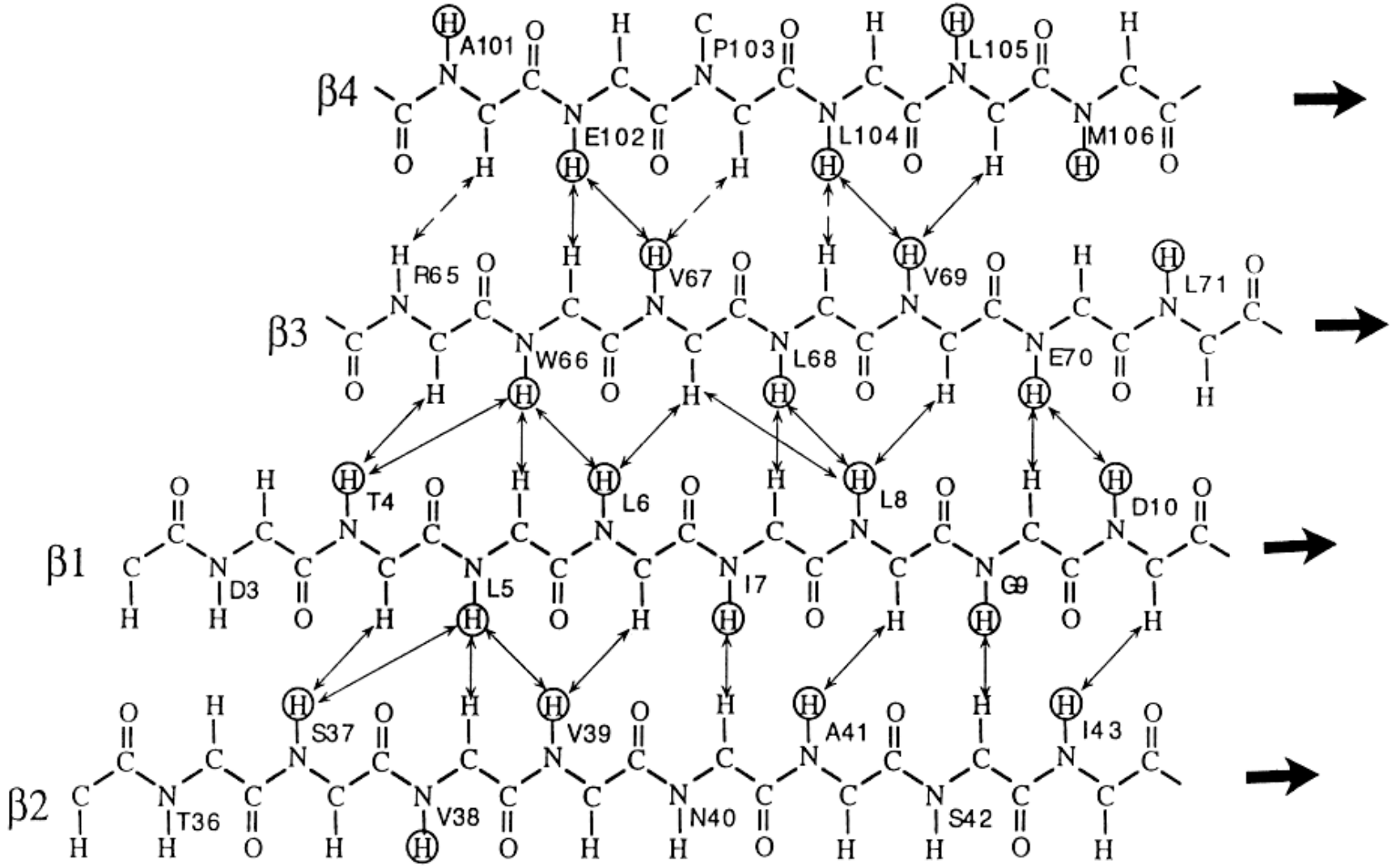
β4
A101
P103
L105
E102
L104
M106
β3
R65
V67
V69
L71
W66
L68
E70
β1
T4
L6
L8
D10
D3
L5
I7
G9
β2
S37
V39
A41
I43
T36
V38
N40
S42

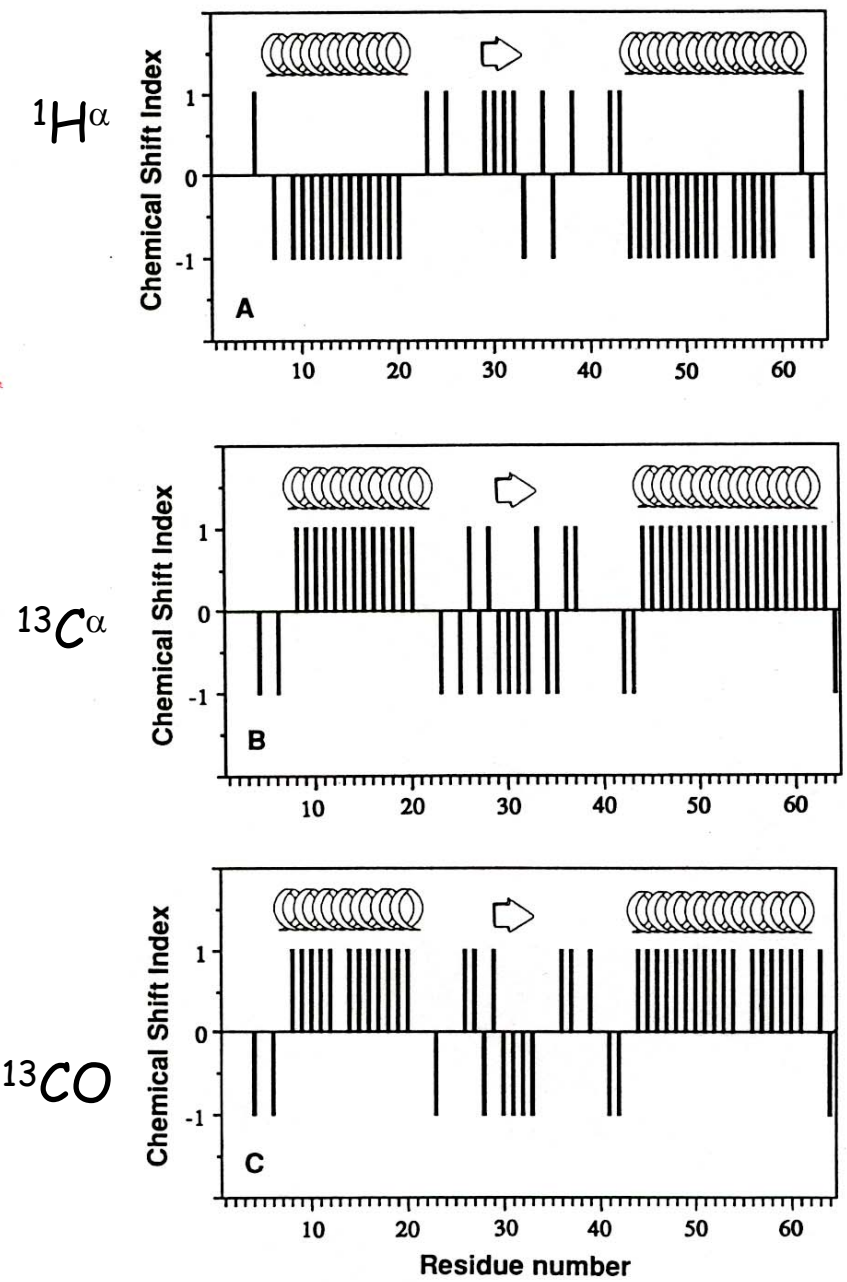

FIG. 2. Chemical shift index plotted for the first 65 residues of interleukin 4 using assignments supplied by Powers *et al.*[44] The chemical shift index is plotted for (A) α-^{1}H resonance assignments, (B) α-^{13}C resonance assignments, and (C) carbonyl ^{13}C resonance

Consensus chemical shift indices

1. For a nucleus, if chemical shift is within the range gives a "0".
2. If greater than the standard deviation range gives "+1"
3. If it is less than that range gives a "- 1".
4. A minimum of four consecutive "- 1" (or "+1" for carbons) is needed to define a helix.
5. A minimum of three consecutive "1" (or "- 1" for carbon) w/o interrupt is needed to define a strand.
6. Repeat for all three nuclei. Need 2/3 agree to define a secondary structure element.

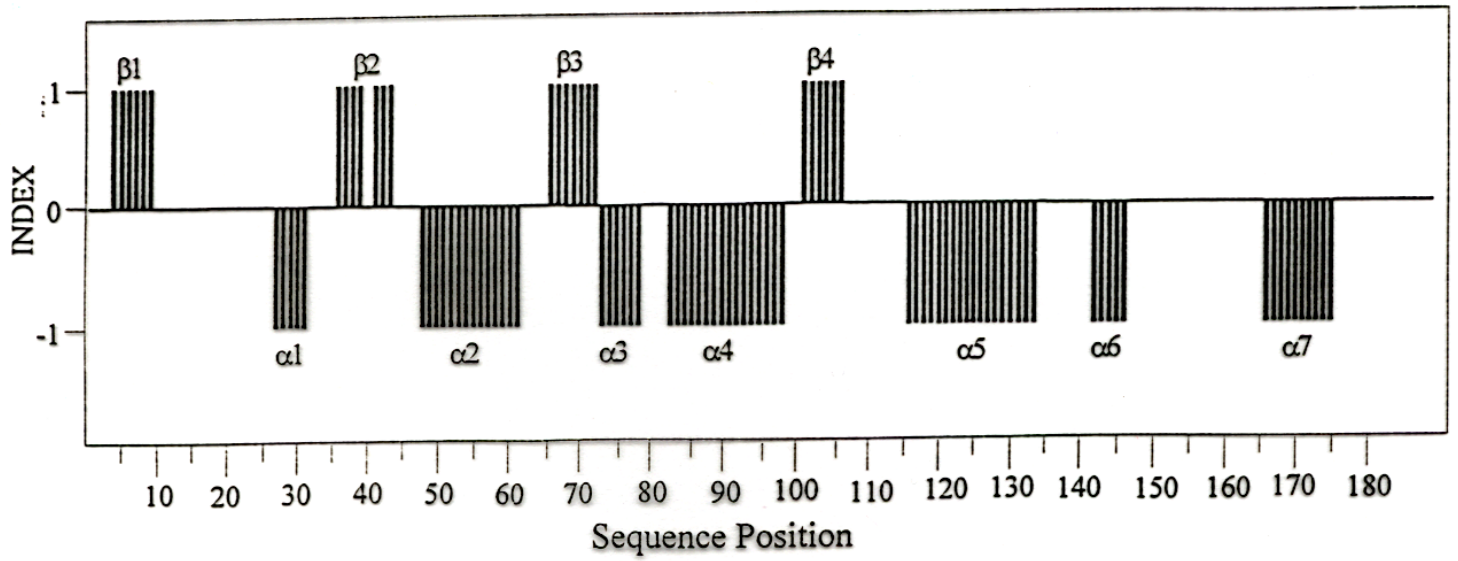

Figure 5. CSI consensus plot for *E. coli* thioesterase/protease I, determined using four nuclei ($^{1}H^{\alpha}$, $^{13}C^{\alpha}$, $^{13}C^{\beta}$, and ^{13}CO). The secondary structural motifs obtained from this program are summarized in the figure.

^1H - ^1H NOESY of RC-RNase

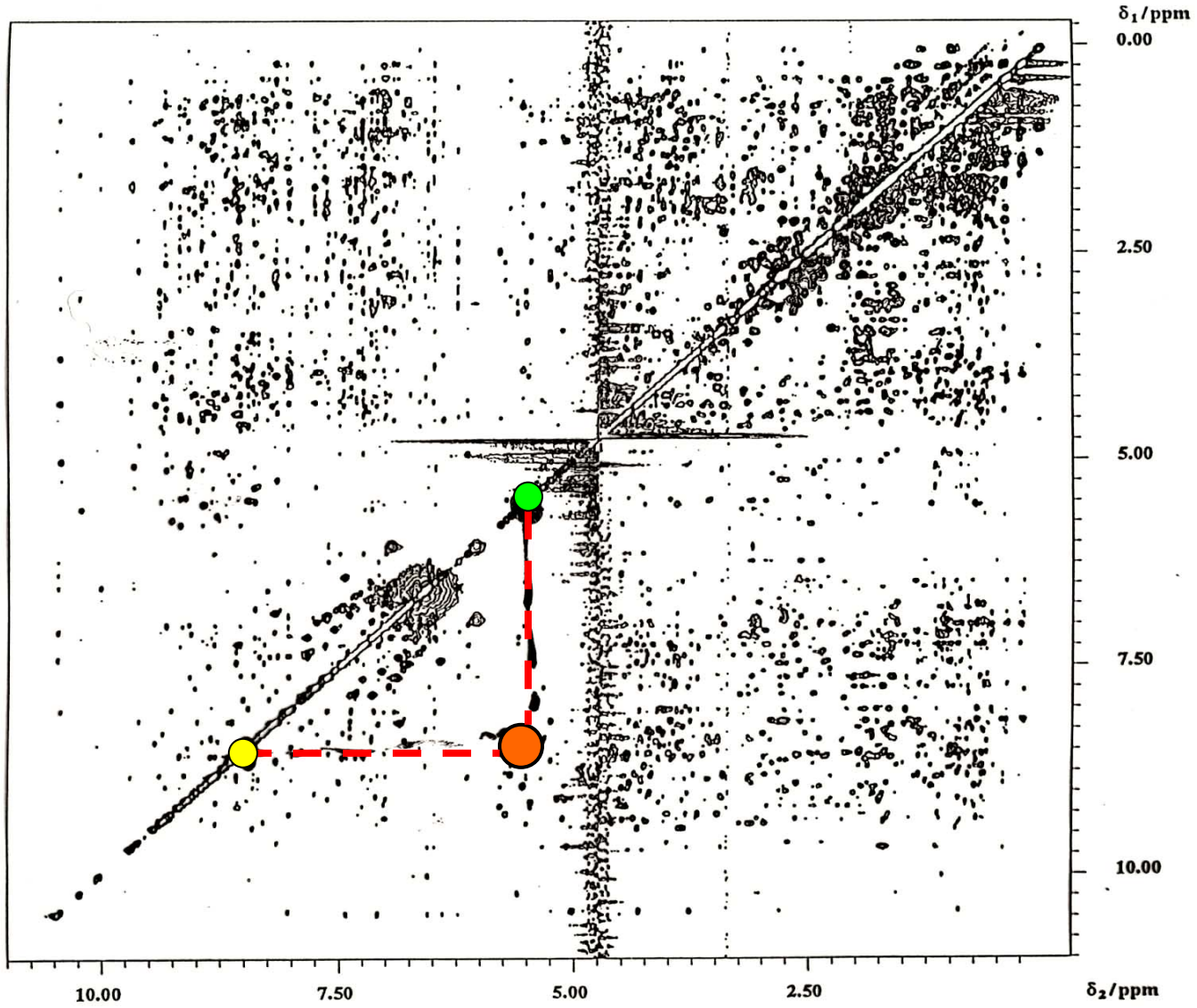

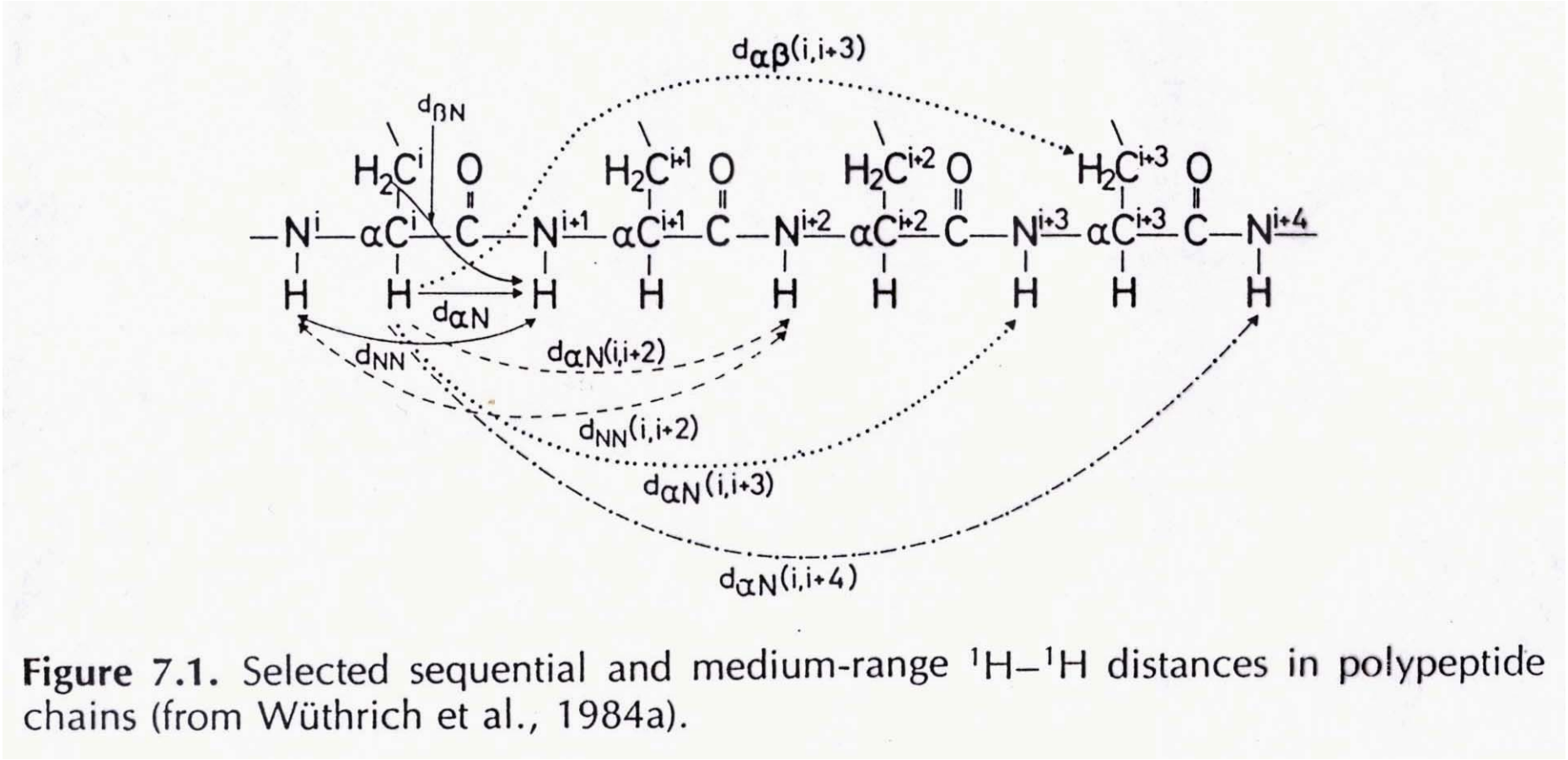

Figure 7.1. Selected sequential and medium-range $^1H-^1H$ distances in polypeptide chains (from Wüthrich et al., 1984a).

J-coupling of backbone nuclei (Hz)

^{3}J(HN-CA) = 4 – 11 Hz depends on secondary structure.

< 6 Hz → α-helix
> 8 Hz → β-stand

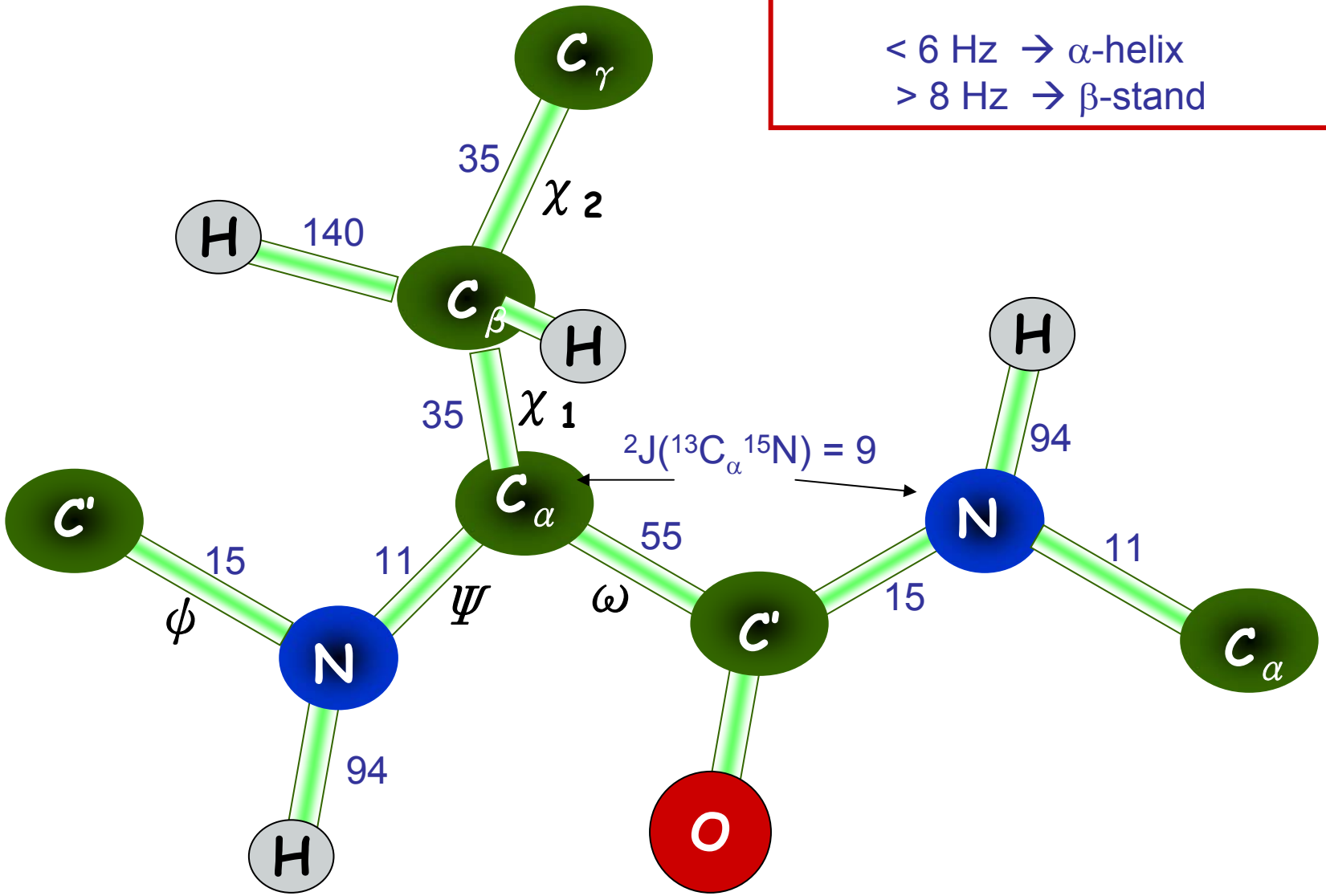

Secondary structure prediction from backbone proton distance

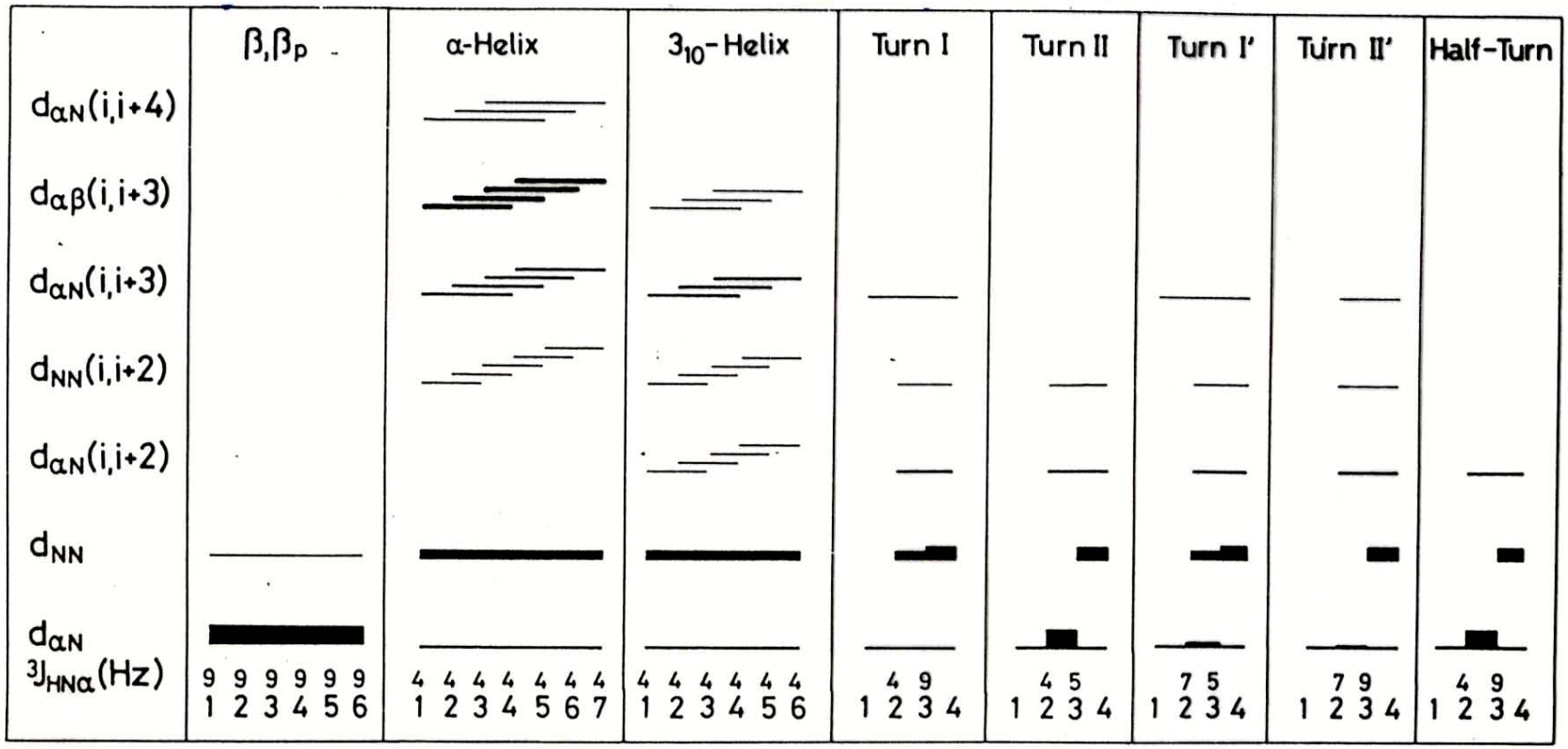

Figure 9.1. Survey of the sequential and medium range $^1H-^1H$ NOE's and the spin–spin coupling constants $^3J_{HN\alpha}$ in the following secondary structures: parallel or antiparallel β sheet, α helix, 3_{10} helix, turns of types I, II, I', and II', and a half-turn derived from a type II tight turn (see text). The numbers at the bottom represent the amino acid residues in the secondary structure elements and the values of $^3J_{HN\alpha}$. Short $^1H-^1H$ distances are indicated by lines linking the residues that contain the connected hydrogen atoms; the thickness of the lines is proportional to r^{-6} and thus represents the NOESY cross-peak intensities (from Wagner et al., 1986a).

Karplus Equations :

$^3J_{HN-HA}$ coupling

$$^3J(H^{\alpha}, H^{N})\phi = 6.4\cos^2(\phi - 60°) - 1.4\cos(\phi - 60°) + 1.9$$

$$^3J(H^{\alpha}, H^{\beta 2})\chi^1 = 9.5\cos^2(\chi^1 - 120°) - 1.6\cos(\chi^1 - 120°) + 1.8$$

$$^3J(H^{\alpha}, H^{\beta 3})\chi^1 = 9.5\cos^2\chi^1 - 1.6\cos\chi^1 + 1.8$$

$$^3J(N, H^{\beta 2})\chi^1 = -4.5\cos^2(\chi^1 + 120°) + 1.2\cos(\chi^1 + 120°) + 0.1$$

$$^3J(N, H^{\beta 3})\chi^1 = -4.5\cos^2(\chi^1 - 120°) + 1.2\cos(\chi^1 - 120°) + 0.1$$

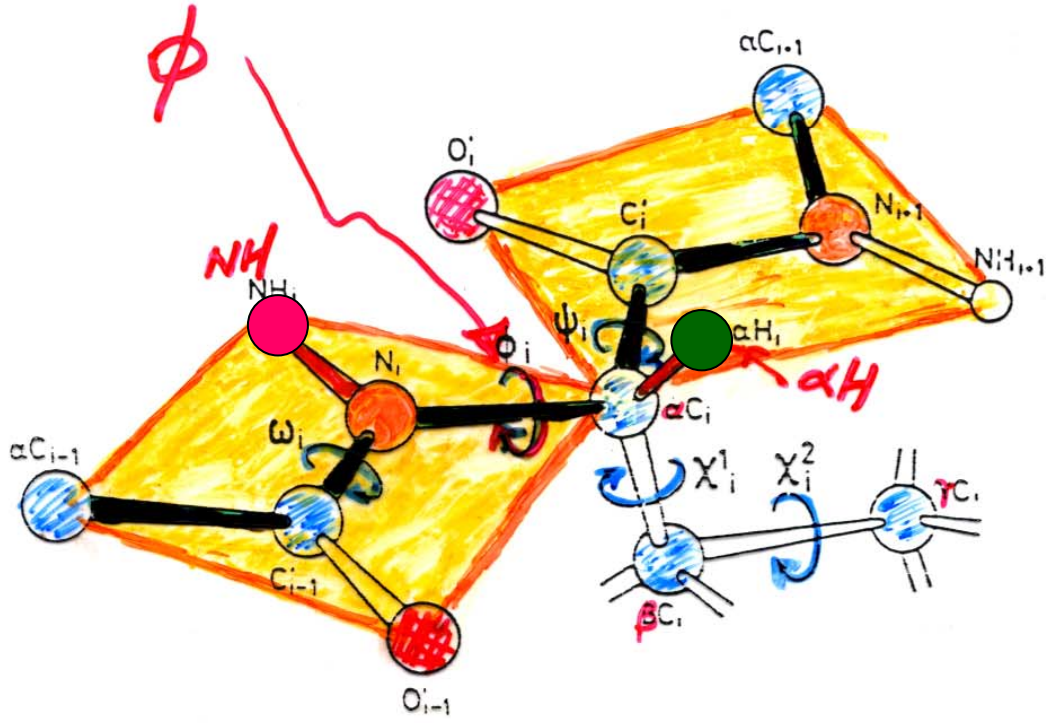

Figure 7.2. Standard nomenclature for the atoms and the torsion angles along a polypeptide chain (IUPAC–IUB Commission on Biochemical Nomenclature, 1970).

Summary plot

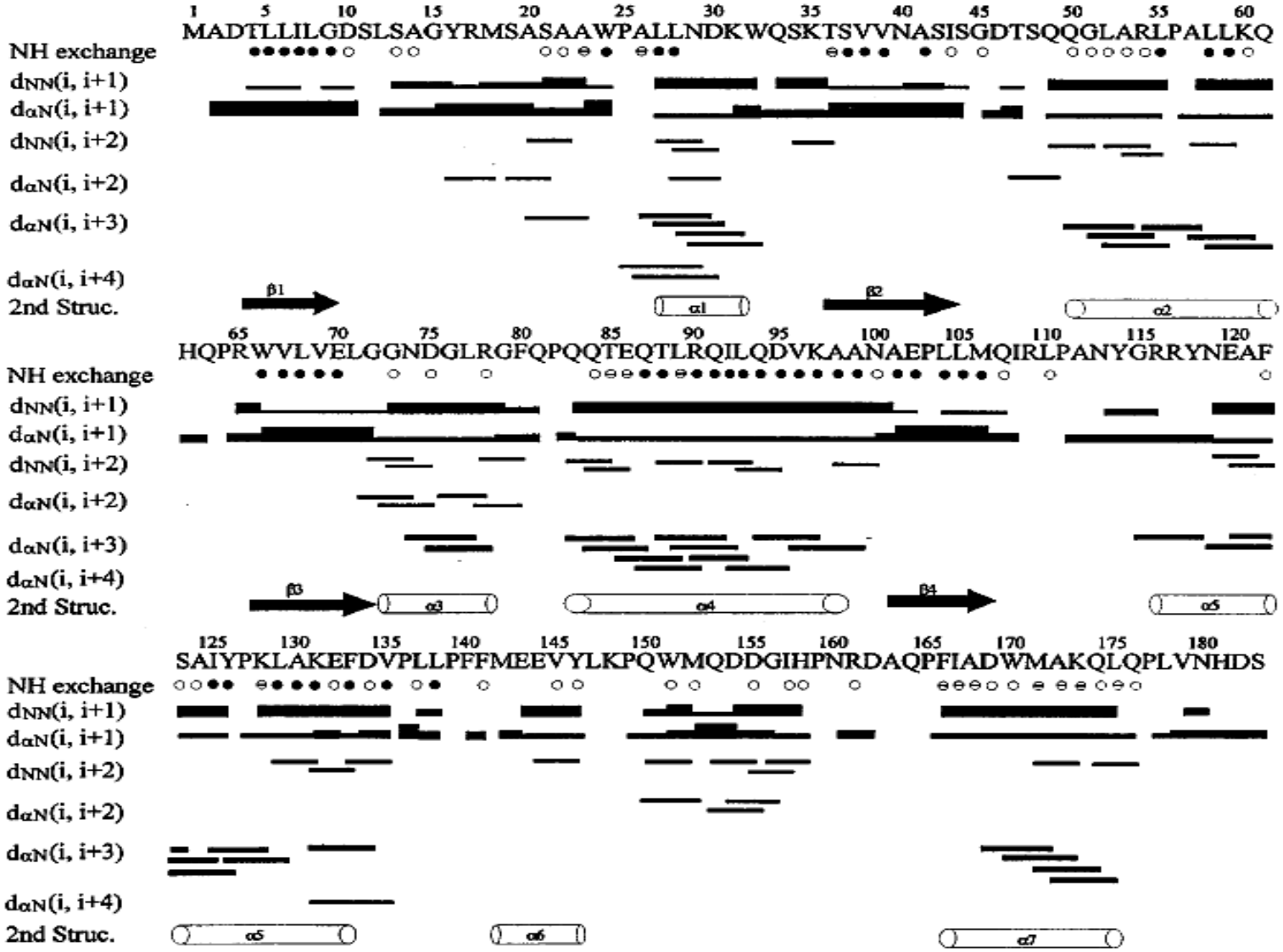

Figure 7. Sequence of *E. coli* thioesterase I, the amide proton exchange rates, and summary of the sequential and medium-range NOEs involving HN and H^{α} protons. Amide protons that remained observable in the 2D ^{15}N-HSQC spectrum after 6 days are labeled with filled circles (very slow-exchange protons), those that were observable after 2 days are marked with open circles with a central horizontal line (slow-exchange protons), those that were observable after 40 min are marked with open circles (medium-exchange protons), and those that were not observable upon the addition of D_2O (fast-exchange protons) are not marked. The NOE intensities are indicated by the thickness of the black bars, with thicker bars representing stronger NOEs.

Secondary Structure Topology Derived by NMR

1. A four-strand β sheet + seven α helices.
2. α/β hydrolase fold

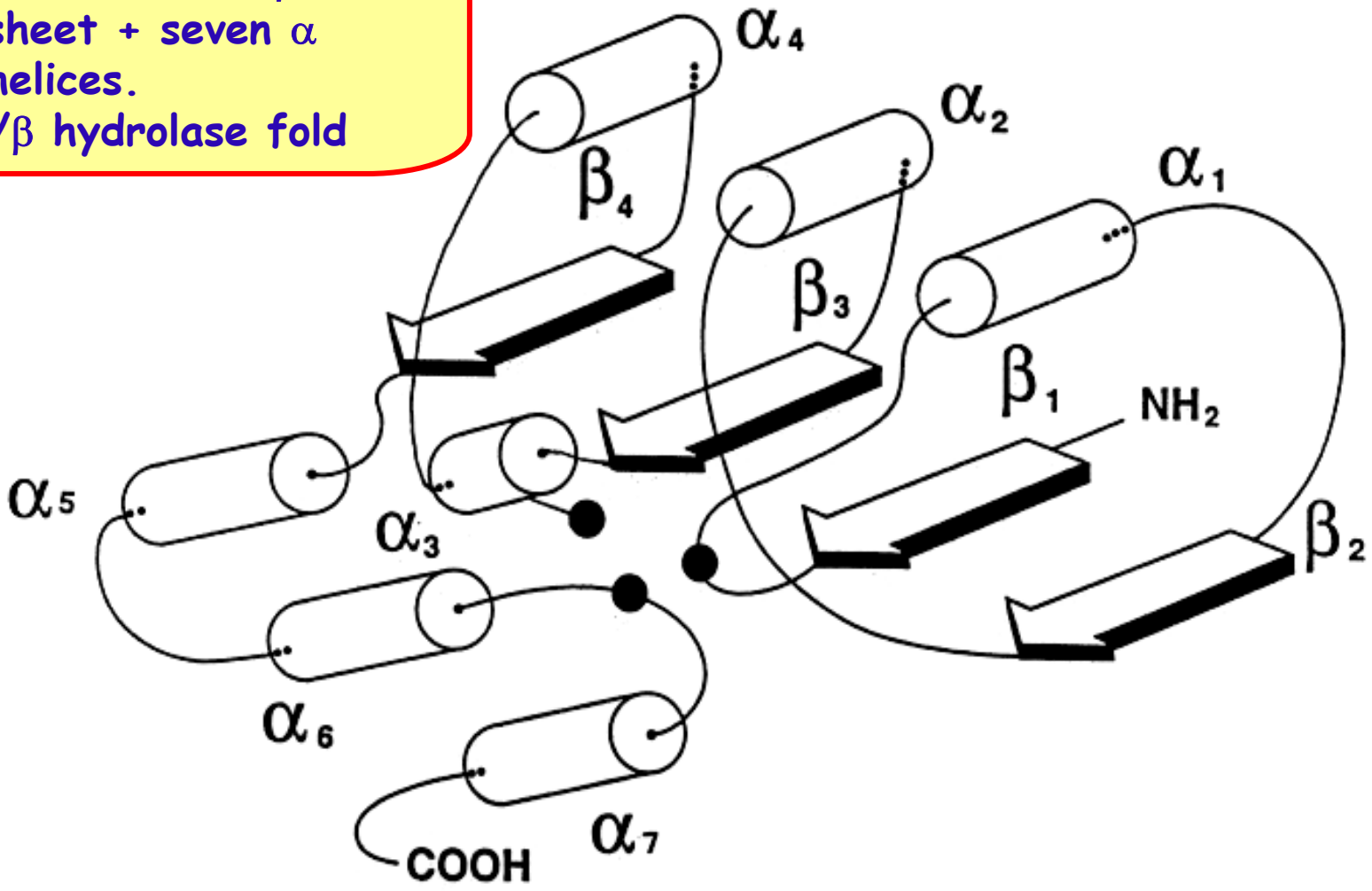

NMR Structural Constraints

1. **Internuclear distances (Nuclear Overhauser Effect)**
   $NOE \propto R^{-6}$

2. **Dihedral angles (J-coupling):**
   $^{3}J_{NH\alpha} = 6.4 \cos^{2}(\Phi\text{-}60) - 1.4\cos(\Phi\text{-}60) + 1.9$

3. **Chemical Shift Index (CSI):**
   Chemical shift difference between observed and random coil chemical shift values $\rightarrow$ 2^{nd} structure determination

4. **Residual dipolar coupling:**
   Partial orientation of protein molecules in liquid crystal media permits observation of residual dipolar coupling for assessing long range orientations of dipolar coupled bonds.

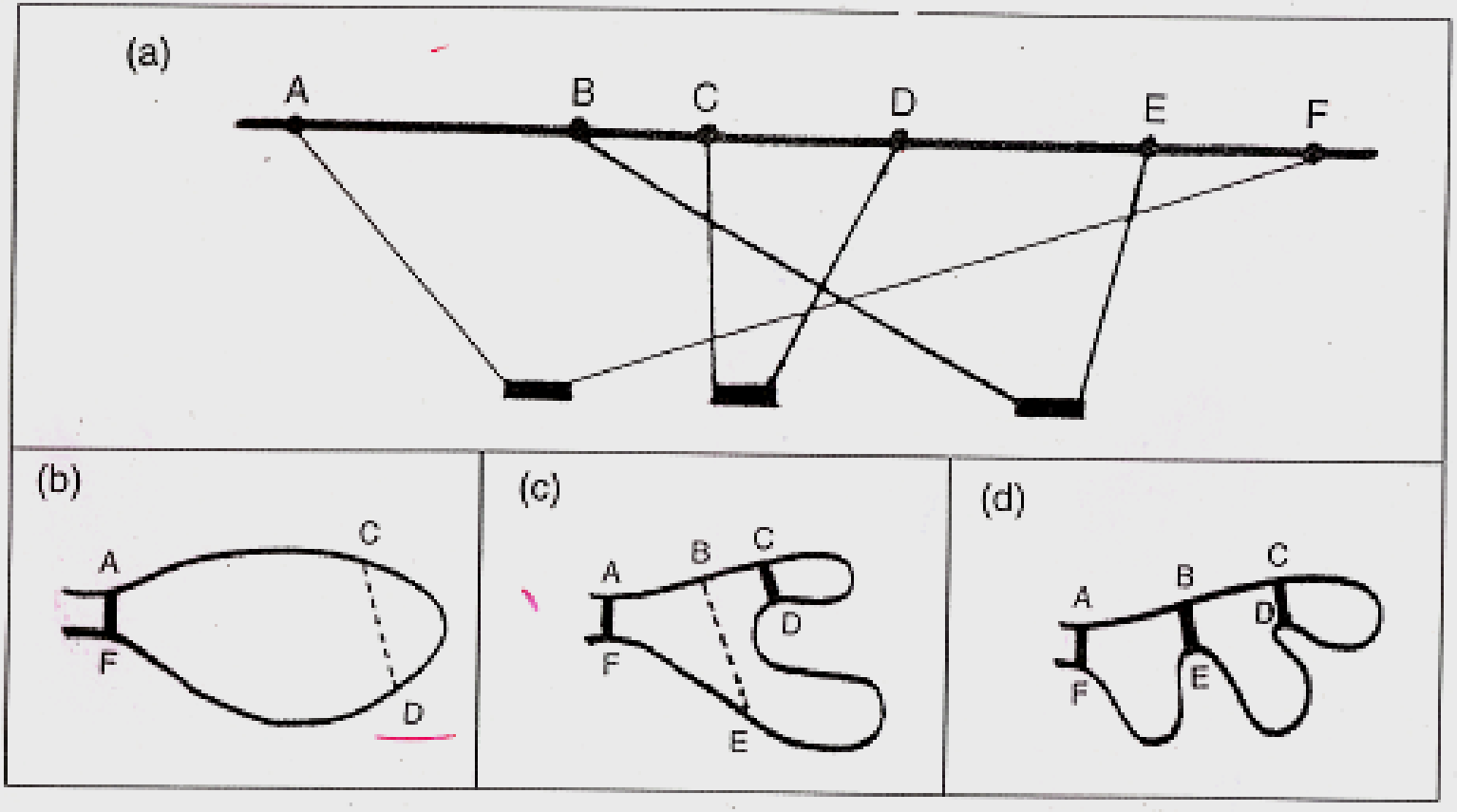

由 NOE 限制找出分子的三度空間結構。

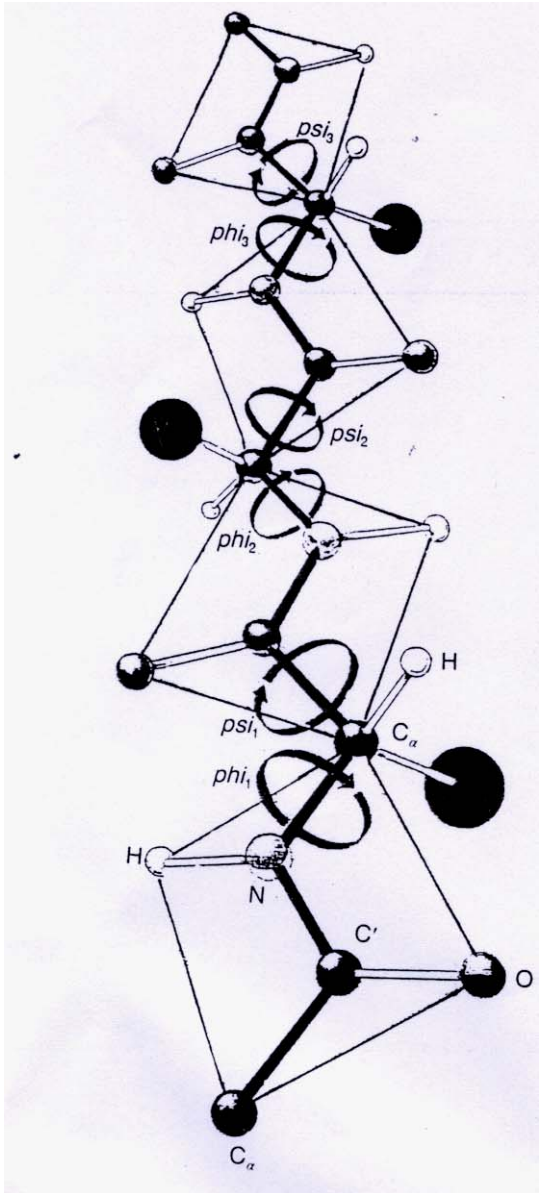

圖三. 蛋白質骨架胜肽平面結構圖

Structure

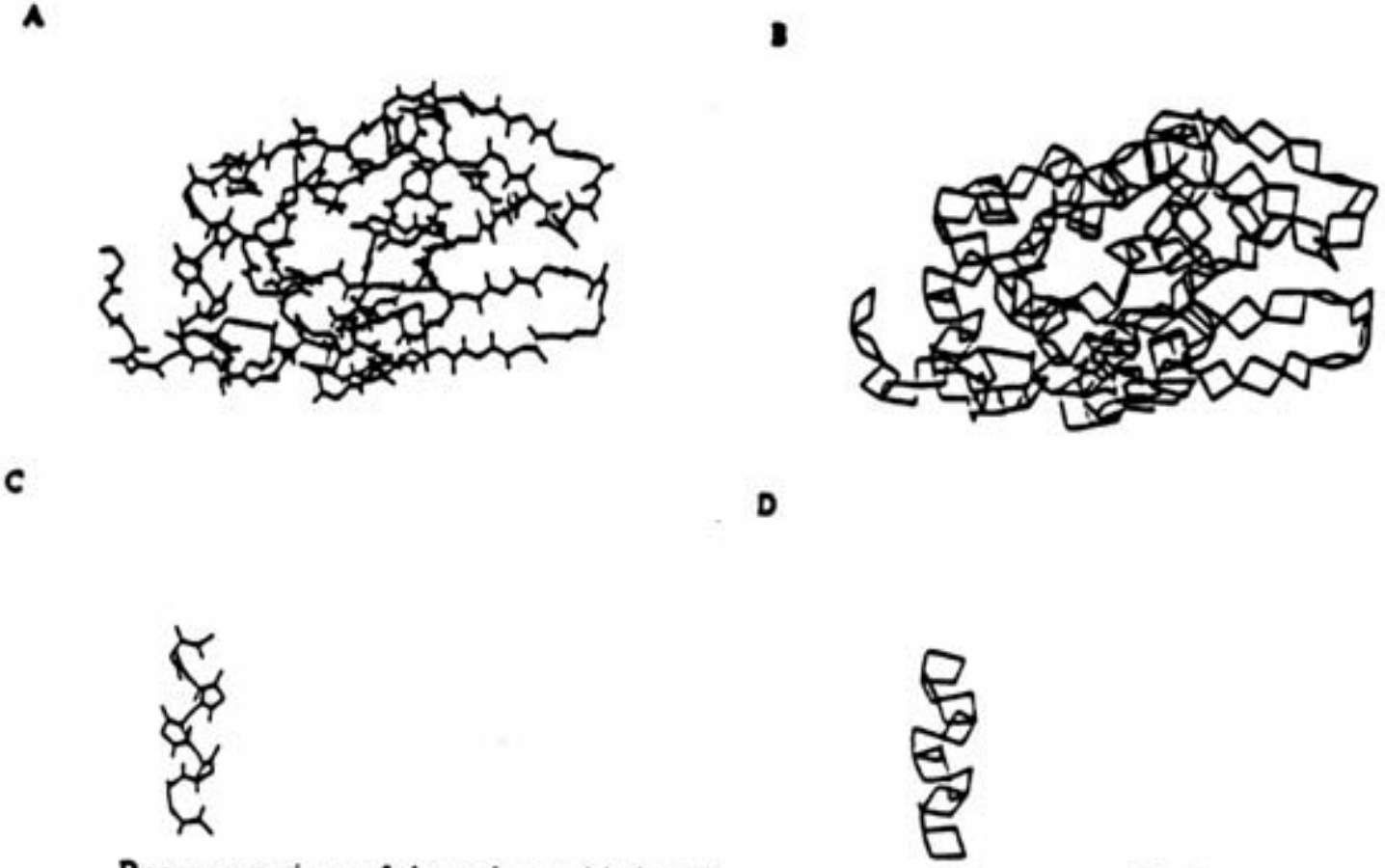

. Representations of the polypeptide backbone structure of lysozyme (Moult *et al*, 1976; Herzberg & Sussman, 1983). (A) all residues with the backbone atoms connected by bonds, (B) Residues 5–15 as in (A). (C) All residues with the peptide planes outlined. (D) Residues 5–15 as in C.

Tertiary Structure Determination

1. Use long range NOE cross peaks, dihedral angles and RDC as constraints.
2. NOE cross peak intensities are affected by molecular motion, multispin interaction and spin diffusion effects. Thus, normally rather loose constraints are used.

   Very Strong: 1.8 – 2.5 Å; Strong: 1.8 – 3 Å
   Medium: 1.8 – 3.5 Å Weak: 1.8 – 4 Å
   Very Weak: 1.8 – 5 Å
3. Need to overcome energy barrier to avoid trapped in local minimum by performing simulated annealing and molecular dynamic calculation.
4. Normally needs to calculate several (50) structures with different initial input conditions to obtain an ensemble of structures.
5. Side chain conformations are hard to define.
6. Use residual dipolar interaction to further refine the structure.
7. Minimize the radius of gyration of the protein to make it more compact:

$$R^2 = \Sigma\, m_i r_i^2 / \Sigma m_i$$

Structure Calculation

1. Build a random structure of the given sequence.
2. Use molecular dynamics and simulated annealing to generate many structures with minimum violation of structure constraints and with minimal energy of the following energy term.

$E_{total} = E_{bond} + E_{angle} + E_{improper} + E_{VDW} + E_{cdih} + E_{NOE} + E_{RDC} + \ldots$

$E_{bond} = \Sigma k_b(b-b_0)^2$; $E_{\varphi} = \Sigma k_{\varphi}(\varphi-\varphi_0)^2$;

$E_{improper} = \Sigma k_{impr}(\omega-\omega_0)^2$; $E_{cdih} = \Sigma k_{cdih}(\Psi-\Psi_0)^2$;

$E_{NOE} = \Sigma k_{NOE}(\gamma-\gamma_0)^2$; $E_{RDC} = \Sigma k_{RDC}(\theta-\theta_0)^2$;

3. Check for wrong assignments and recalculate the structure.
4. Selcet 20 structures of least NOE violation (> 0.5 Å)
5. Criteria for good structures:
   a. No NOE violation
   b. RMSD < 0.5 Å
   c. No violation in dihedral angle (Inspect Ramachandran diagram)(Atomic hindrance).

Table 1. Summary of structural constraints and structural statistics

NMR-derived restraints	
Upper inter-proton restraints	1245
Intra-residue	460
Sequential	435
Medium-range	146
Long-range	204
Hydrogen bond restraints	66 for 33 hydrogen bonds
Dihedral angle (ϕ, ψ, χ^1)	87, 81, 28
Total constraints	1507
Residual constraint violations[a]	
CYANA target function value (Å^2)	1.58 ± 0.31
NOE upper distance constraint violations	
Maximum (Å)	0.36 ± 0.20
Number >0.2 Å	3 ± 2
Dihedral angle constraint violations[b]	
Maximum (deg.)	4.86 ± 1.14
Number >5 (deg.)	1 ± 1
van der Waals violations	
Maximum (Å)	0.17 ± 0.02
Number >0.1 Å	0 ± 0

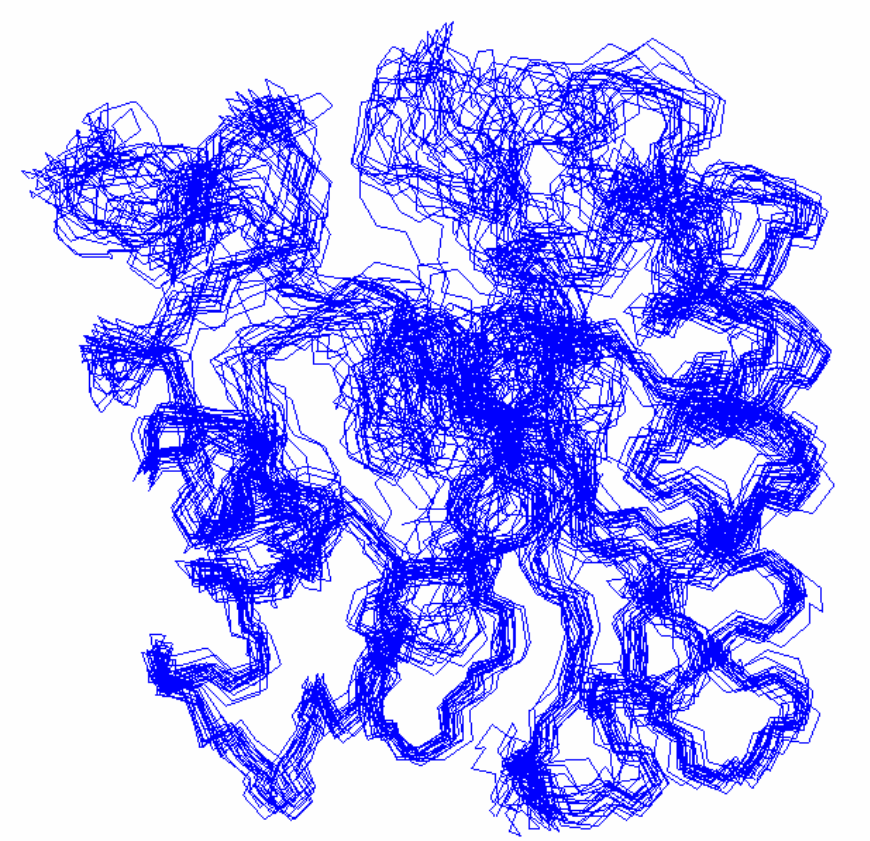

Oxyanion Hole residues

S^{10}, G^{44} & N^{73}

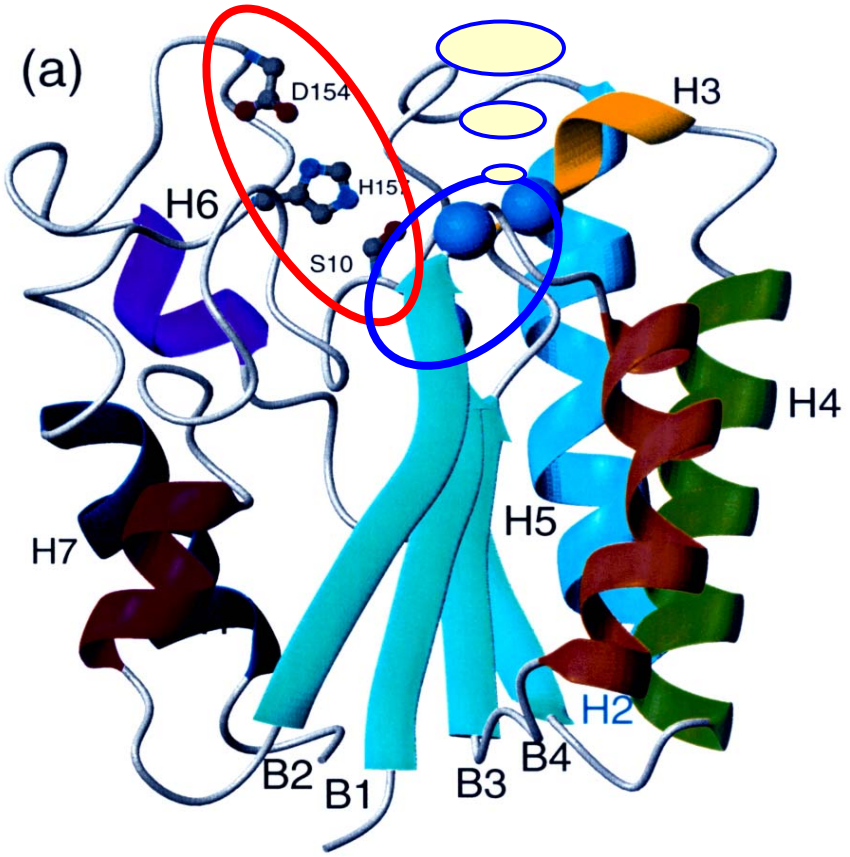

Average pairwise r.m.s. deviations (Å)[c]	
Backbone, N, C^{α}, C (10–93)	0.67 ± 0.12
Heavy atoms (10–93)	1.17 ± 0.18
Backbone, N, C^{α}, C (secondary region)[d]	0.39 ± 0.06
Heavy atoms (secondary region)	0.98+0.12
Ramachandran statistics	
Most favorable region (%)	73.1
Additional allowed region (%)	24.8
Generally allowed region (%)	2.0
Disallowed region (%)	0.1

[a] For the 20 conformers with lowest CYANA target function values.

[b] Dihedral angles predicted from the program TALOS.

[c] r.m.s. deviations relative to the mean coordinates.

[d] Residues 15–20, 23–31, 45–49, 54–58, 63–64, 66–72, 80–90.

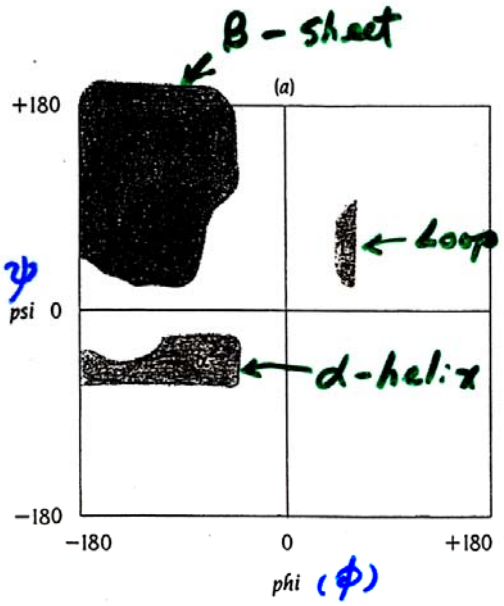

Figure 1.7 Ramachandran plots showing allowed combinations of the conformational angles phi and psi defined in Figure 1.6. Since phi (ϕ) and psi (ψ) refer to rotations of two rigid peptide units around the same C_α atom, most combinations produce steric collisions either between atoms in different peptide groups or between a peptide unit and the side chain attached to C_α. These combinations are therefore not allowed. (a) Colored areas show sterically allowed regions. The areas labeled α, β, and L correspond approximately to conformational angles found for the usual right-handed α helices, β strands, and left-handed α helices, respectively. (b) Observed values for all residue types except glycine. Each point represents ϕ and ψ values for an amino acid residue in a well-refined x-ray structure to high resolution. (c) Observed values for glycine. Notice that the values include combinations of ϕ and ψ that are not allowed for other amino acids. (From J. Richardson, *Adv. Prot. Chem.*34: 174–175, 1981.)

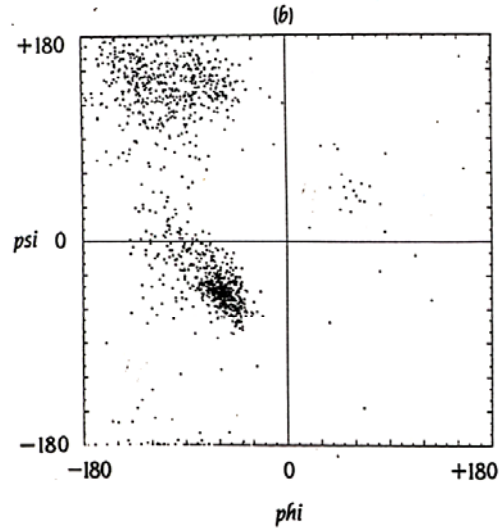

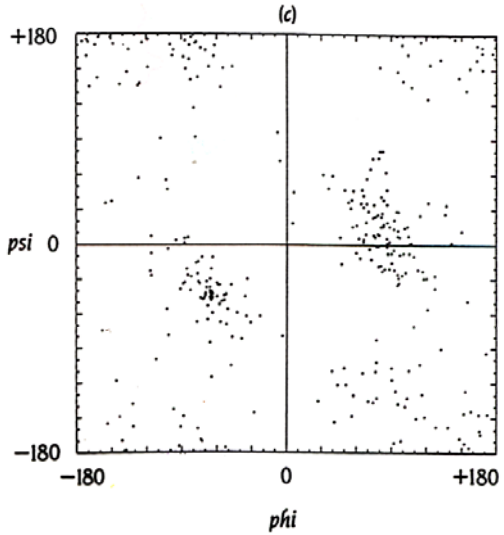

Ramachandran plot

Ramachandran plot (ϕ v.s. Ψ plot)

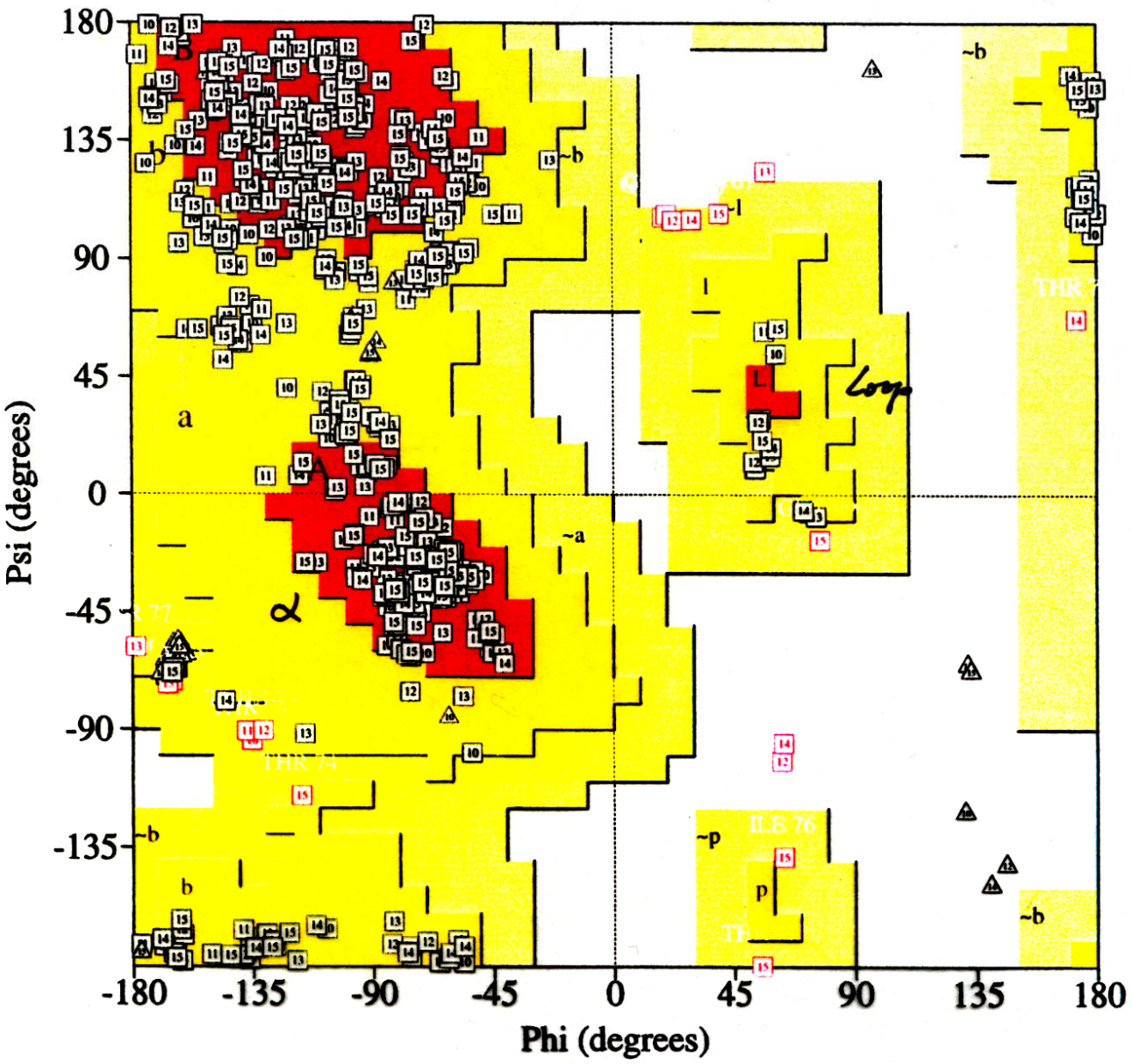

II. Catalytic Mechanism

1. Hydrogen bonding in the catalytic triad.

2. Structure of the Michaelis complex.

Catalytic mechanism

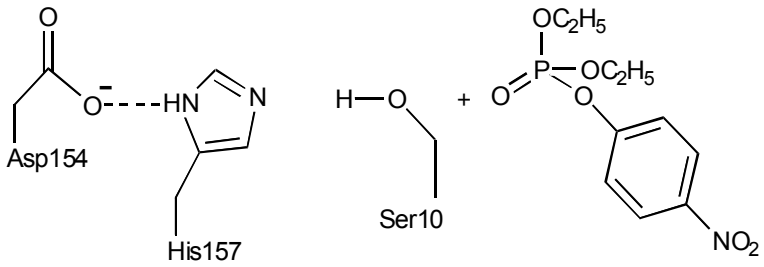

Free Enzyme + Inhibitor

k_1 k_{-1}

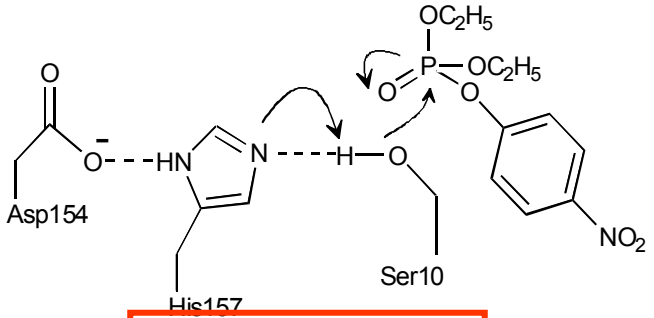

Michaelis-type complex

k_2

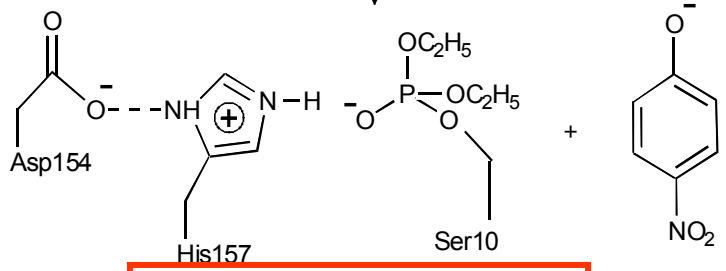

Transition state analogue complex

The catalytic triad of serine proteases

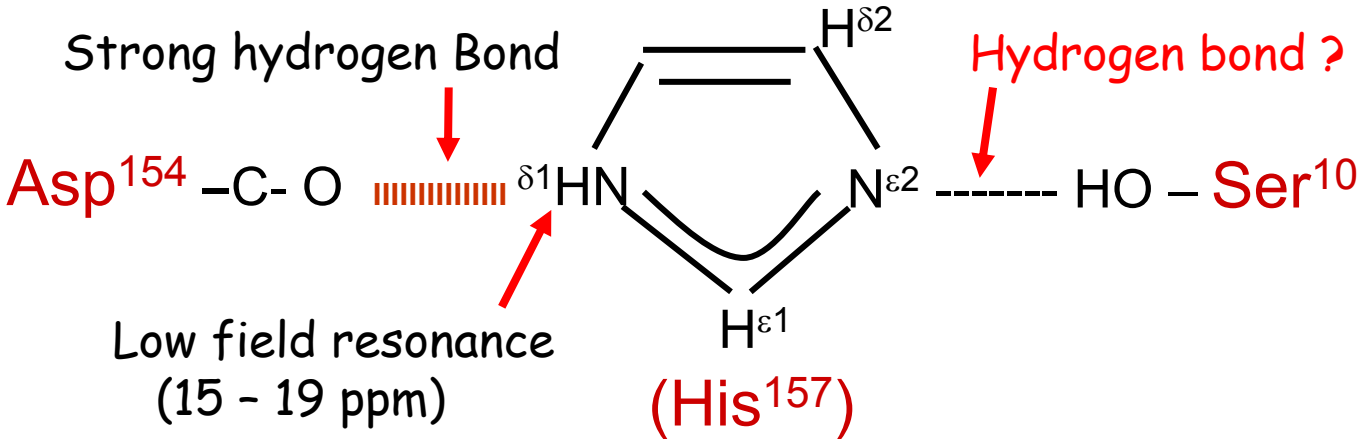

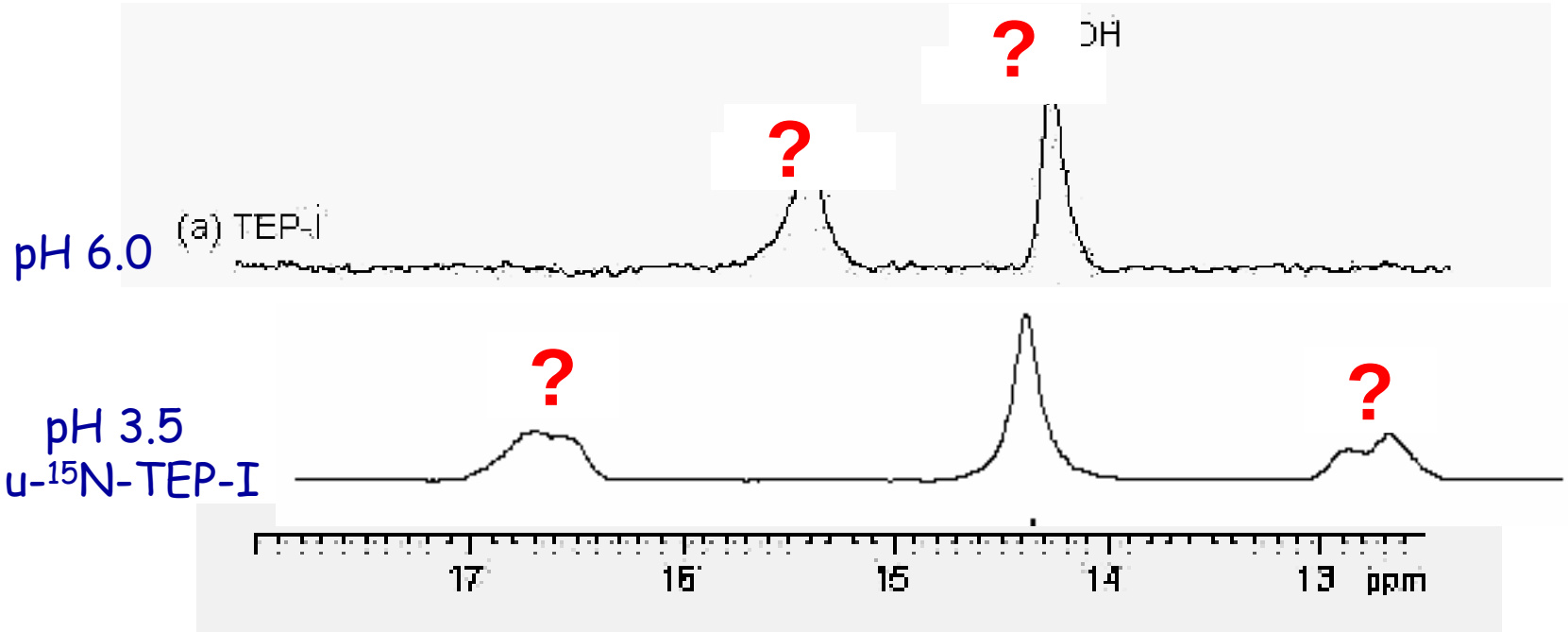

Assignment of low field resonances by Mutant studies

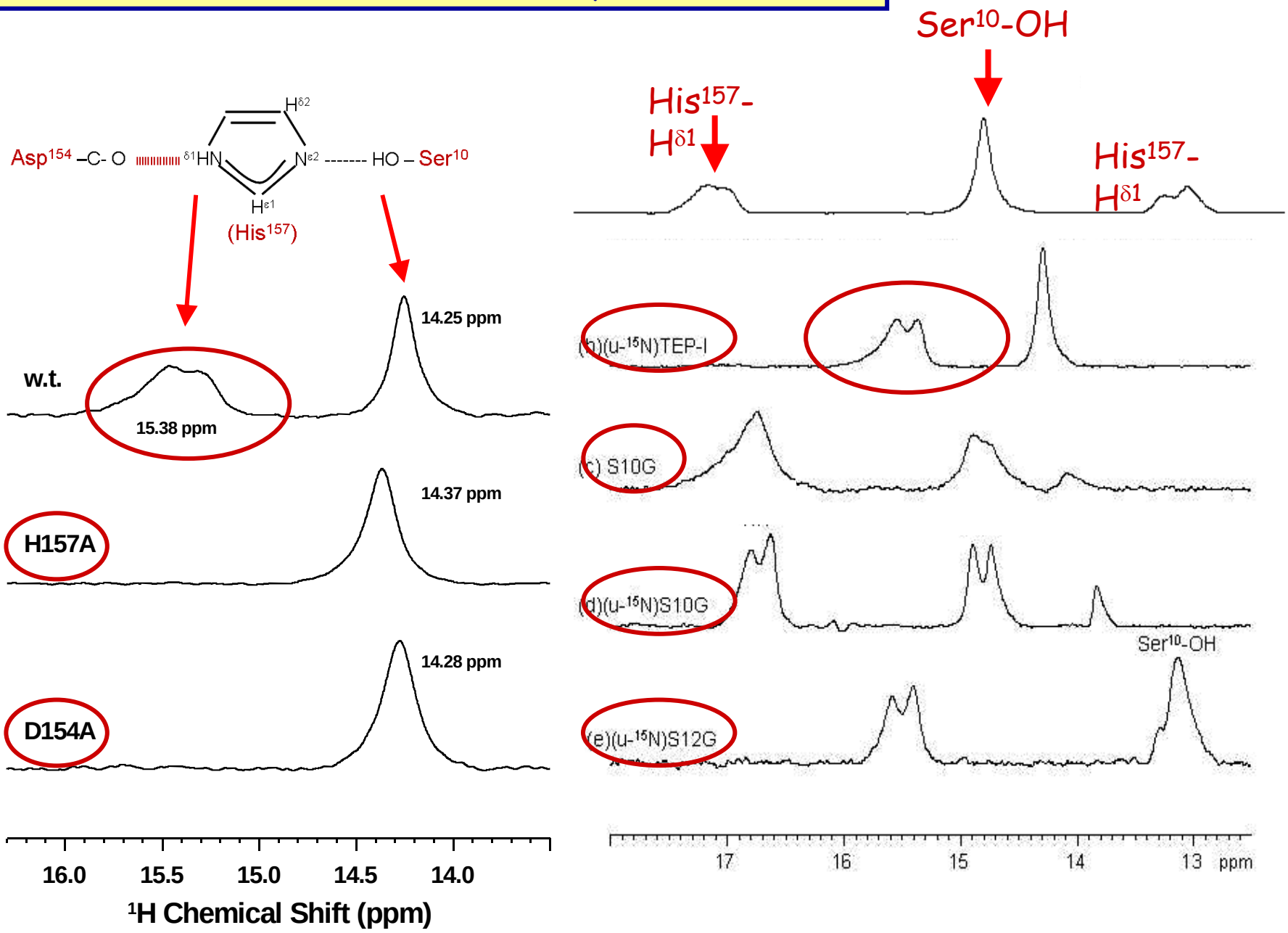

pH titration of the low field resonances

(1°C)

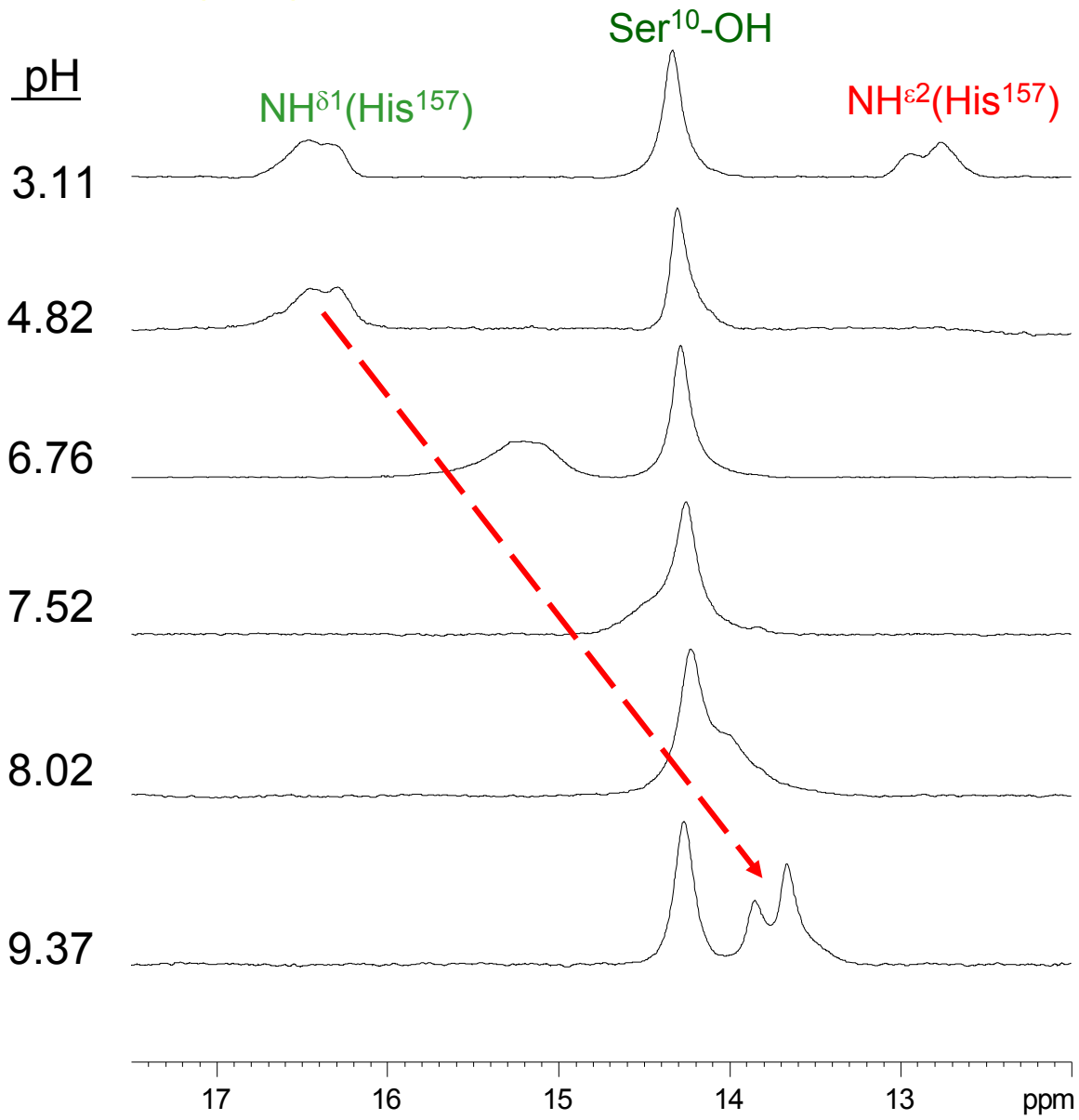

pH titration of the low field resonances

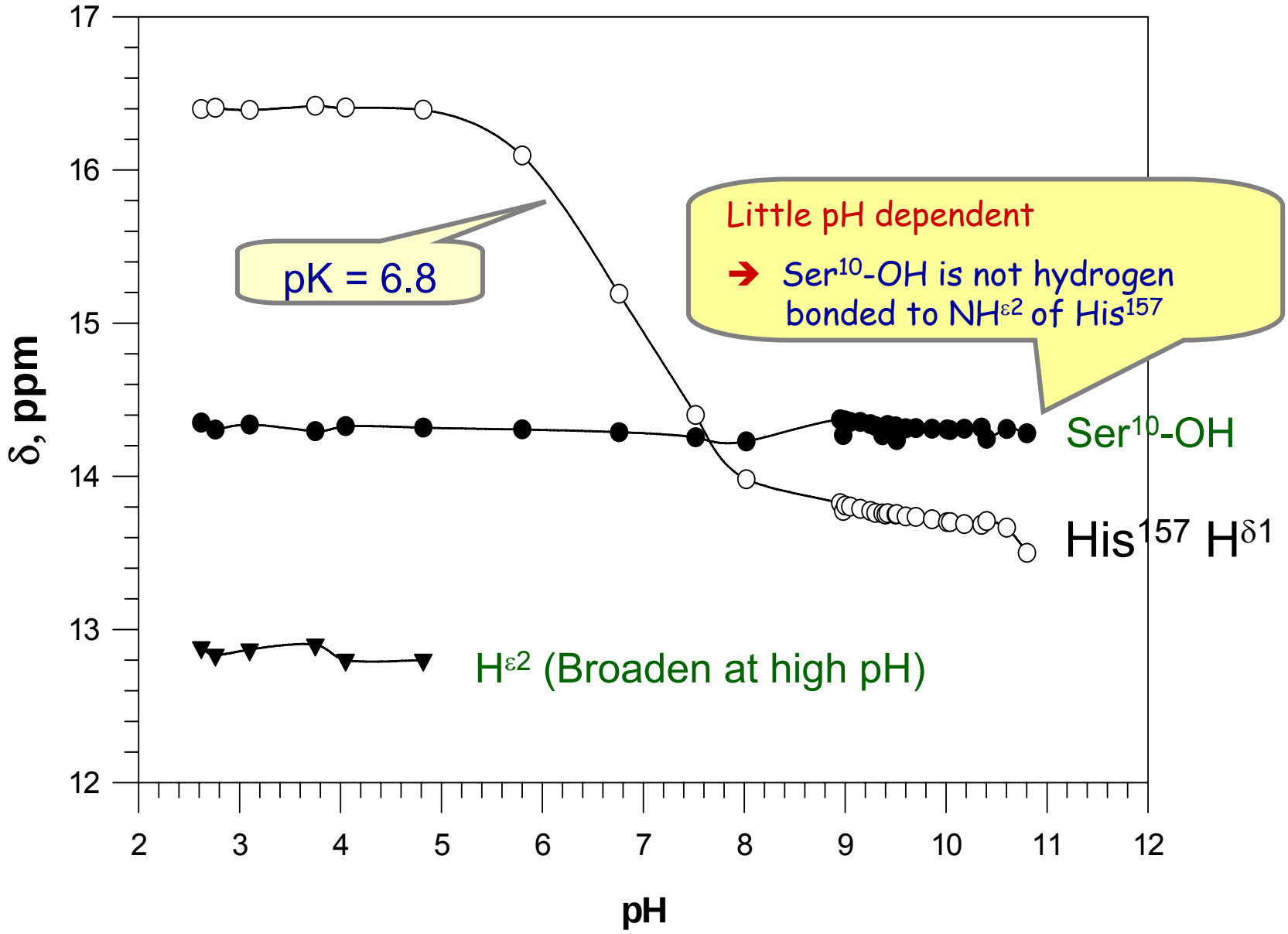

Effect of DENP binding

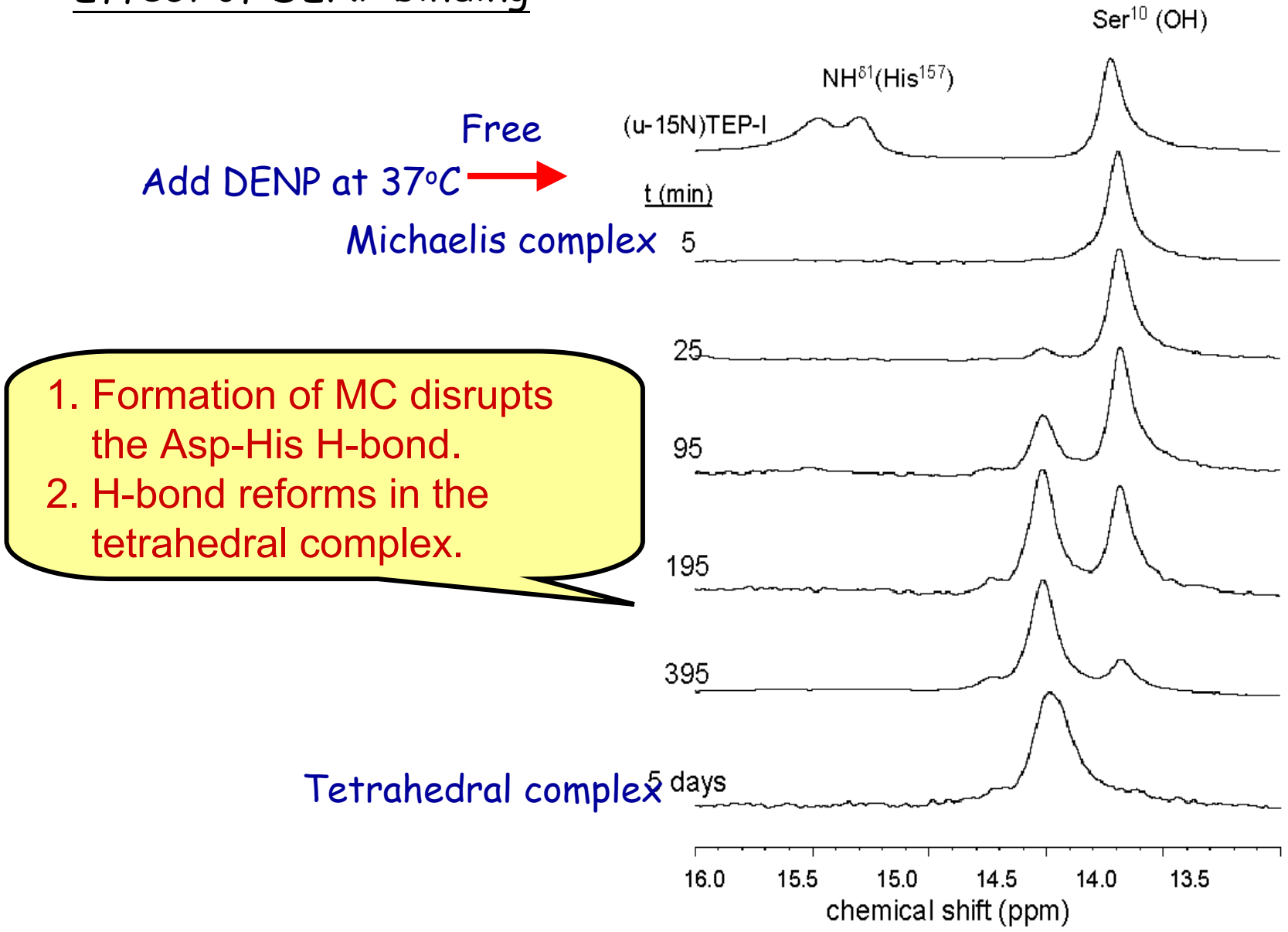

1. Formation of MC disrupts the Asp-His H-bond.
2. H-bond reforms in the tetrahedral complex.

Hydrogen bond of the catalytic triad

1. We have detected and have assigned the low field hydrogen bond resonances of Asp^{154}-$His^{157}$and Ser^{10}-OH.

2. We found that in the free form Ser^{10}-OH is not hydrogen bonded to His^{157} in the free form.

3. In the Michaelis complex the Asp^{154}-His^{157} hydrogen bond cannot be detected.

4. In the TEP-I/DENP tetrahedral complex the Asp^{154}-His^{157} may be reformed, but its nature is still unclear.

Structure of the Michaelis complex

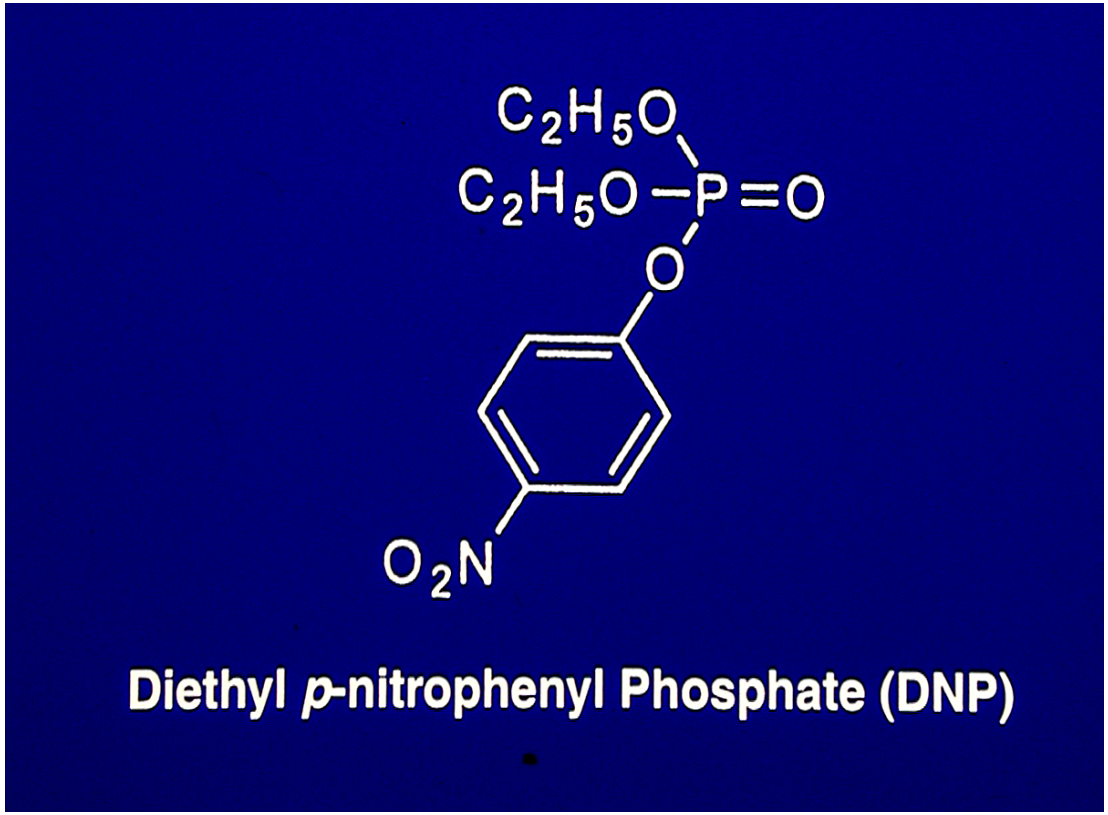

- DENP is a Transition state analogues
- DENP forms long lived Michaelis complex with TEP-I

Mechanism of DENP binding

- Tight binder
- Slow exchange

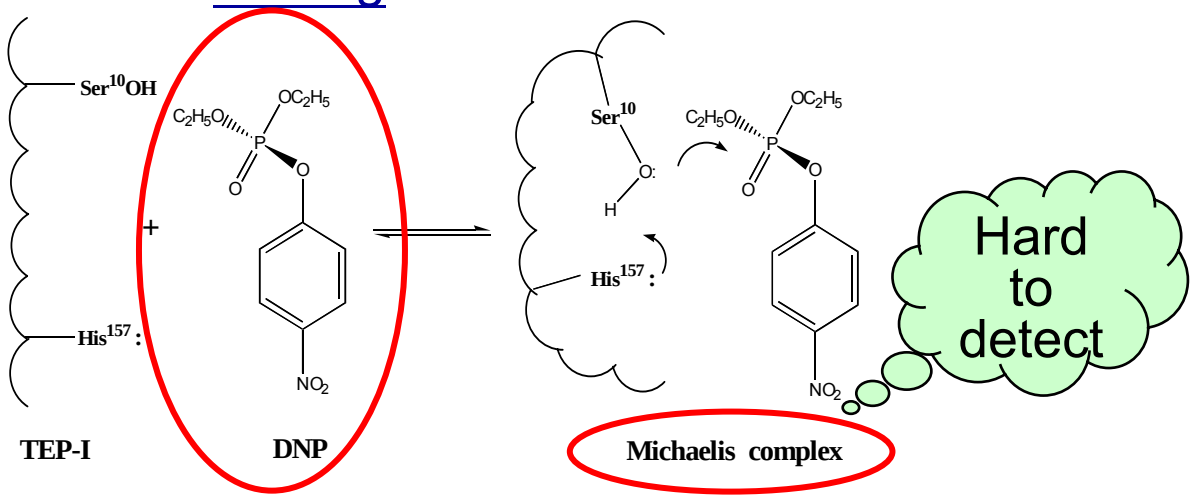

Structure of the Michaelis complex ?

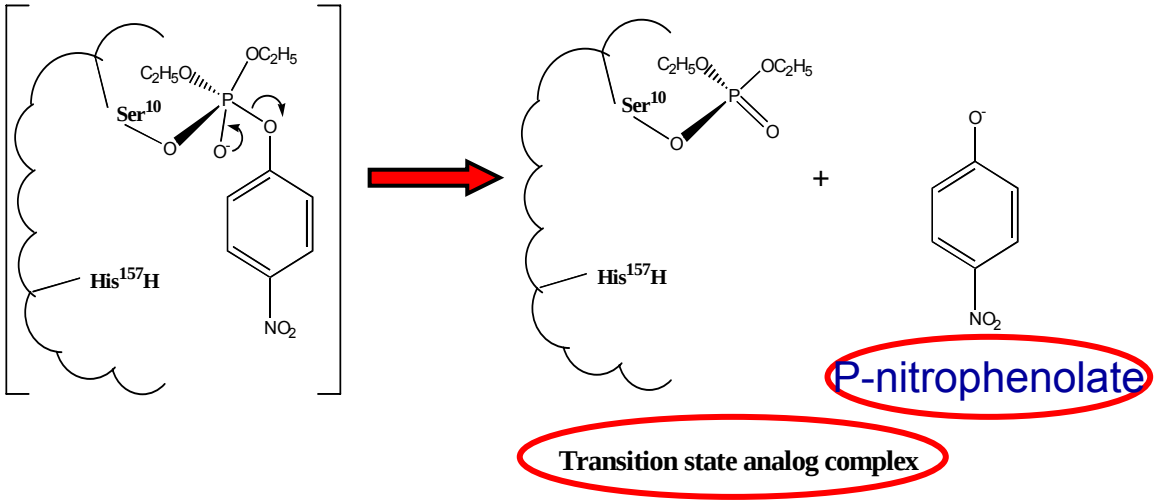

Use of chemical shift perturbation for characterizing ligand binding.

^{15}N-HSQC

Excellent dispersion & Detailed structural information

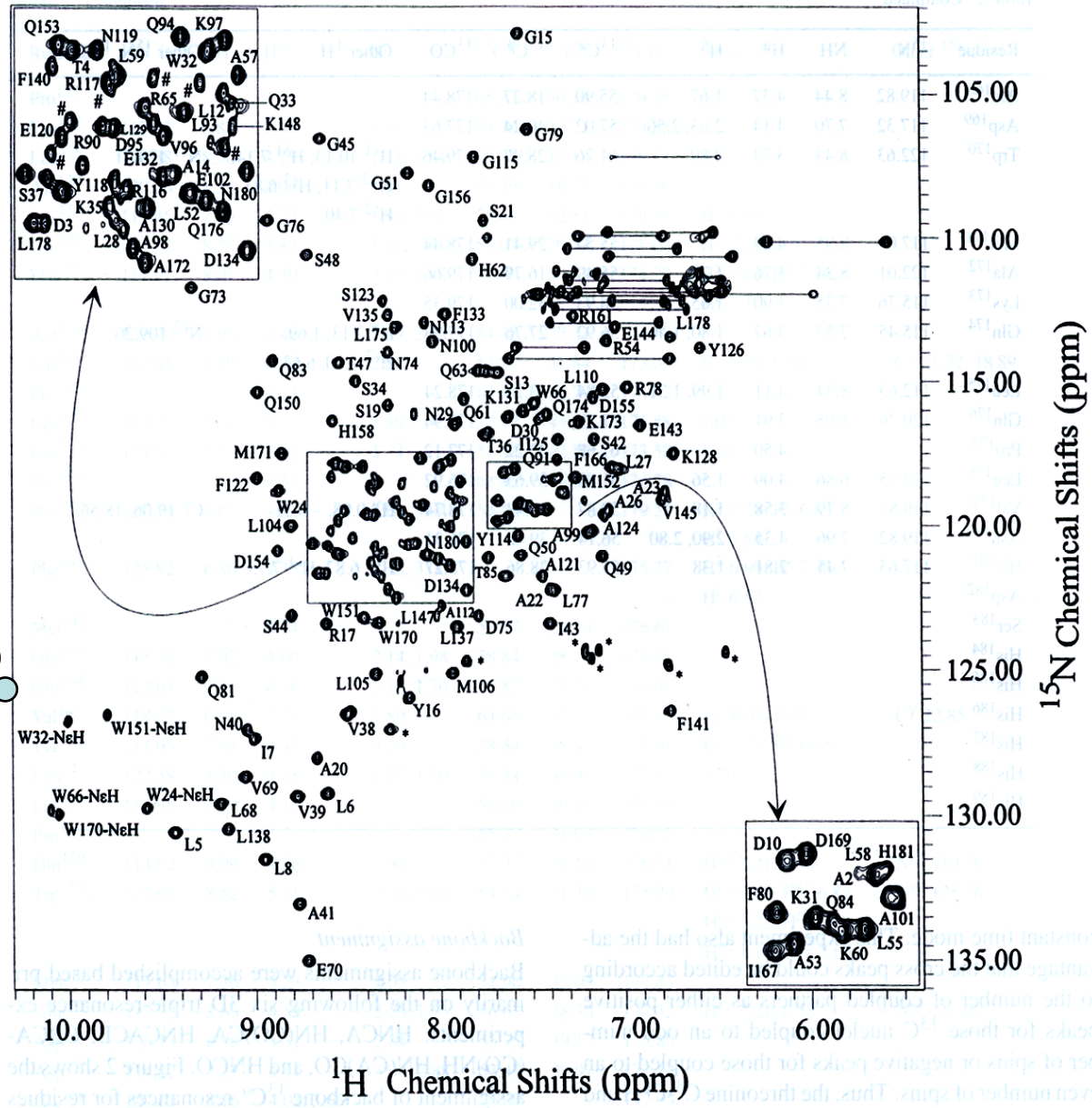

Superposition of two ^{15}N-HSQC spectra (pH 6.1, 2°C)

Blue: Pure TEP-I; Red: TEP-I/DNP complex

Two sets of spectra were observed in TEP-I/DNP complex

Individual species can be detected separately

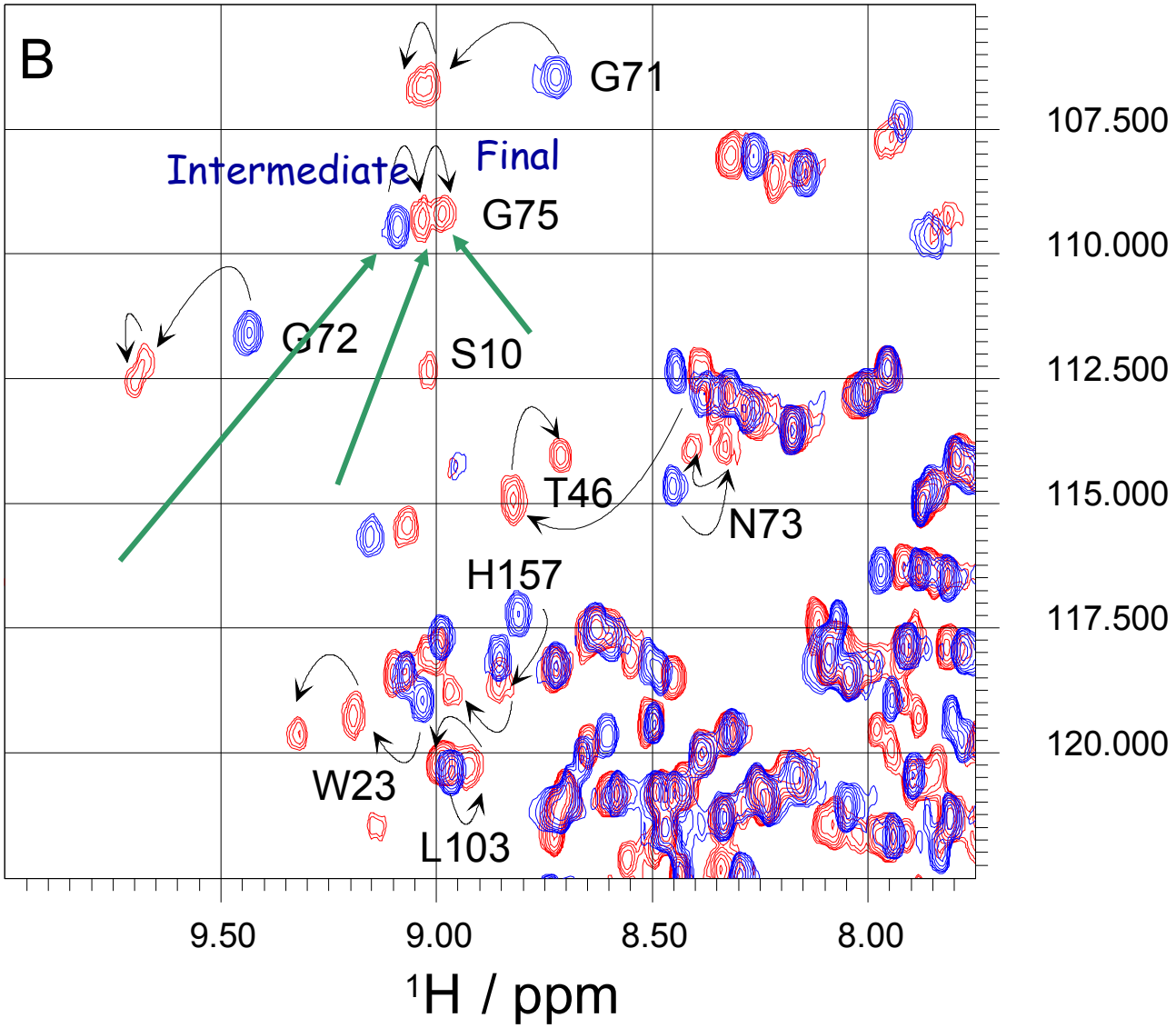

What are the identities of these species

- Free form: Free enzyme.
- Intermediate species: Michaelis complex.
- Final complex: Tetrahedral Adduct.

(u-^{15}N-Leu)-TEP-I

Blue: Free TEP-I
Red: Michaelis

Blue: Intermediate
Red: Final complex

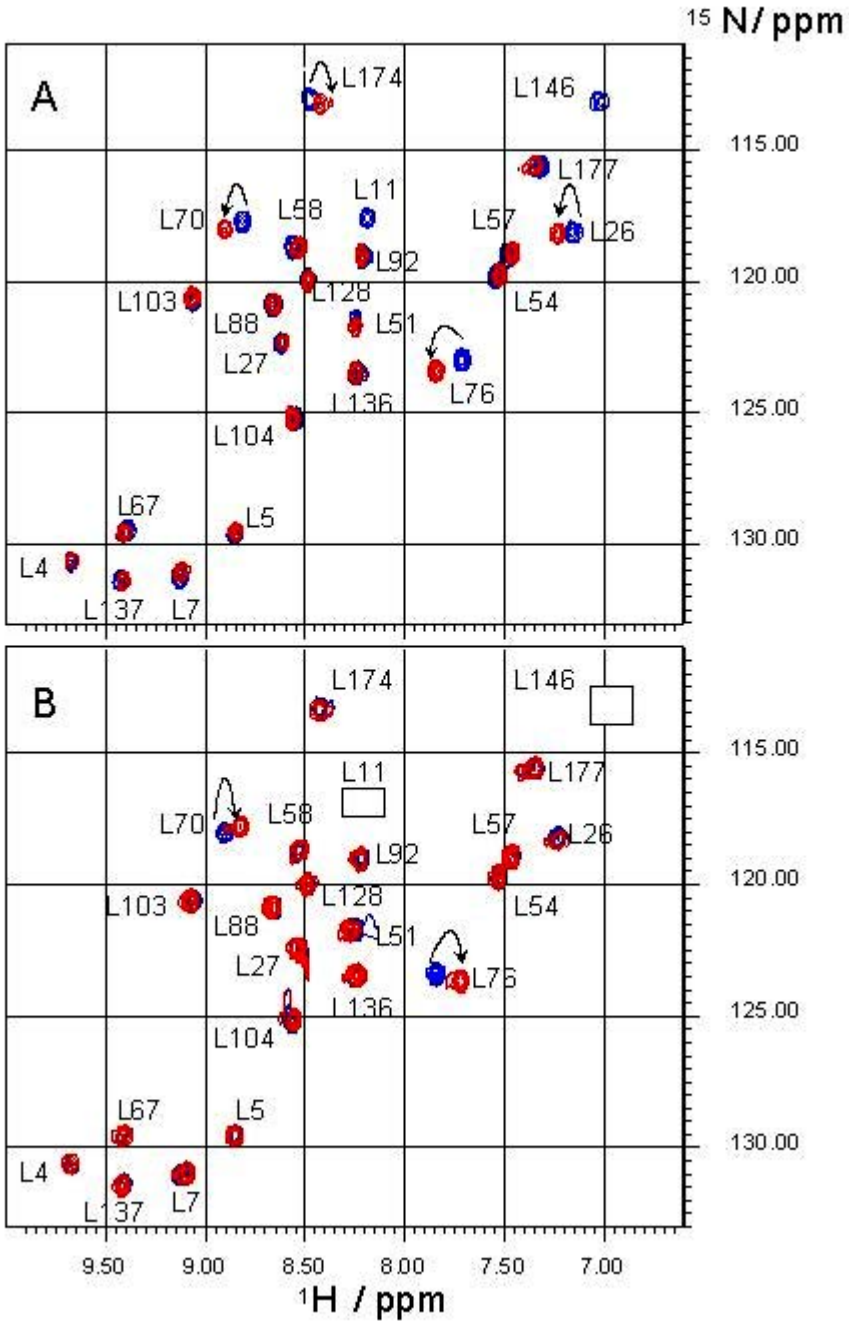

Chemical shift purturbatiopn: Free enzyme ➔ Michaelis complex

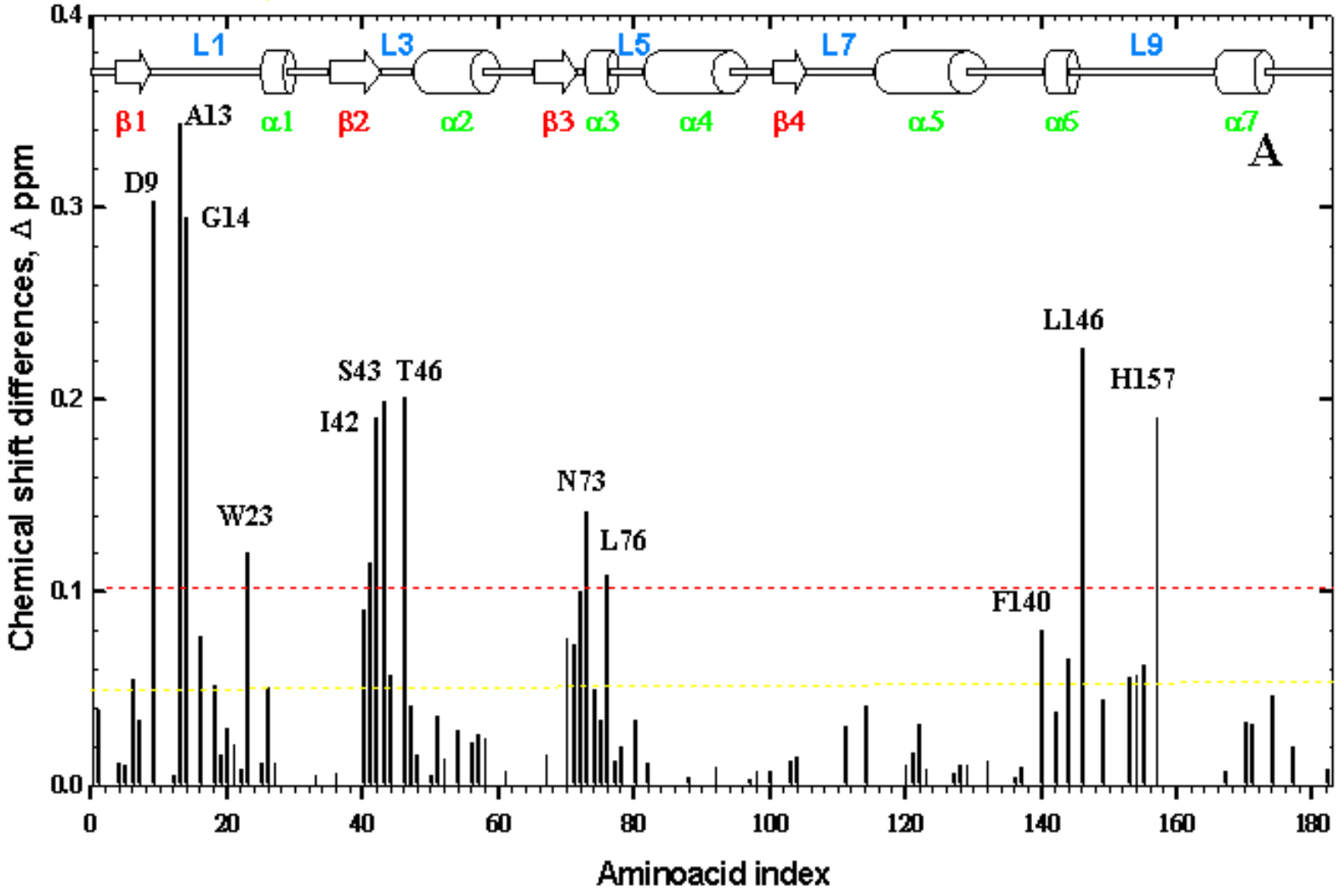

Michaelis complex ➔ Tetrahedral adduct

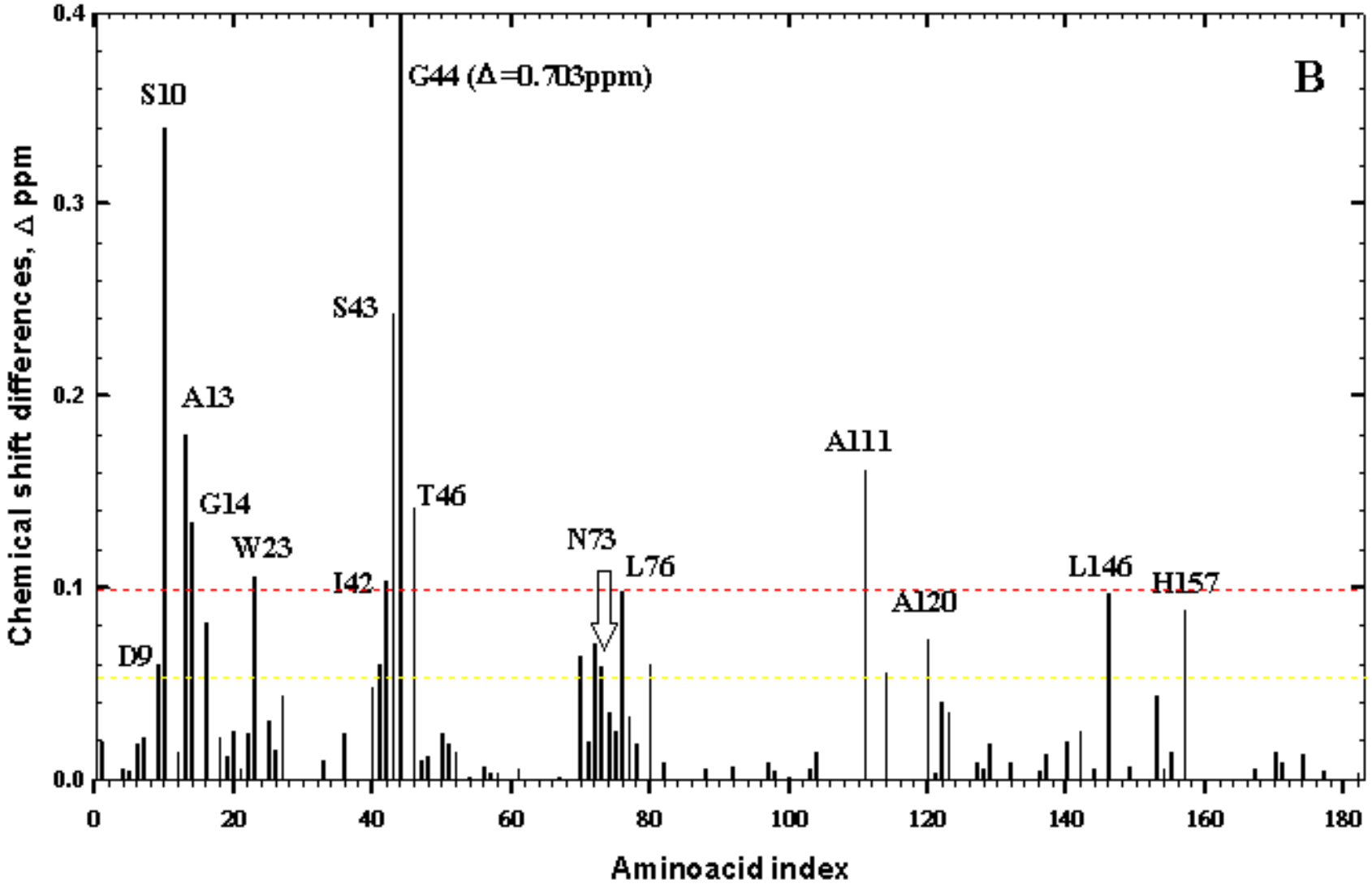

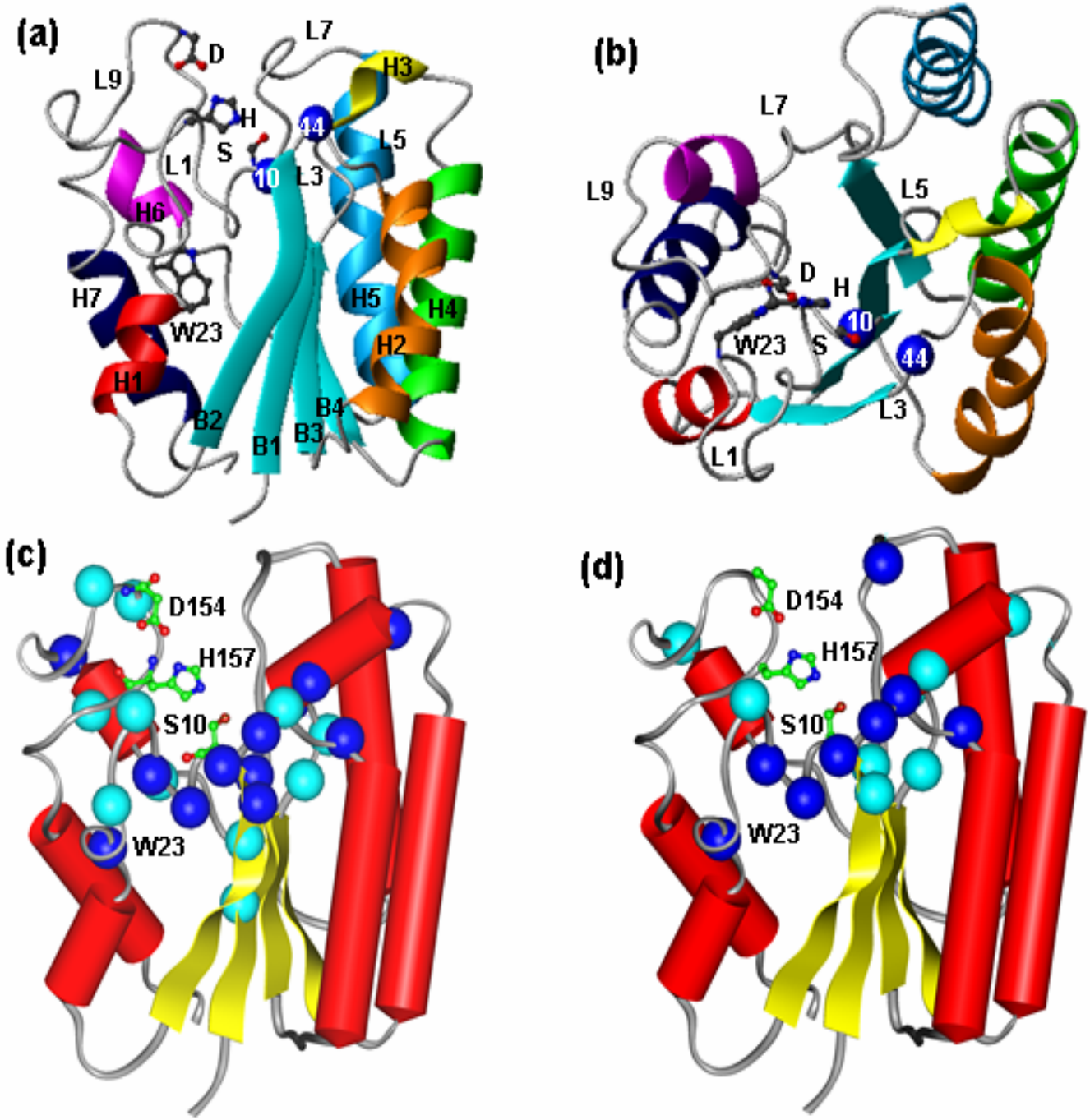
(a)
L7
D
L9
H3
H
44
S
L5
L1
10
L3
H6
H7
H5
H4
W23
H2
H1
B4
B2
B1
B3
(b)
L7
L9
L5
D
H
10
W23
S
44
L3
L1
(c)
D154
H157
S10
W23
(d)
D154
H157
S10
W23

Chemical shift purturbatiopn: Free enzyme ➔ Michaelis complex

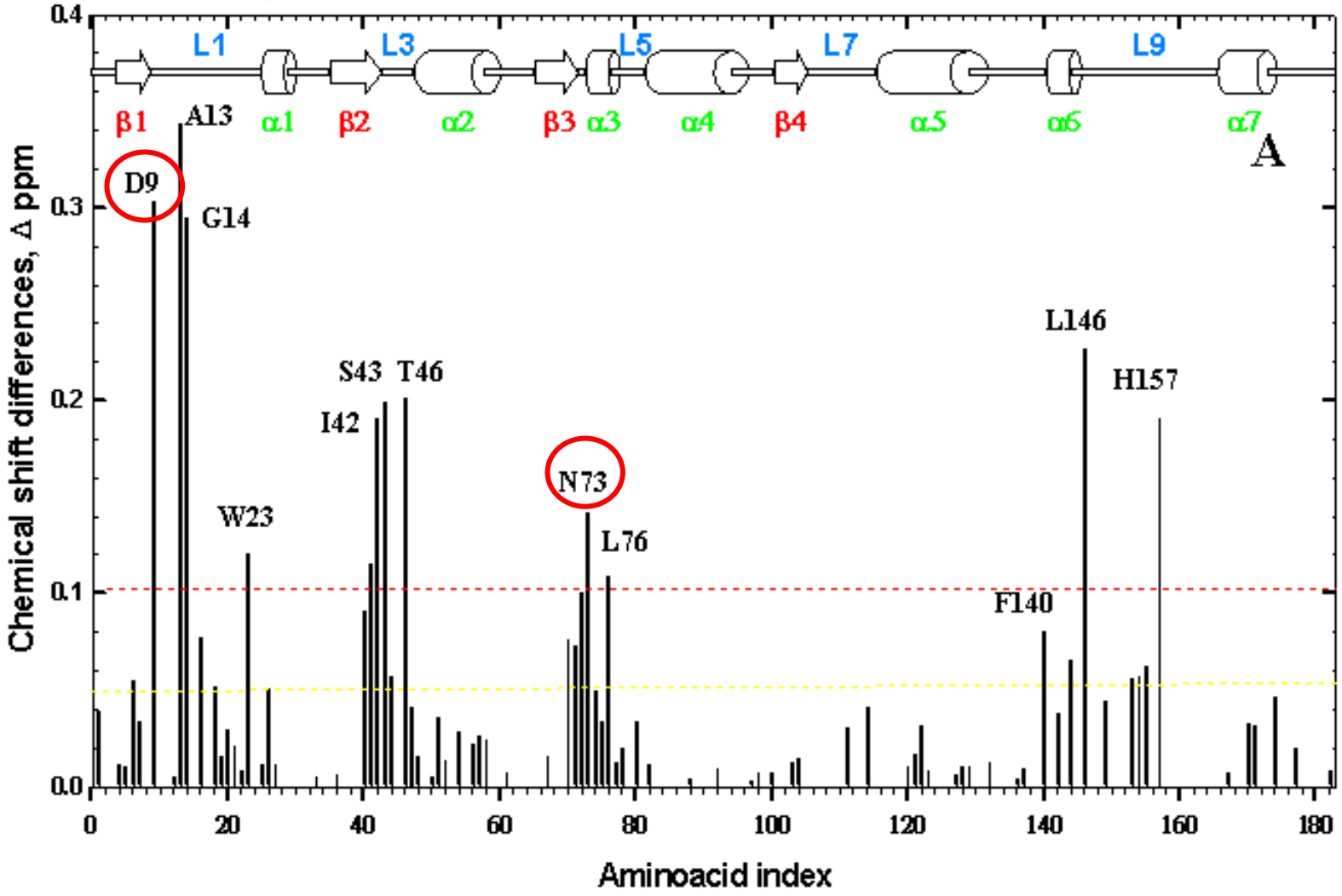

➔ Active site residues: S10, D154, & H157

Oxyanion holes: D9, G44 & N73

Michaelis complex ➔ Tetrahedral adduct

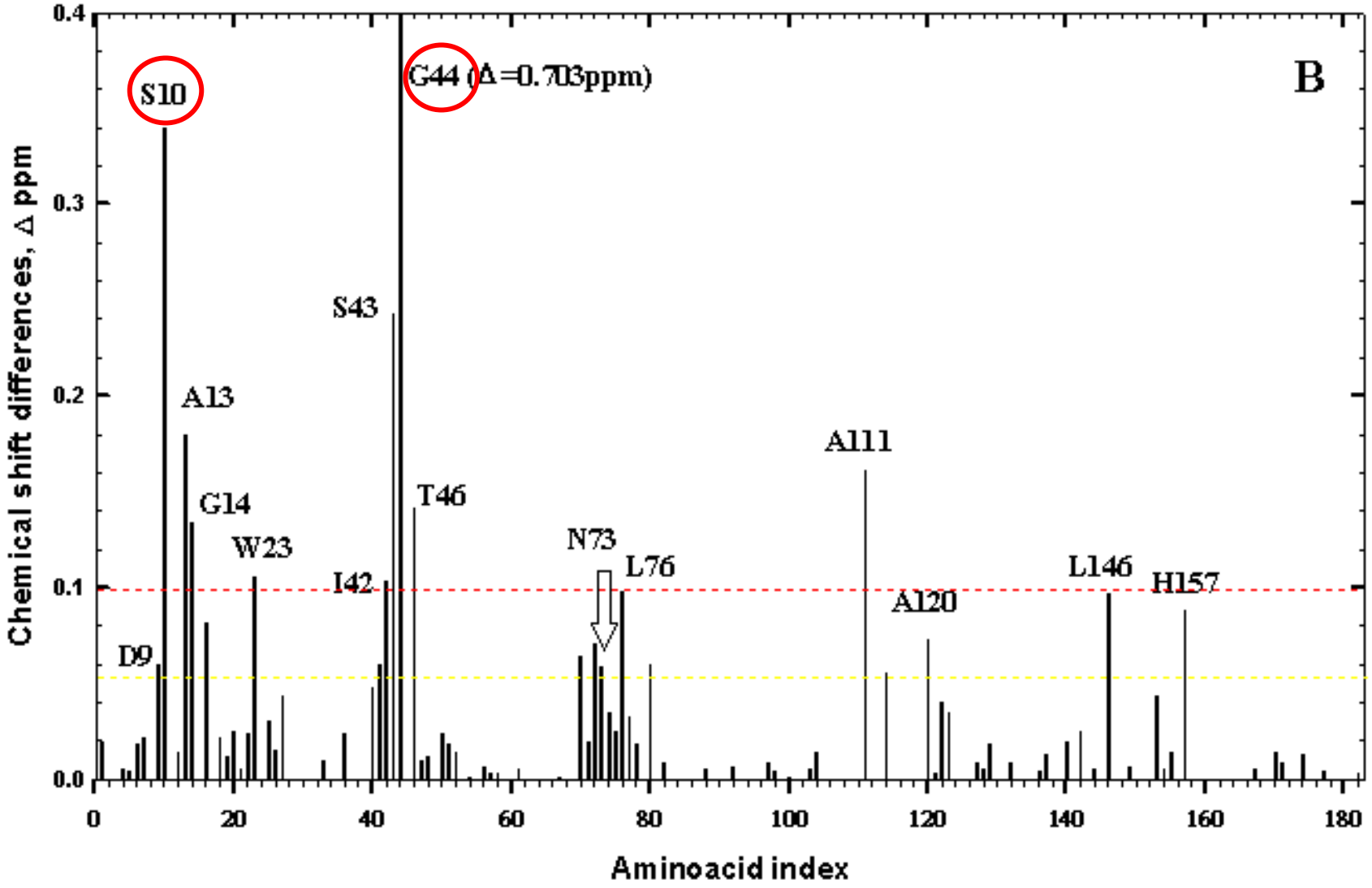

Sequential Binding of DNP to the oxyanion holes

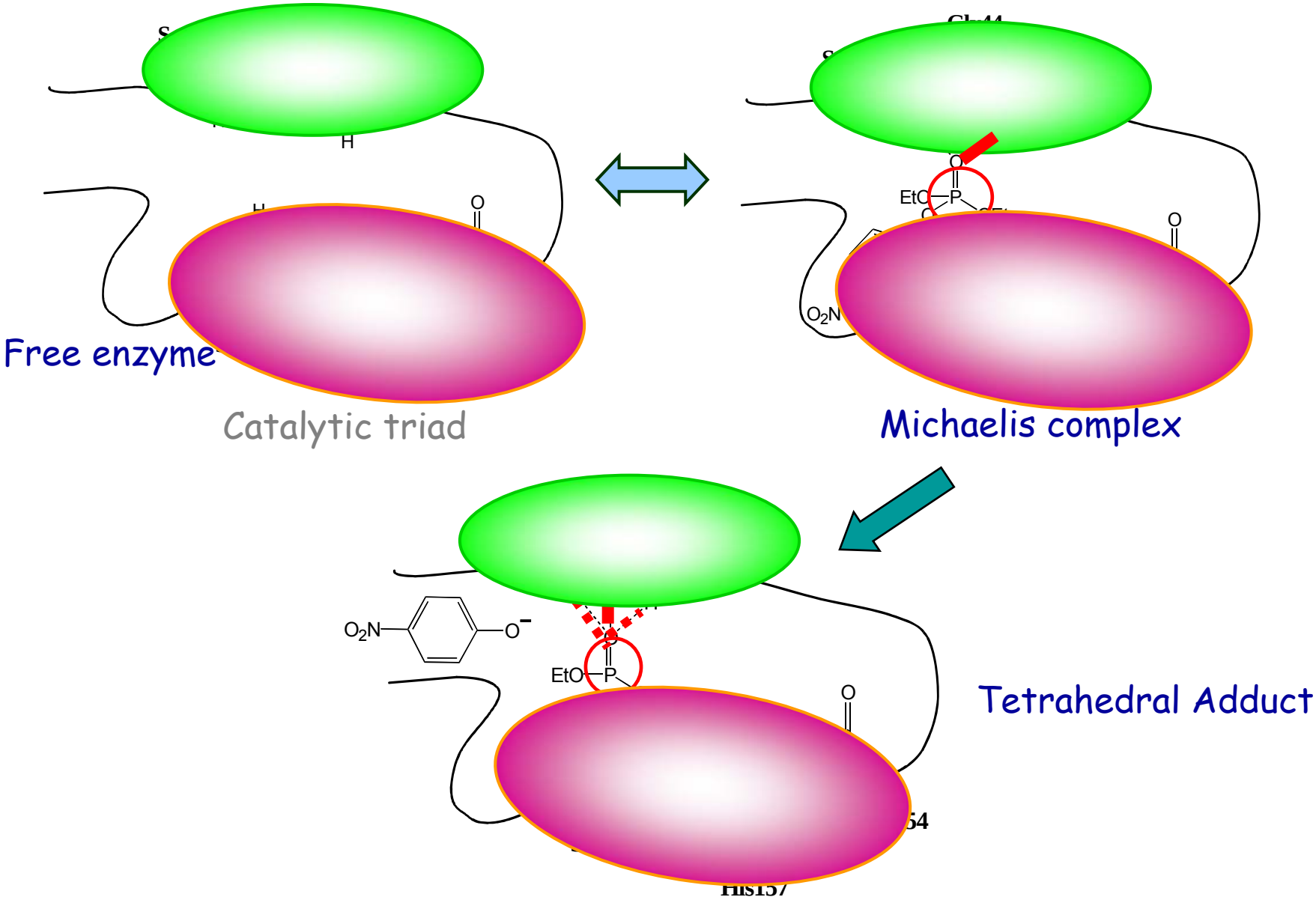

III. Dynamics - 4-dimensional structure

- Many biological functions of proteins can not be explained by static structure.

- Determine ^{15}N-T_1, ^{15}N-T_2, (^1H-^{15}N)NOE of (u-^{15}N)TEP-I at 500 and 600 MHz.

- Data were analyzed by Modelfree approach, assuming axially symmetric anisotropic diffusion tensor to extract:
  - Order parameters (ΔS^2);
  - Conformational exchange rates (R_{ex}); and
  - Rotational correlation time (τ) etc

NMR Relaxation

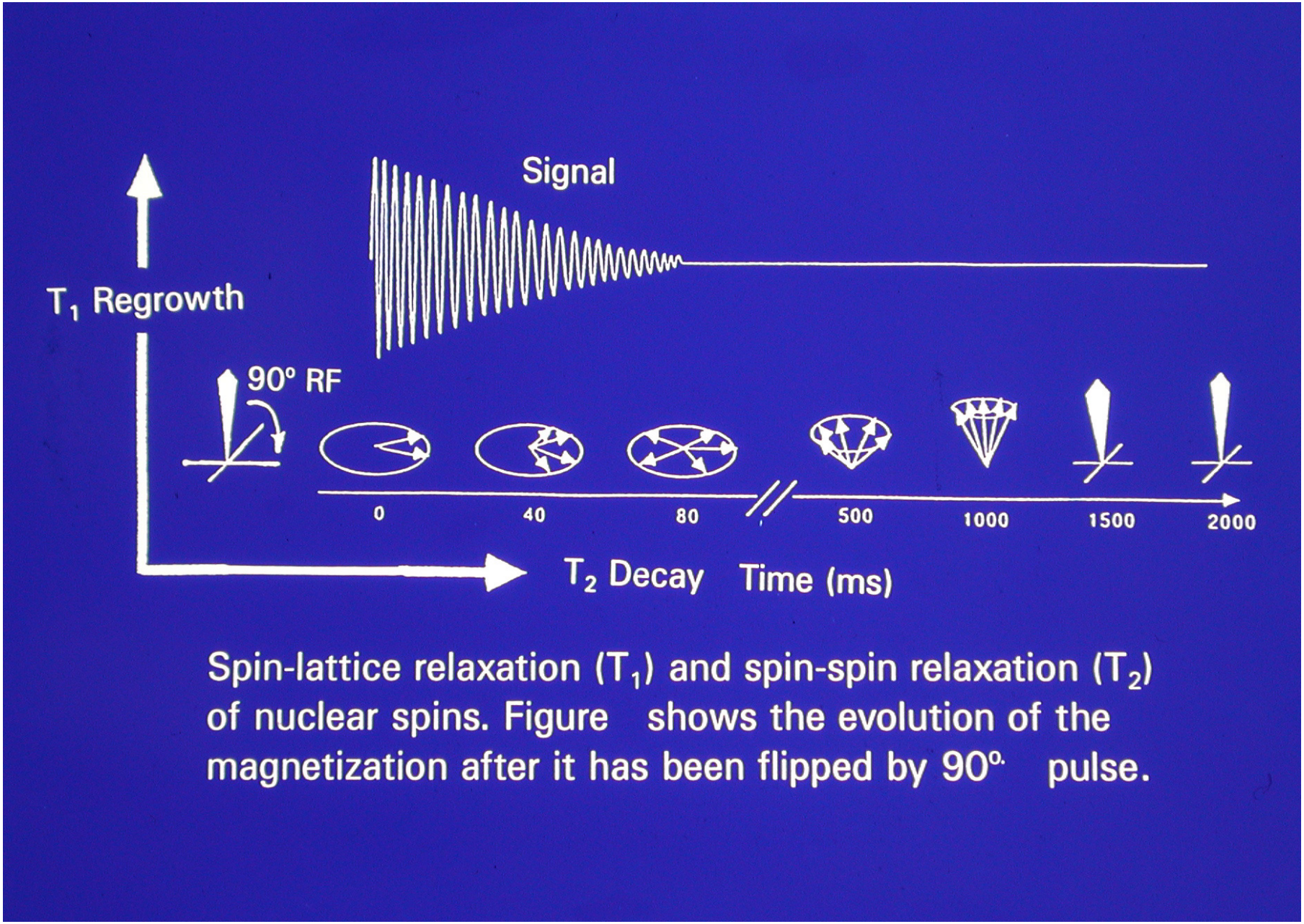

Spin-lattice relaxation (T_1) and spin-spin relaxation (T_2) of nuclear spins. Figure shows the evolution of the magnetization after it has been flipped by 90°. pulse.

Nuclear Overhauser Effect (NOE)
(Energy transfer through dipolar effect)

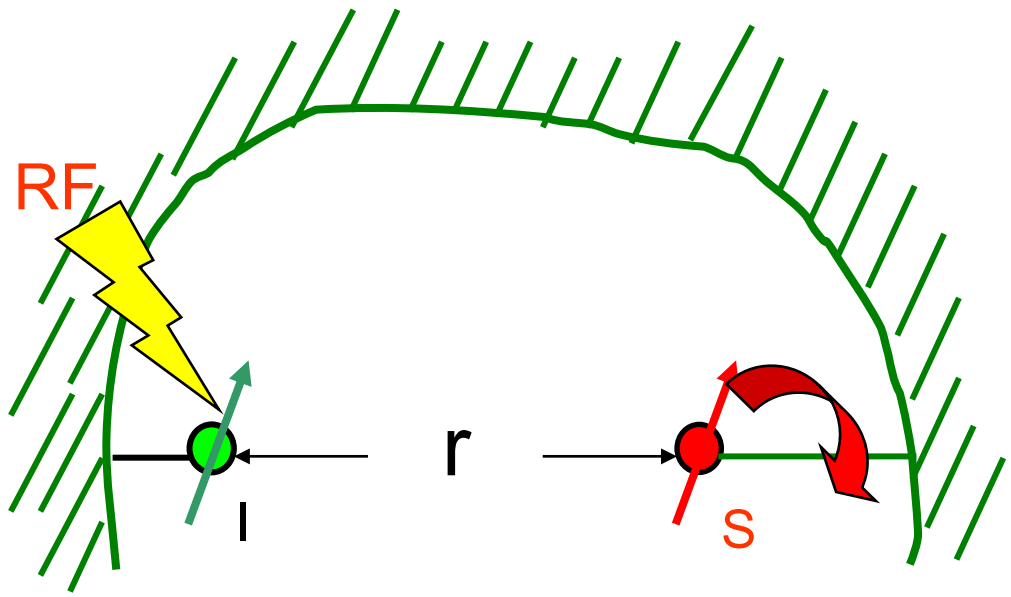

$$XNOE = 1 + (d^2/4)(\gamma_H/\gamma_N)[6J(\omega_H + \omega_N) - J(\omega_H - \omega_N)]T_1$$

where $d = (\mu_o h \gamma_N \gamma_H / 8\pi^2)(r_{NH}^{-3})$,

Relaxation Mechanism

Dominated by dipolar and chemical shift anisotropic interactions, and are related to the spectral density functions, $J(\omega)$, by :

$$1/T_1 = (d^2/4)[J(\omega_H - \omega_N) + 3J(\omega_N) + 6J(\omega_H + \omega_N)] + c^2 J(\omega_N) \text{ -------} \quad (1)$$

$$1/T_2 = (d^2/8)[4J(0) + J(\omega_H - \omega_N) + 3J(\omega_N) + 6J(\omega_H) + 6J(\omega_H + \omega_N)] + (c^2/6)[4J(0) + 3J(\omega_N)] + R_{ex} \text{ ----------} \quad (2)$$

$$NOE = 1 + (d^2/4)(\gamma_H/\gamma_N)[6J(\omega_H + \omega_N) - J(\omega_H - \omega_N)]\, T_1 \text{ ----------} \quad (3)$$

where $d = (\mu_o h \gamma_N \gamma_H / 8\pi^2)(r_{NH}^{-3})$, (Dipolar term) & $c = \omega_N(\sigma_{\parallel} - \sigma_{\perp})/\sqrt{3}$. (Chemical shift term)

μ_o : permeability constant of free space;
γ_i : magnetogyric ratio of spin i;
r_{NH} = 1.02 Å: N-H bond length;
$\sigma_{\parallel} - \sigma_{\perp}$ = -170 ppm (^{15}NH CSA tensor).
h: Planck constant;
ω_i: Larmor frequency of spin i;
R_{ex}: exchange rate;

J(ω) and molecular motion - Modelfree analysis

For a rigid macromolecule undergoing Brownian motion with a rotational correlation time τ_m and local internal motion with rotational correlation time τ_s the spectral density function, $J(\omega)$ can be expressed as:

$$J(\omega) = \frac{2}{5}\left[\frac{S^2\tau_m}{1+(\omega\tau_m)^2} + \frac{(1-S_f^2)\tau'_f}{1+(\omega\tau'_f)^2} + \frac{(S_f^2-S^2)\tau'_s}{1+(\omega\tau'_s)^2}\right]$$

S^2 : Order parameters (Magnitude of motion)

τ's : Correlation times (Speed of motion)

R_{ex} : Chemical exchange rate (Slow motion in ms or μs regime)

→ Fitting T_1, T_2 and NOE data to determine S^2, τ and R_{ex}

Dynamics

1. Measured T_1, T_2 and (^1H, ^{15}N) NOE at 500 and 600 MHz at 310 K.

2. Total of 128 resonances were measured at 500 MHz and 134 resonances were determined at 600 MHz.

3. Average:

   R_1 = 1.108 $\pm$ 0.056 S-1 (1.506 $\pm$ 0.096 S-1),

   R_2 = 10.31 $\pm$ 1.40 S-1(9.236 $\pm$ 1.17 S-1)

   XNOE = 0.742 $\pm$ 0.044 (0.705 $\pm$ 0.039) at 14.09 T (11.74 T).

Relaxation Data

Obtained in two fields:

- ○ : 500 MHz
- ● : 600 MHz

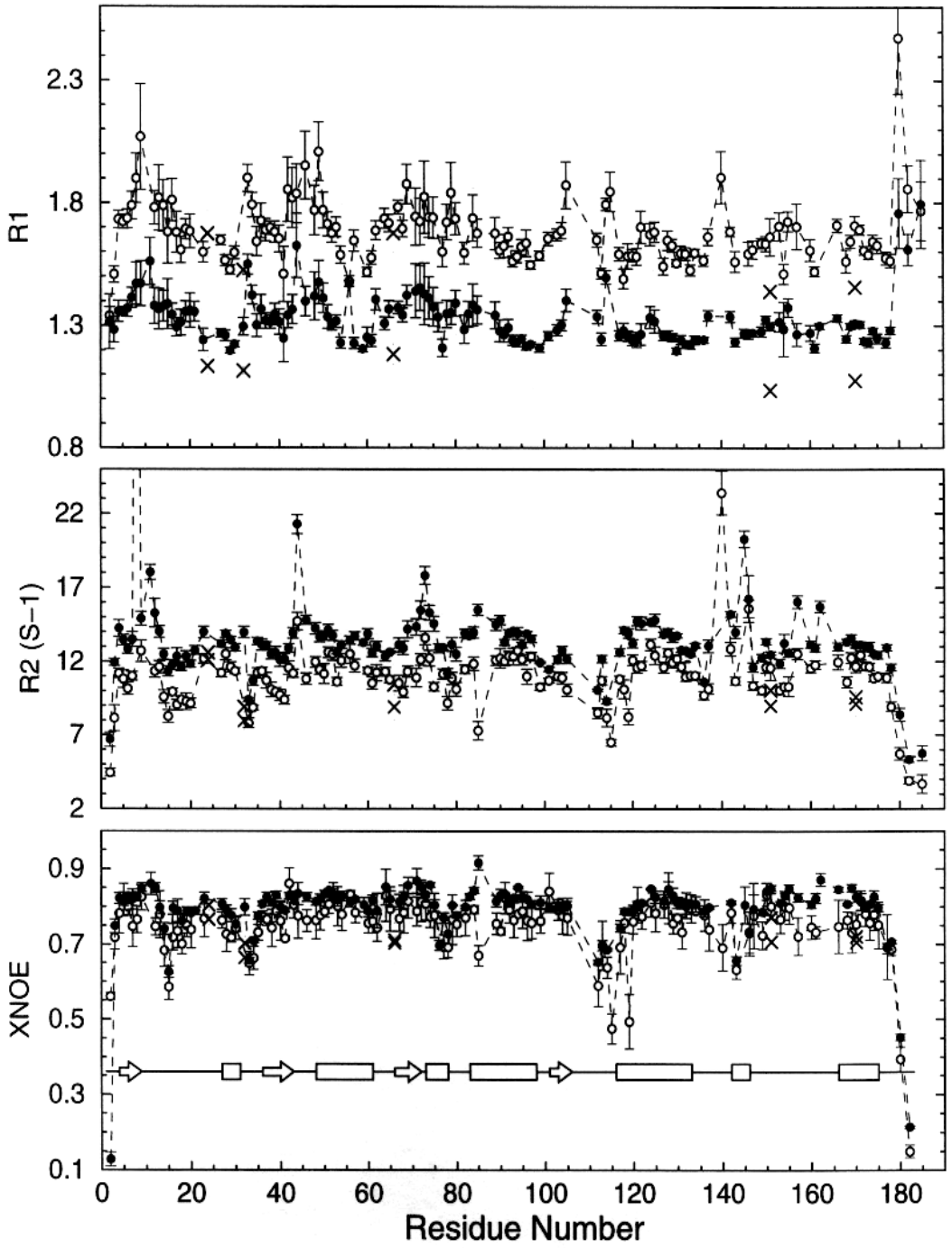

Order parameter – Flexibility

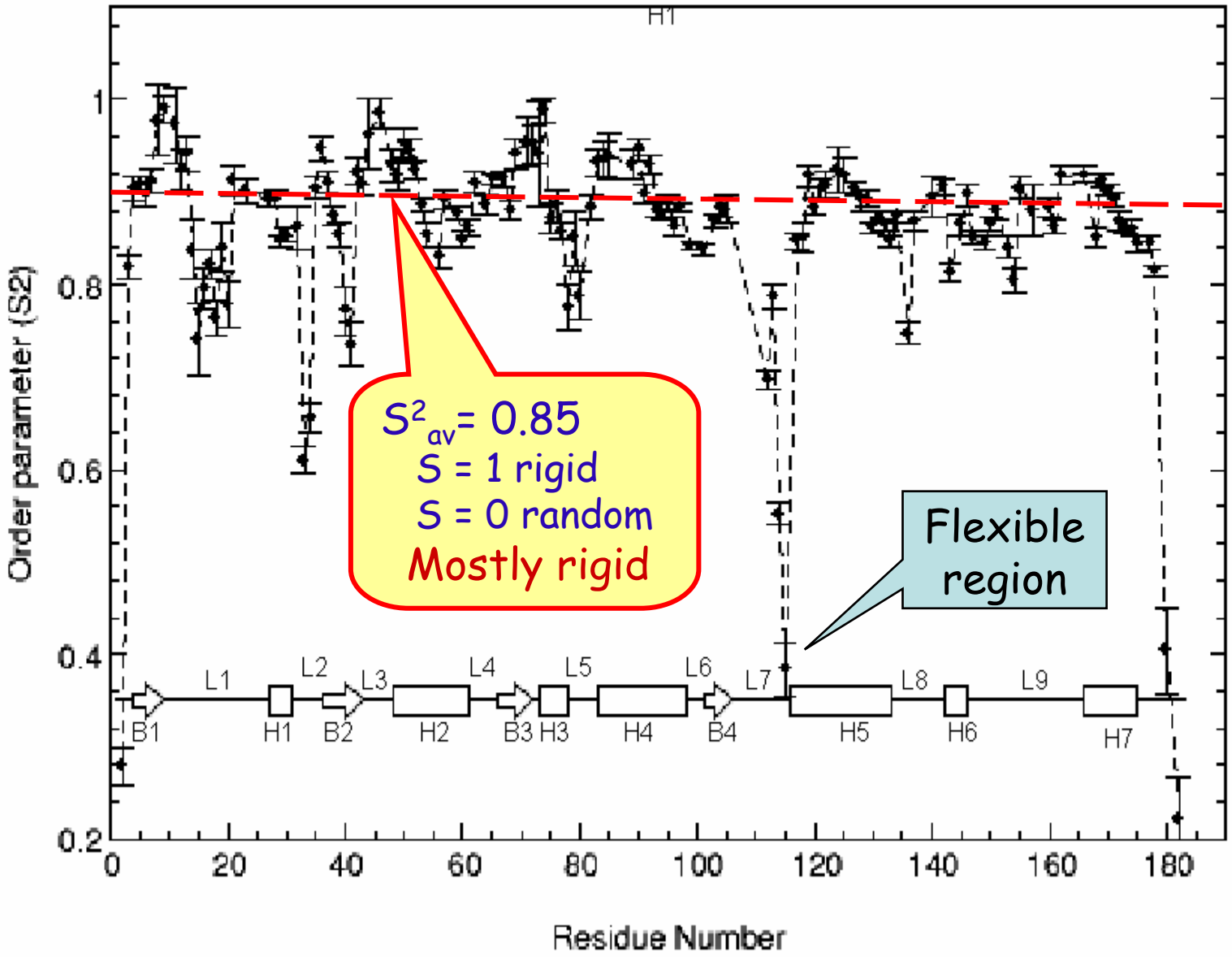

Exchange rate – Residues with low motion

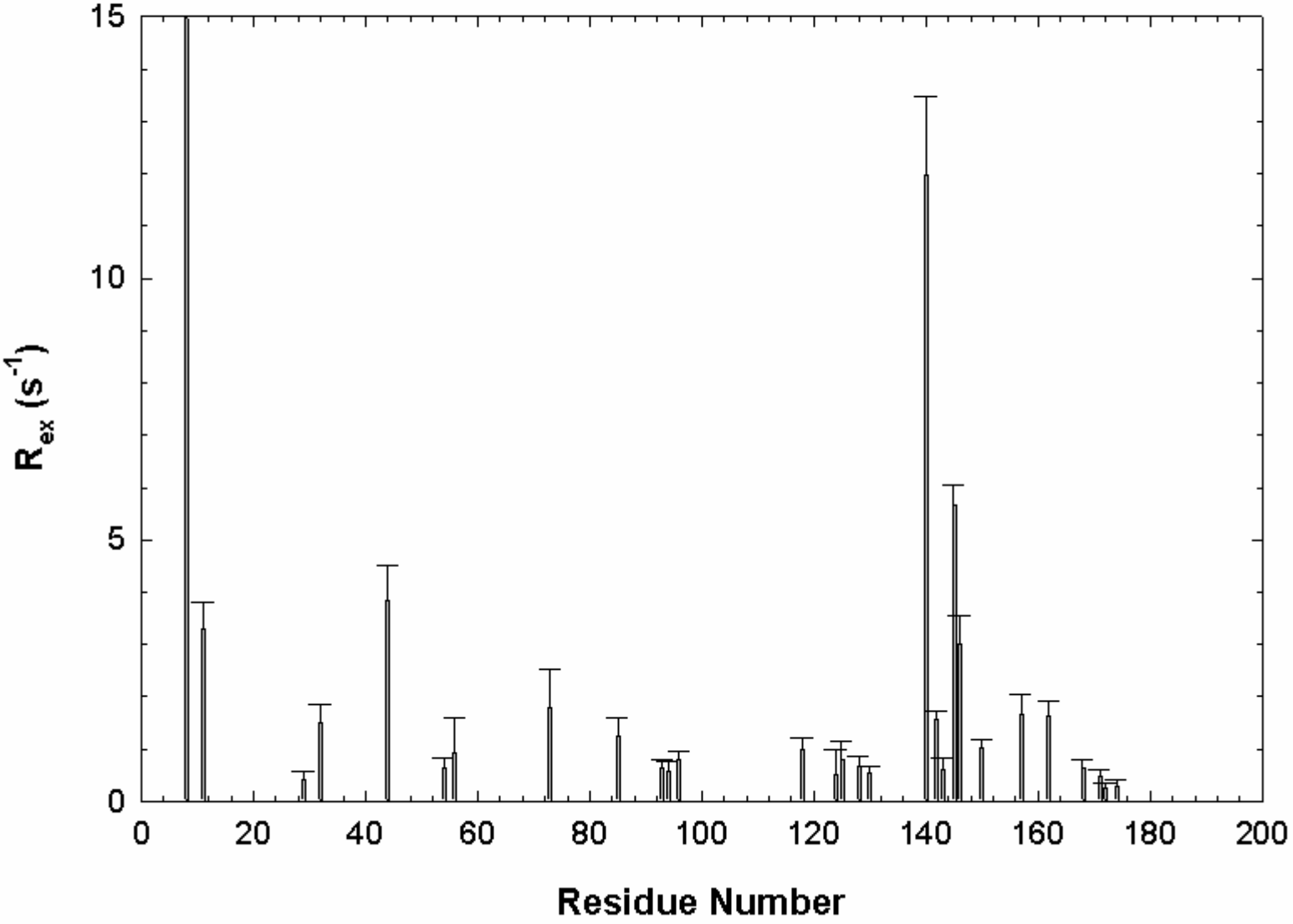

Sausage representation of the backbone structure of TEP-I

(a) Order parameter:

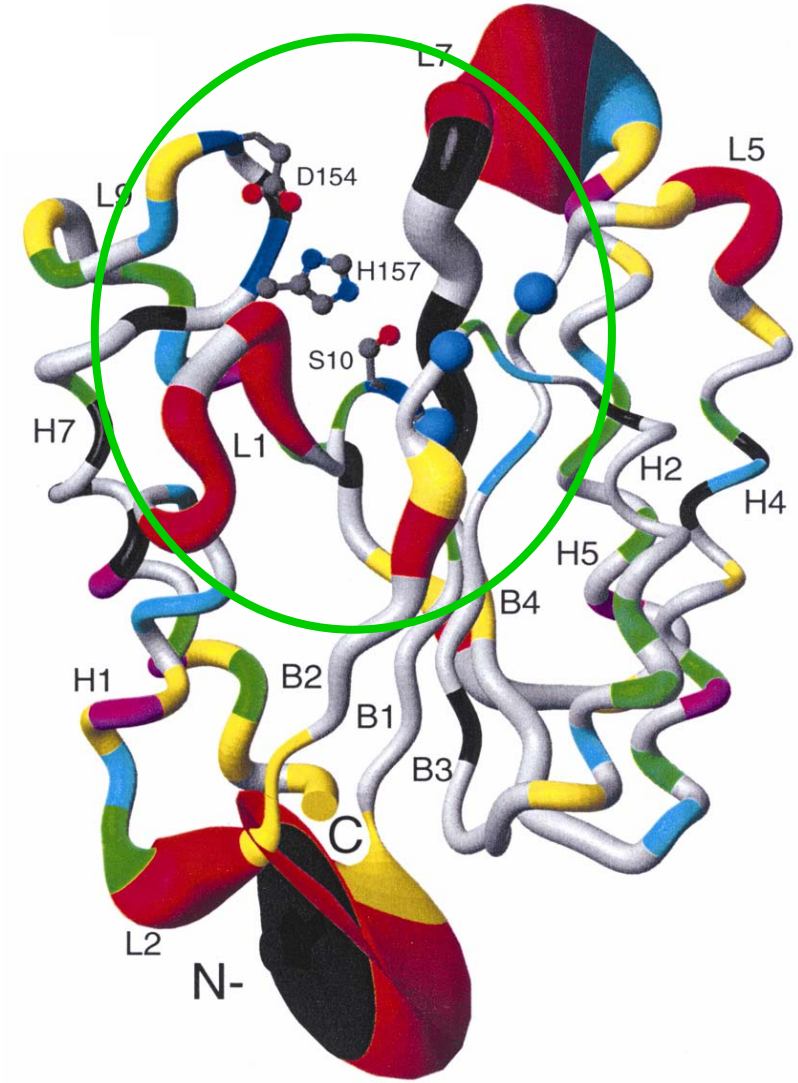

(b) Exchange rate :

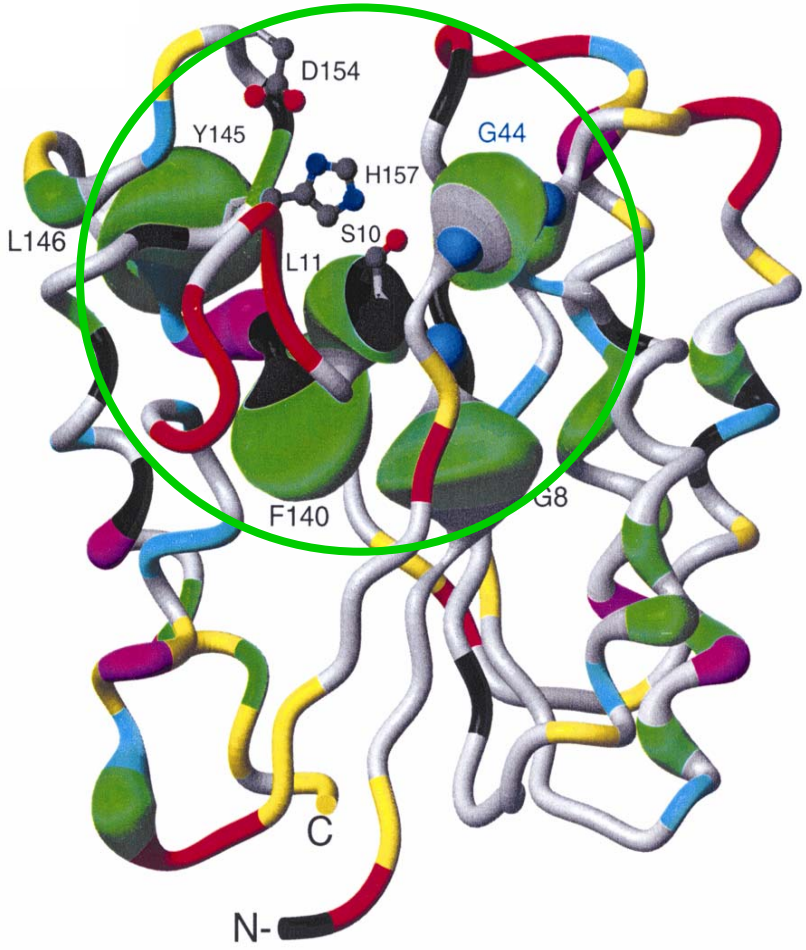

Acknowledgements

Structure: 陳金榜　林達顯　黃耀德　Vitaly Gorbatyu

Dynamics: 黃耀德，周靜瑜

DENP binding & H-bond: Serge Tyukhtenko　Sacha Livinchuk

Material: 蕭介夫　李雅玲 etc
Oksana Gorbatyuk

Technical Support: 張七鳳

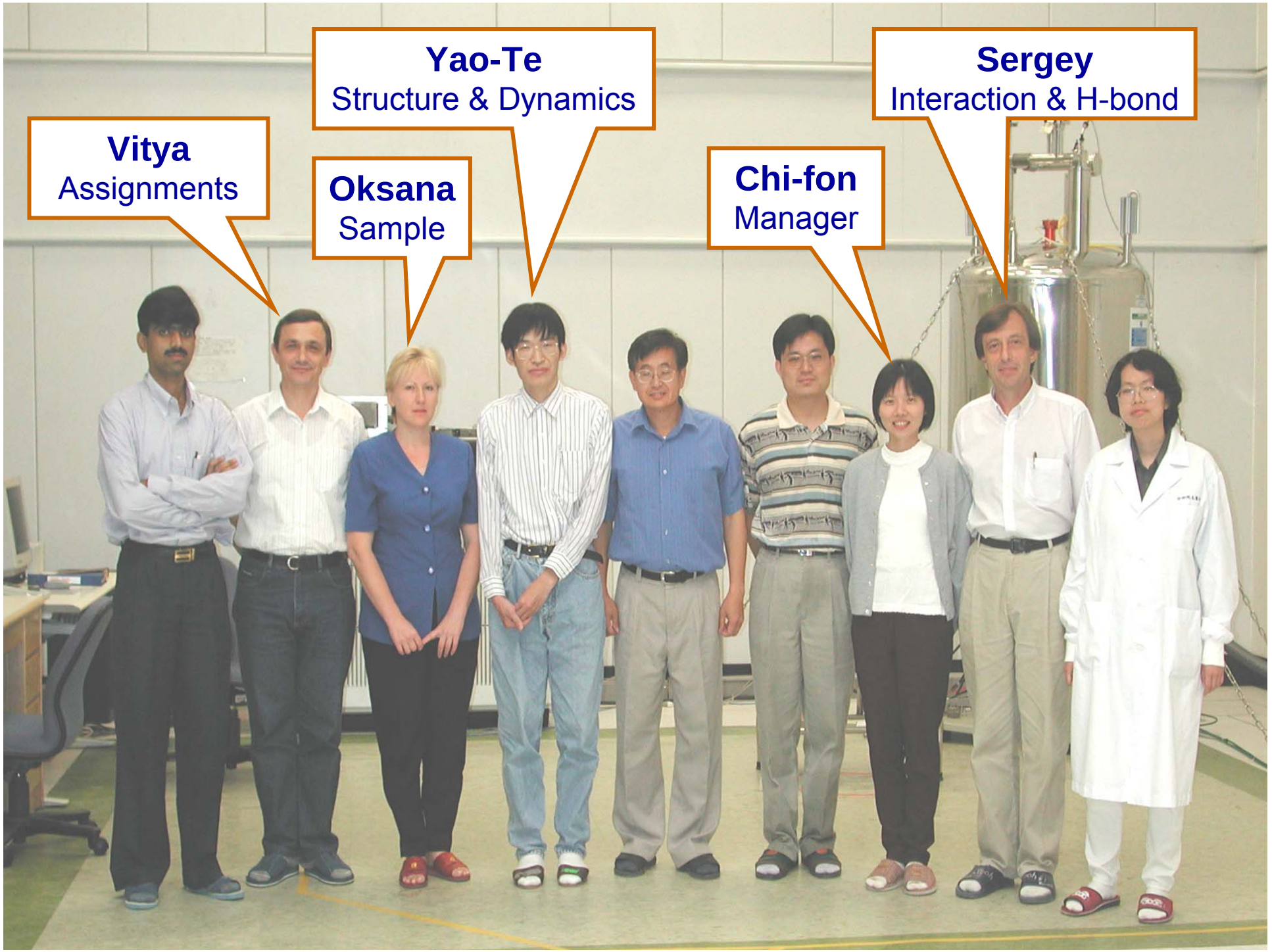
Vitya
Assignments
Oksana
Sample
Yao-Te
Structure & Dynamics
Chi-fon
Manager
Sergey
Interaction & H-bond

The joy of Surprises – The case of a Heparin-Binding Human Hepatoma-Derived Growth Factor

Tai-huang Huang
Institute of Biomedical Sciences
Academia Sinica
Taiwan, R.O.C.

ICMRBS, Hyderabad, India
January 18, 2005

Human Hepatoma-derived Growth Factor (hHDGF)

- First isolated from human hepatoma-derived Huh7 cells.
- Mitogenic activities toward various cell lines, including fibroblasts, endothelial cells and smooth muscle cells.
- Stimulates DNA synthesis in Swiss 3T3 cells and promote proliferation of renal epithelial cells, smooth muscle cells, and fetal hepatocytes.
- Involved in the development of vascular tissue, kidney and liver, and in lung remodeling after injury. ➔ Treatment of restenosis.
- The first member of a new family of heparin binding growth factors of important functions.

Properties of HRPs

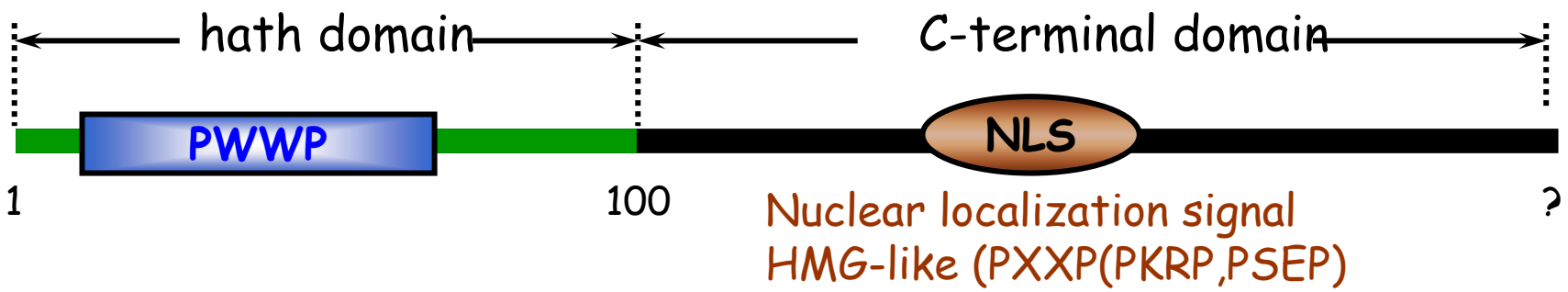

- All contain highly homologous N-terminal "HATH" (Homology to the Hmino Terminal of HHDGF) domain (100 a.a.) and varied C-terminal domains.
- The conserved "HATH" domain causes protein internalization.
- The non-conserved C-terminal alone is capable of stimulating DNA synthesis but "HATH" domain alone can not.
- The HATH domain contains a PWWP motif implicated in protein-protein interactions.
- HRPs bind to heparin

Outline

1. Structure of hHDGF
2. hHDGF-heparin interaction.
3. Heparin-binding and internalization
4. HATH-forms a dimer.
5. Model of HATH-dimer structure.

Structure of hHDGF (240 a.a.)

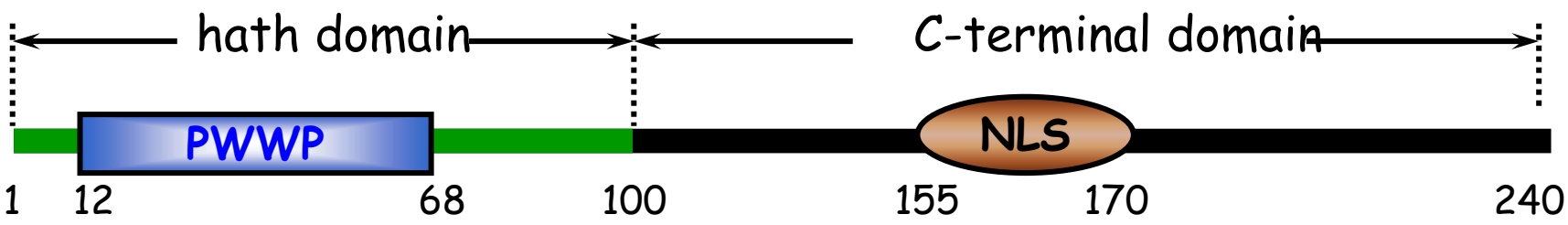

^{15}N-HSQC spectrum

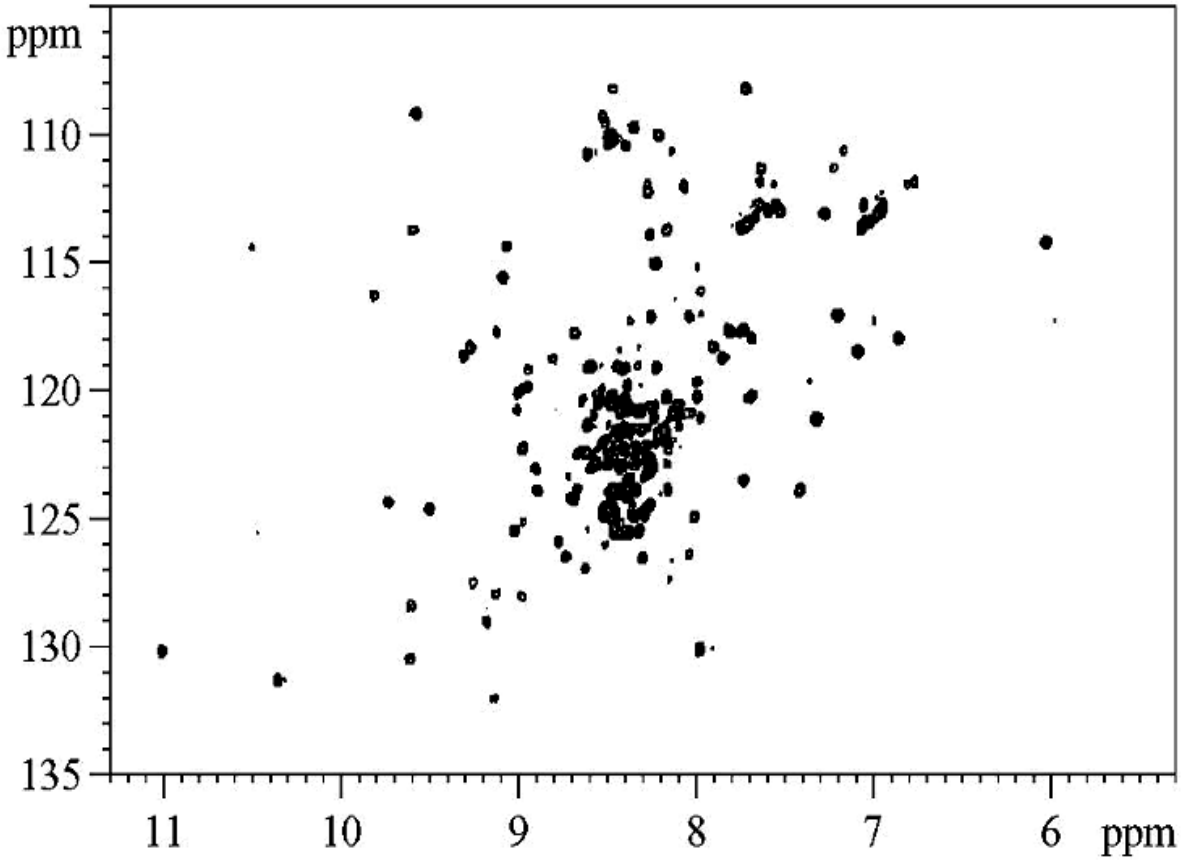

Organization of hHDGF (240 a.a.)

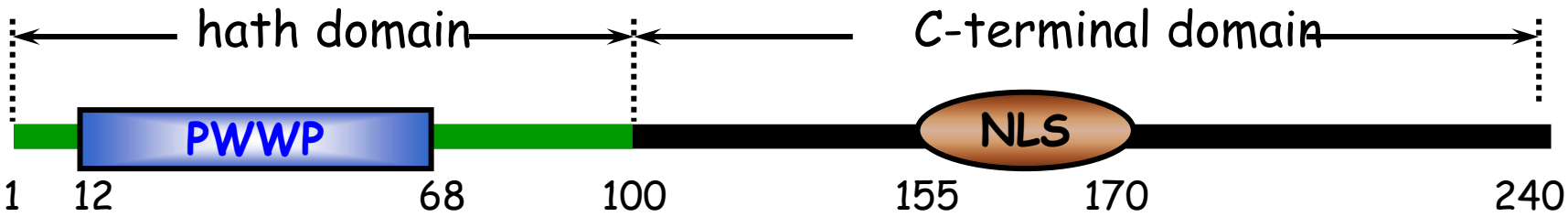

Divide and conquer

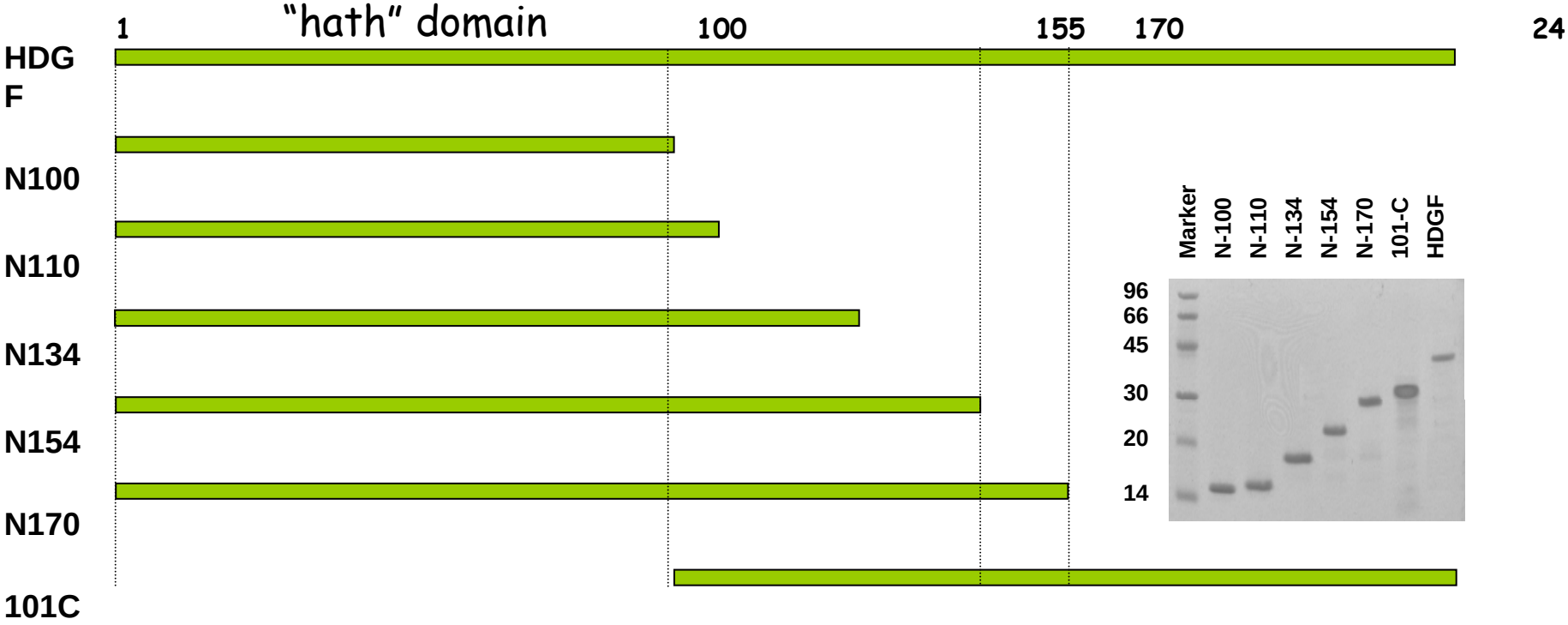

Full length

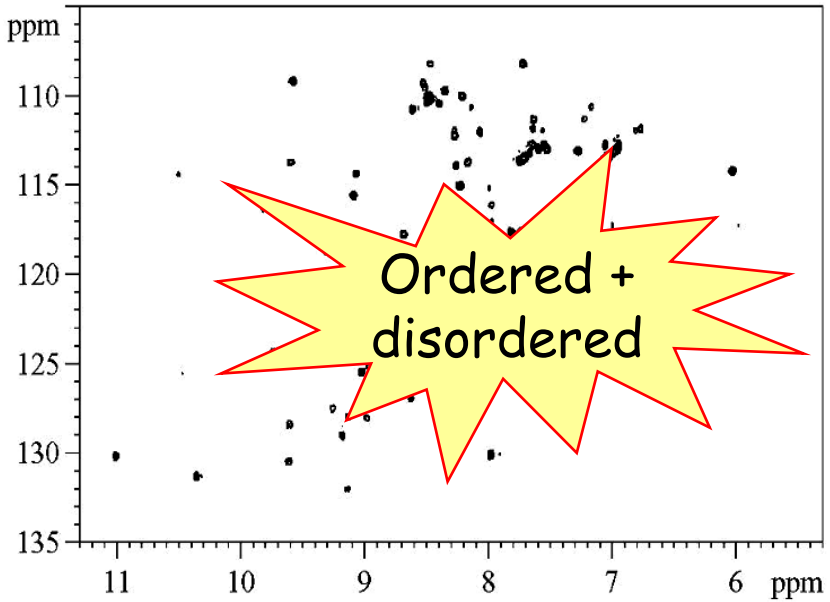

N-terminal 1-100 (Hath)

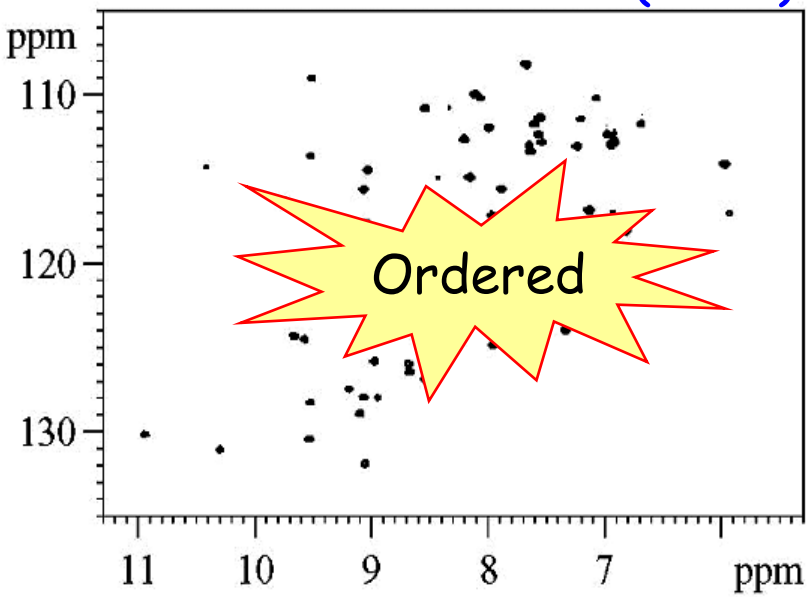

+

C-terminal (101-240)

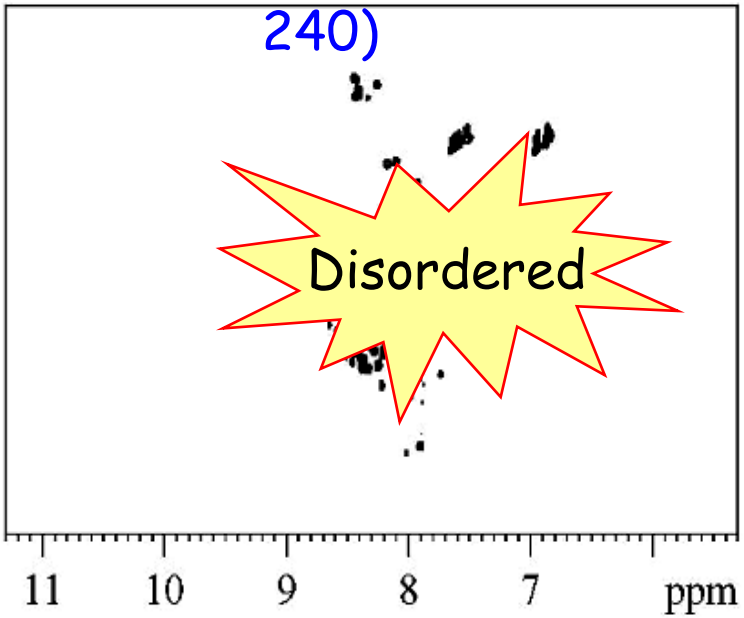

Structure hHDGF

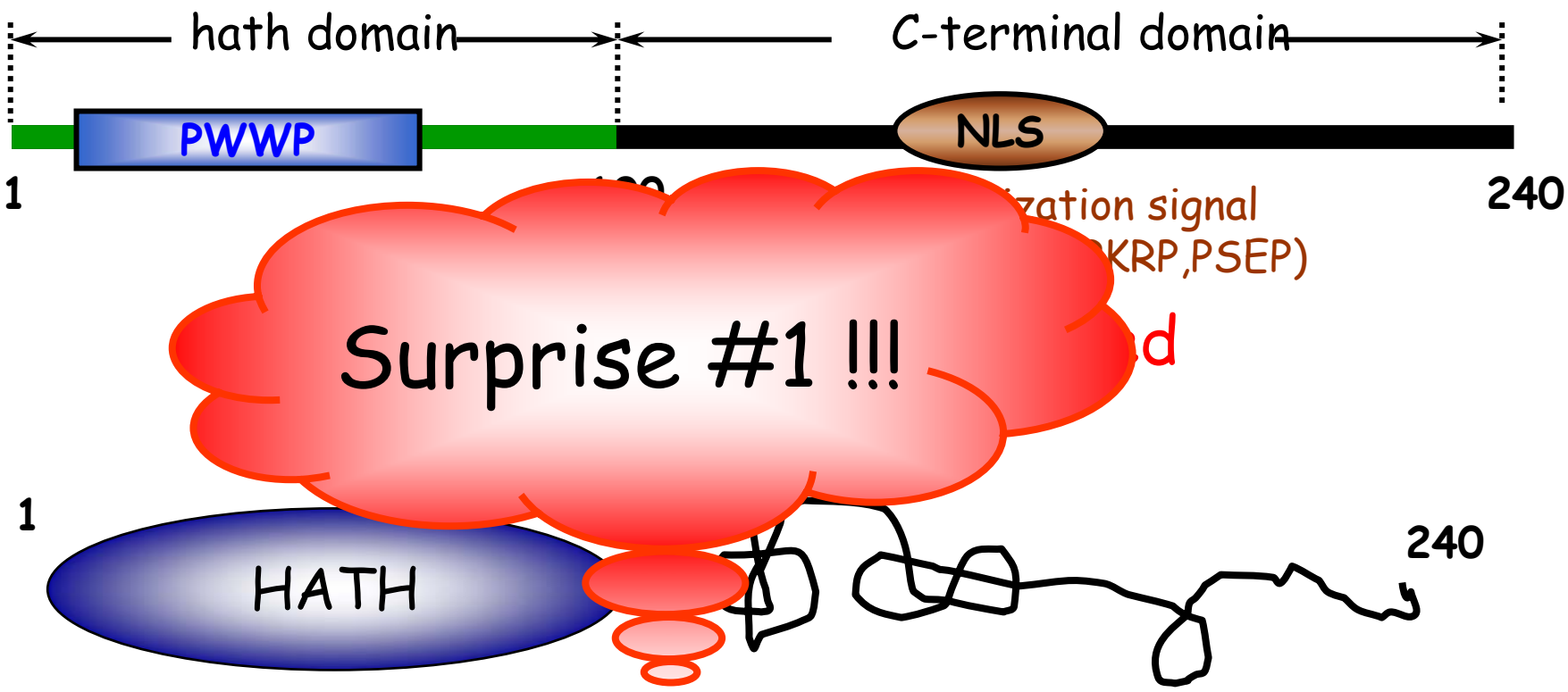

Internalization

DNA synthesis

➔ Intrinsically disordered regulatory protein

Solution Structure of HATH domain

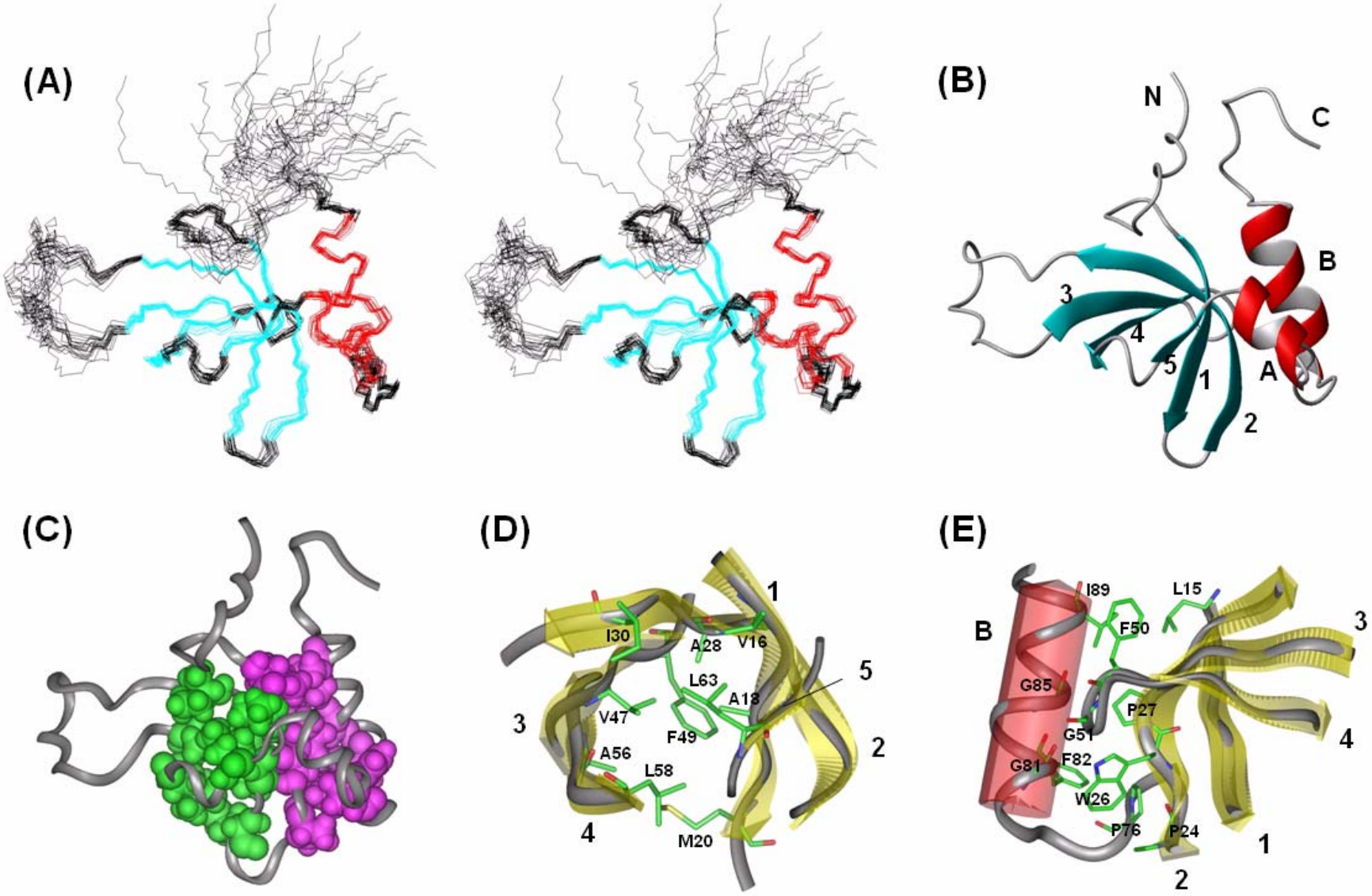

Identification of heparin binding site.

SPR study of heparin binding to hHDGF fragments

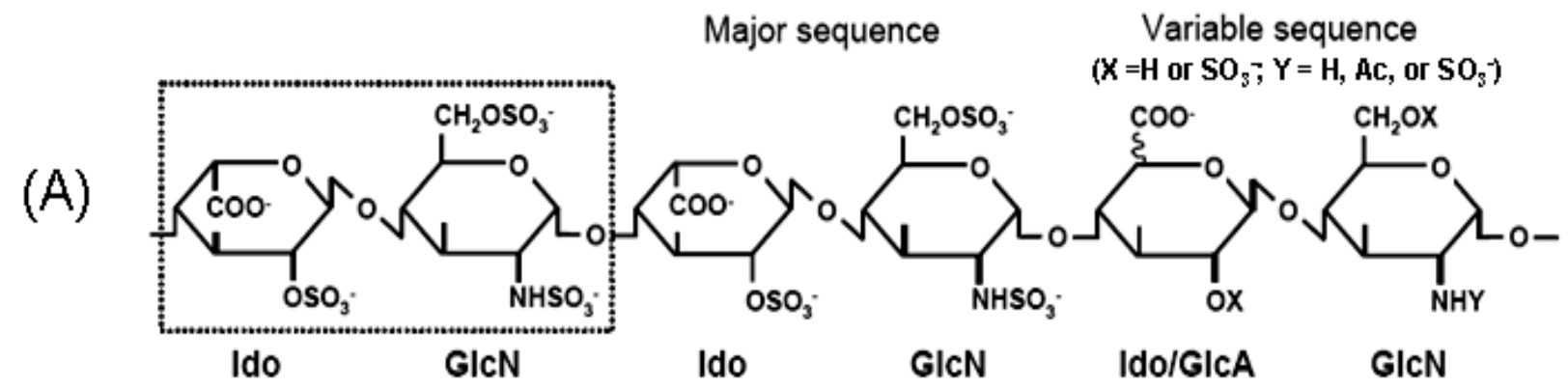

Binding of various fragments

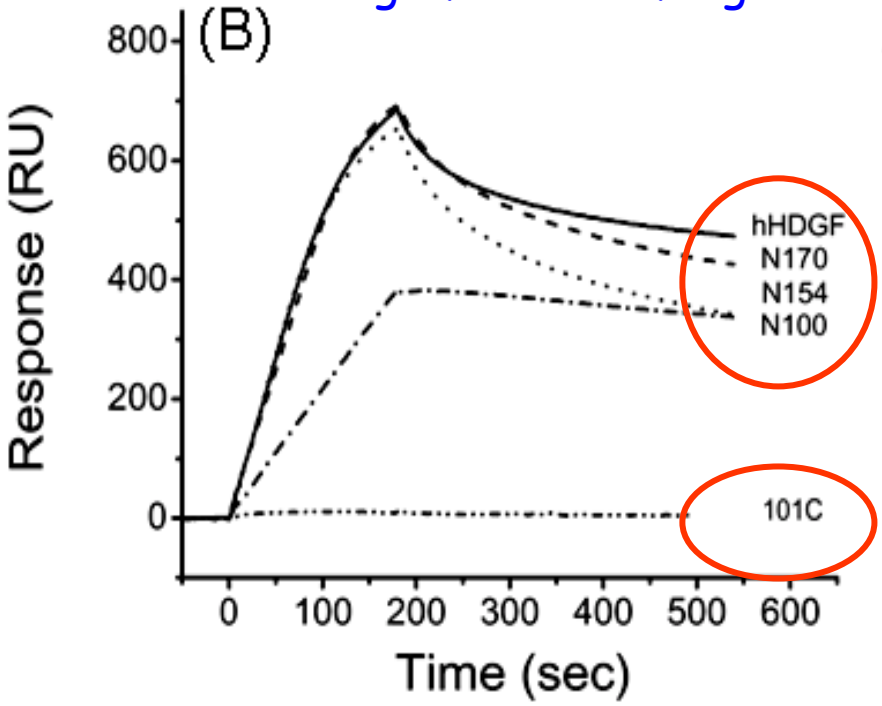

Binding of N100 at various conc.

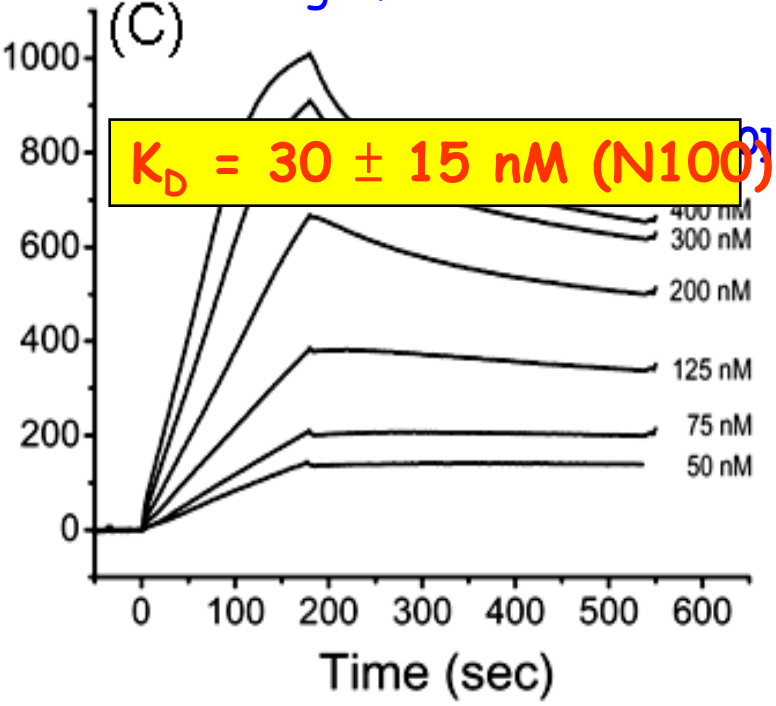

Heparin binds primarily to the N-terminal domain HATH domain

Chemical shift perturbation

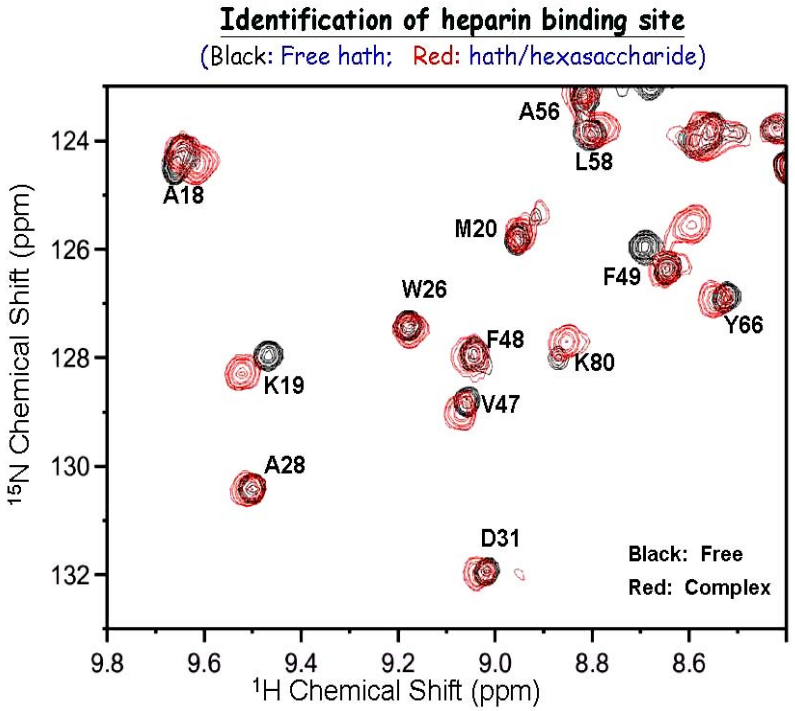

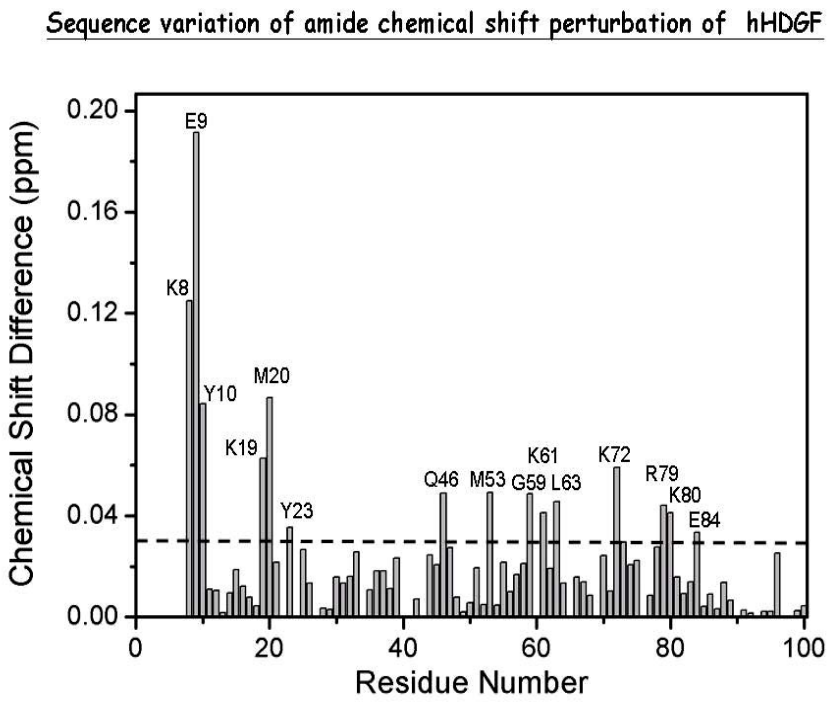

Mapping the heparin binding surface

Residues perturbed

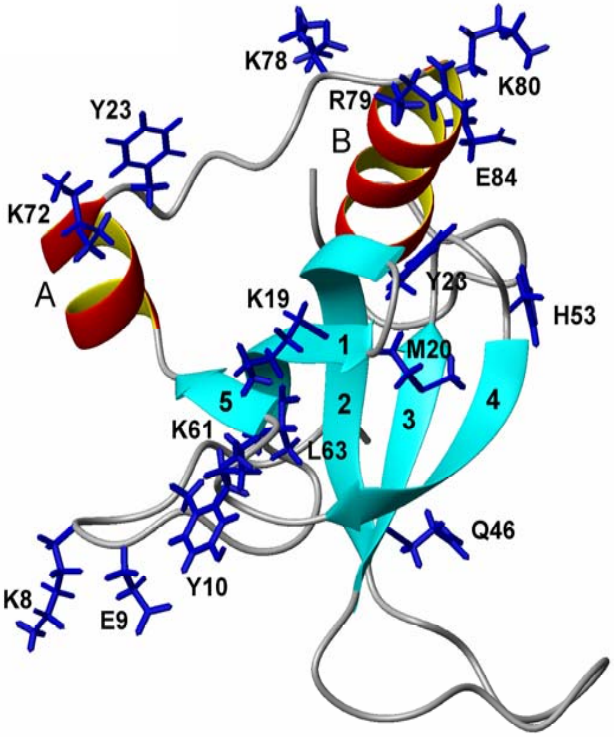

Charge surface

"+": blue; "-": Red

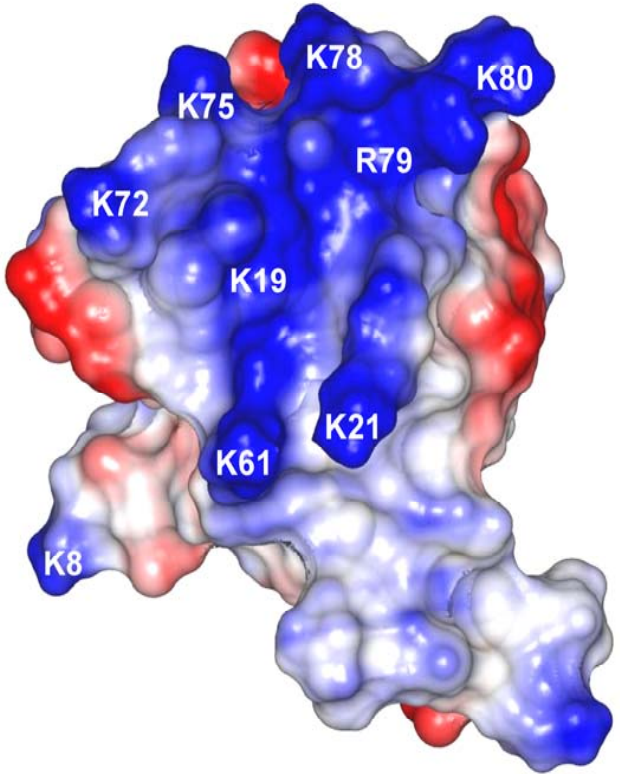

Docking of octasaccharide onto the binding surface

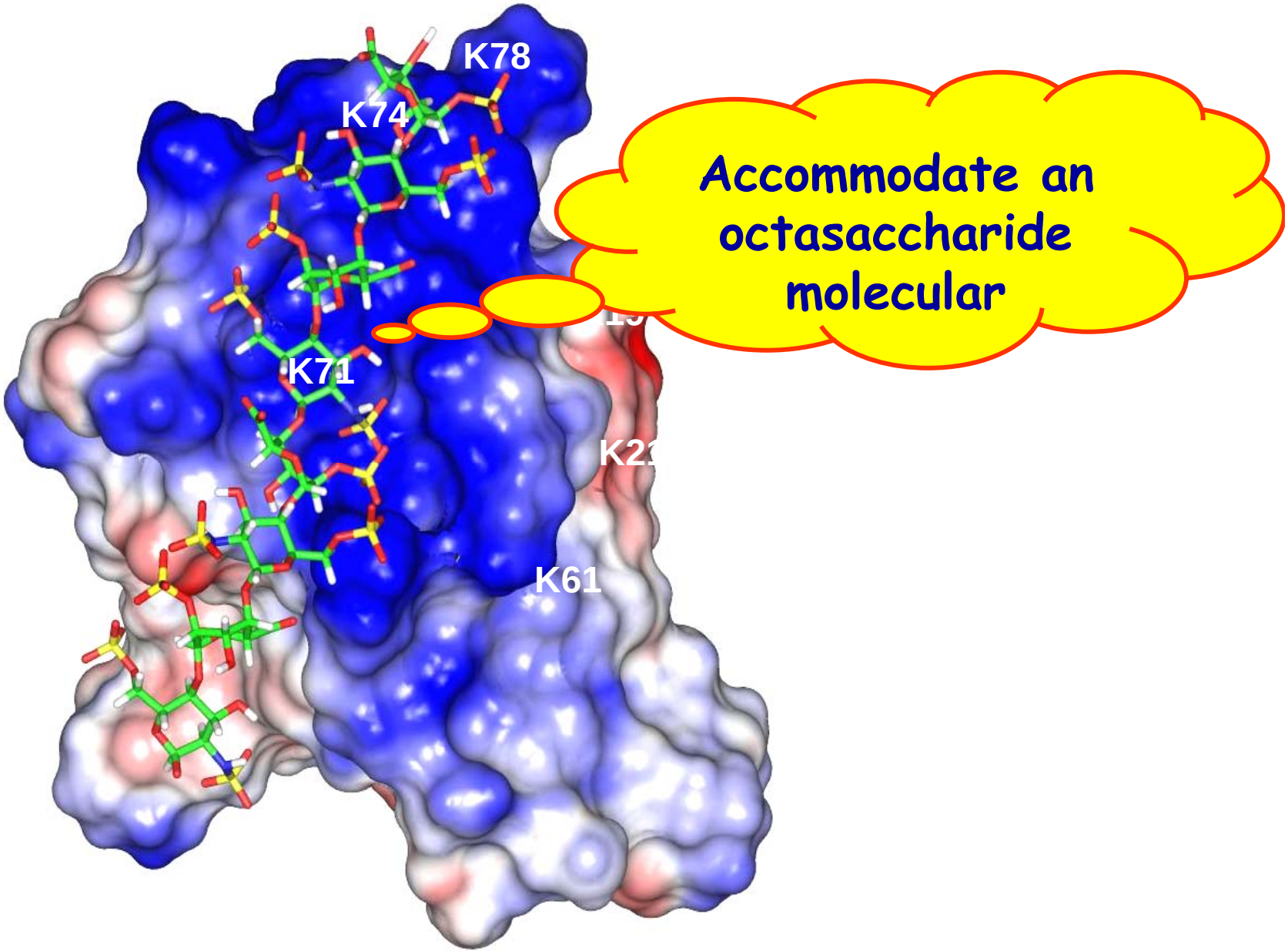

HATH domain forms a dimer

Size exclusion chromatogram

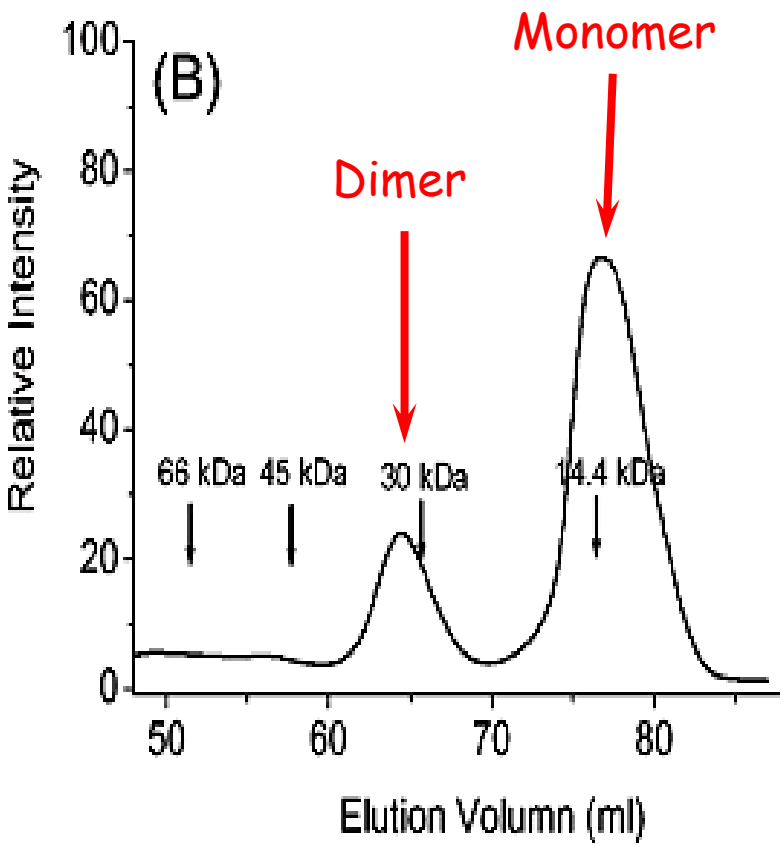

Mass spectra

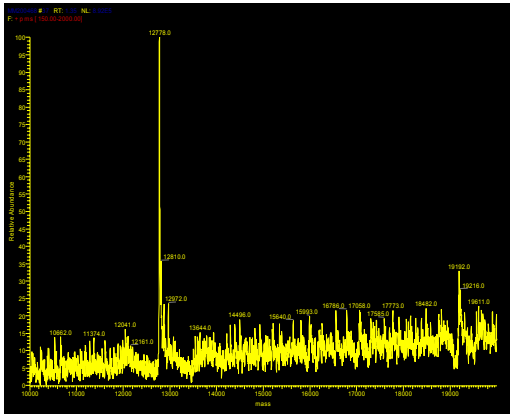

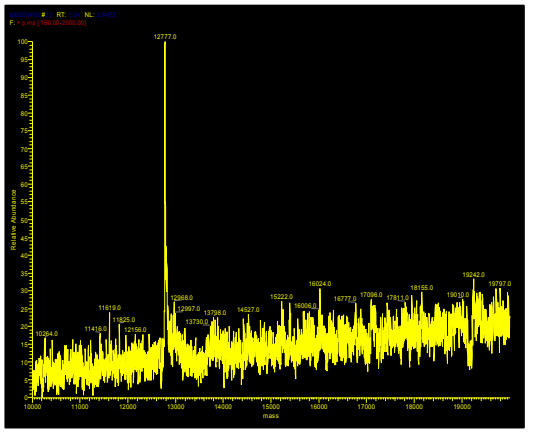

Masses of the two peaks are the same

➔ HATH forms dimer !

➔ Is there any physiological consequence ?

SPR of the Binding Affinities of Monomer & Dimer

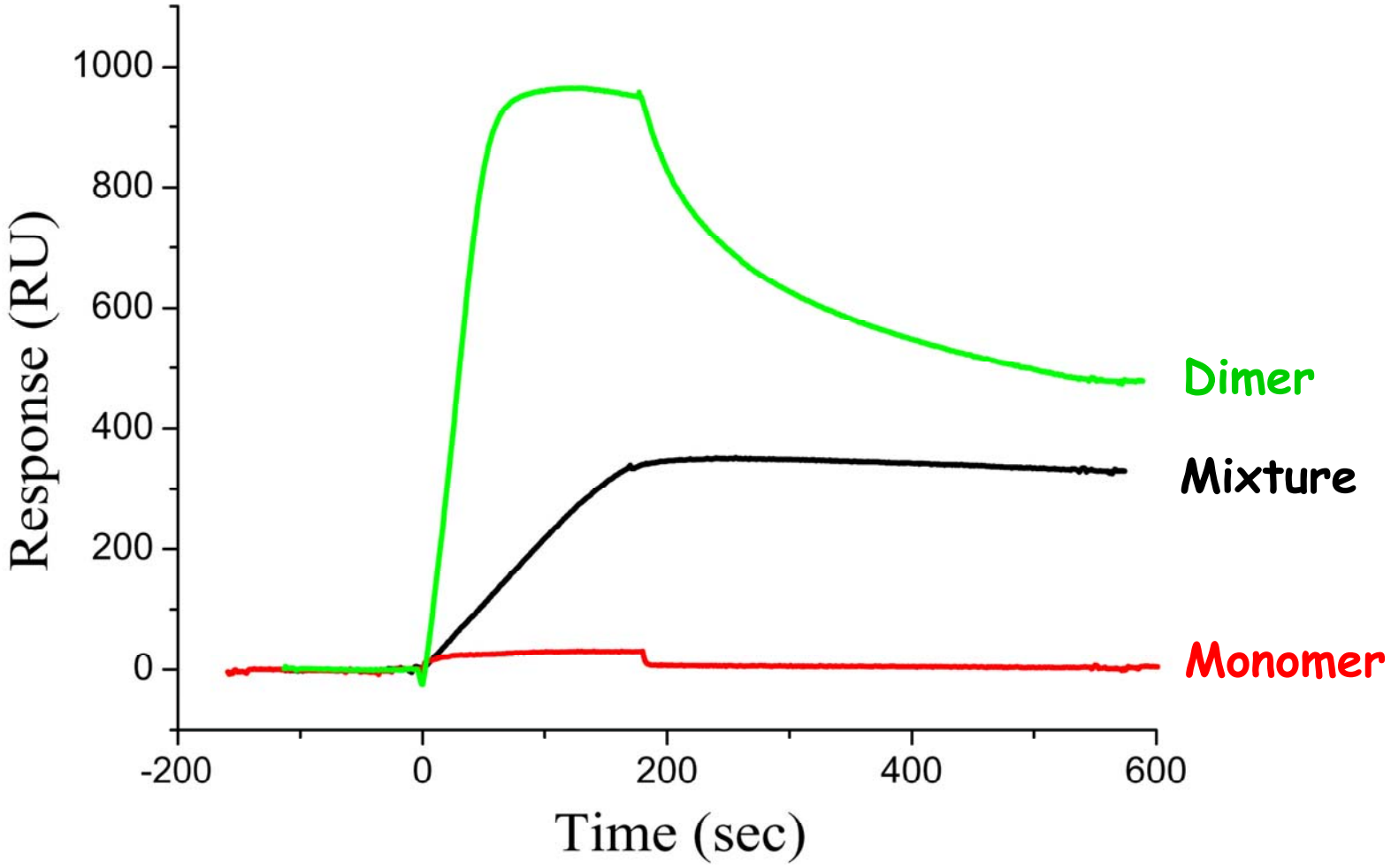

➔ Dimer binds to heparin with much higher affinity.

Measuring binding constants

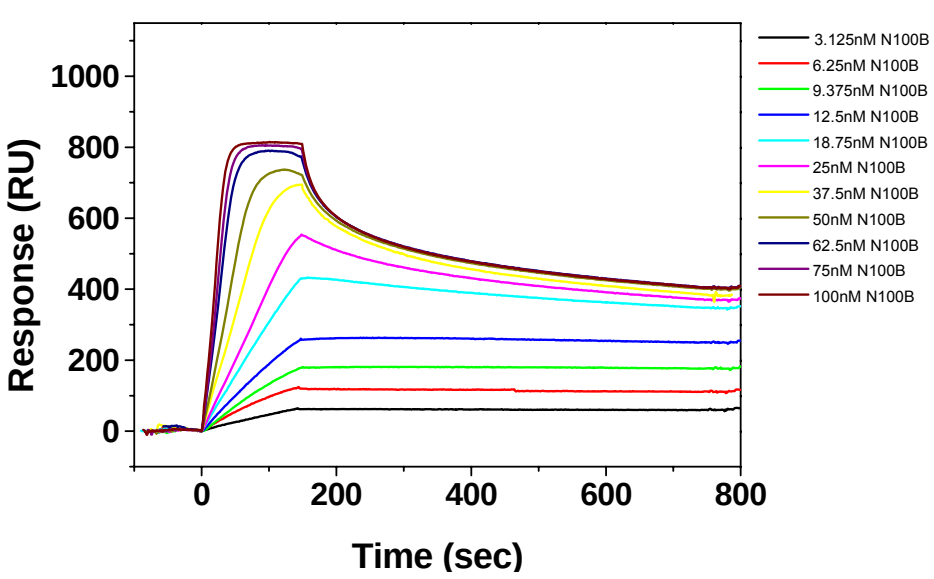

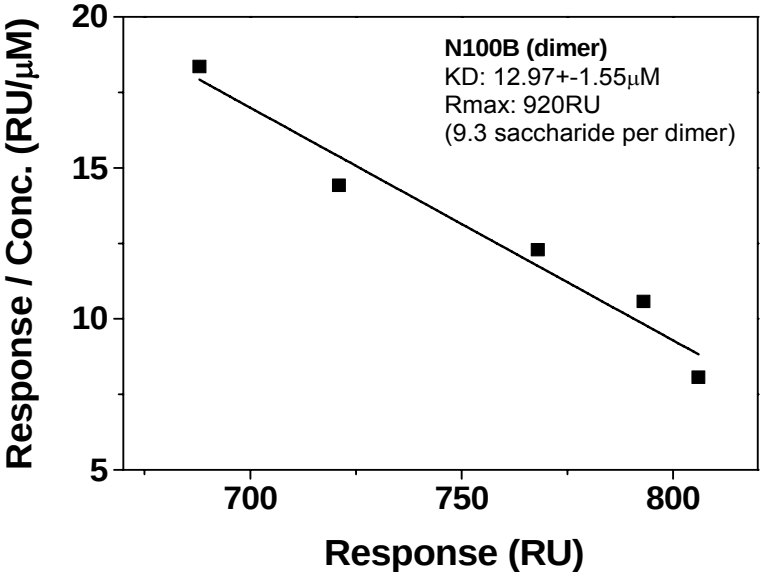

K_D = 1.5 ± 0.1 mM (monomer)

= 12.5 ± 1.5 nM (Dimer)

80 x difference !!!

Identification of Dimer interface.

Identification of dimer interface by chemical shift differences

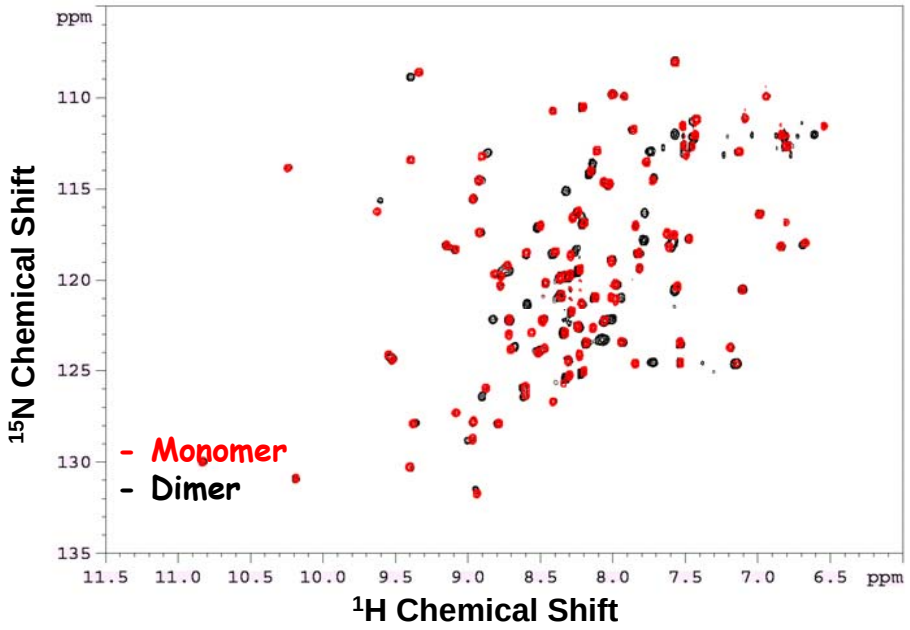

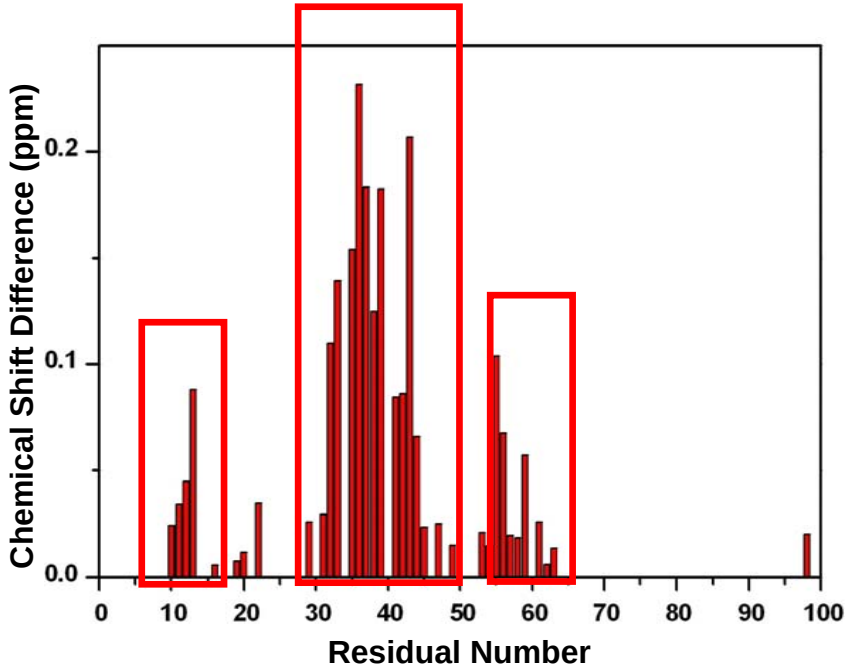

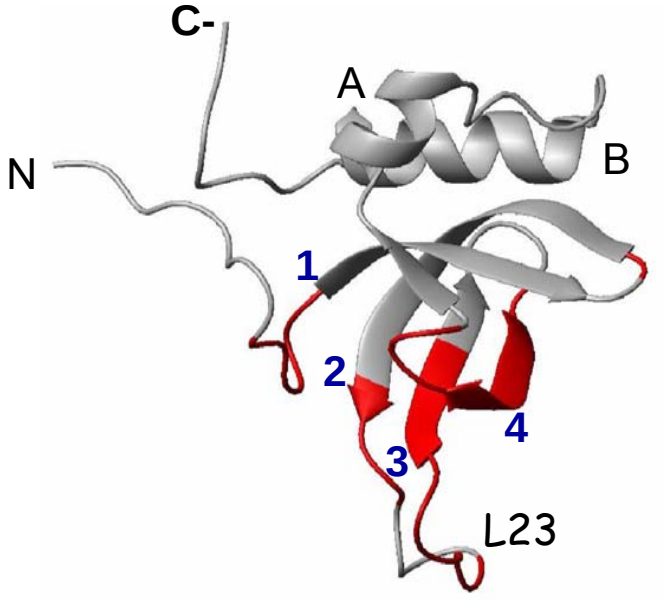

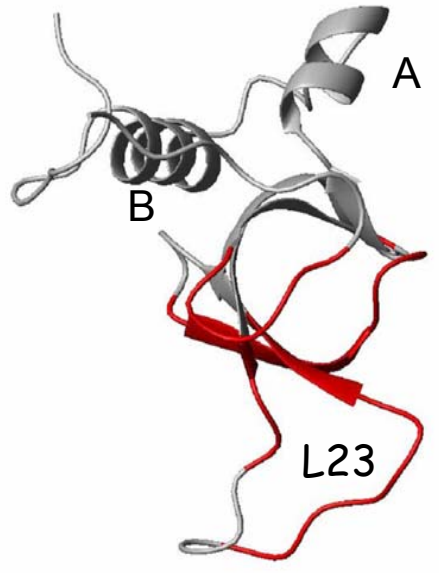

Proposed Model:

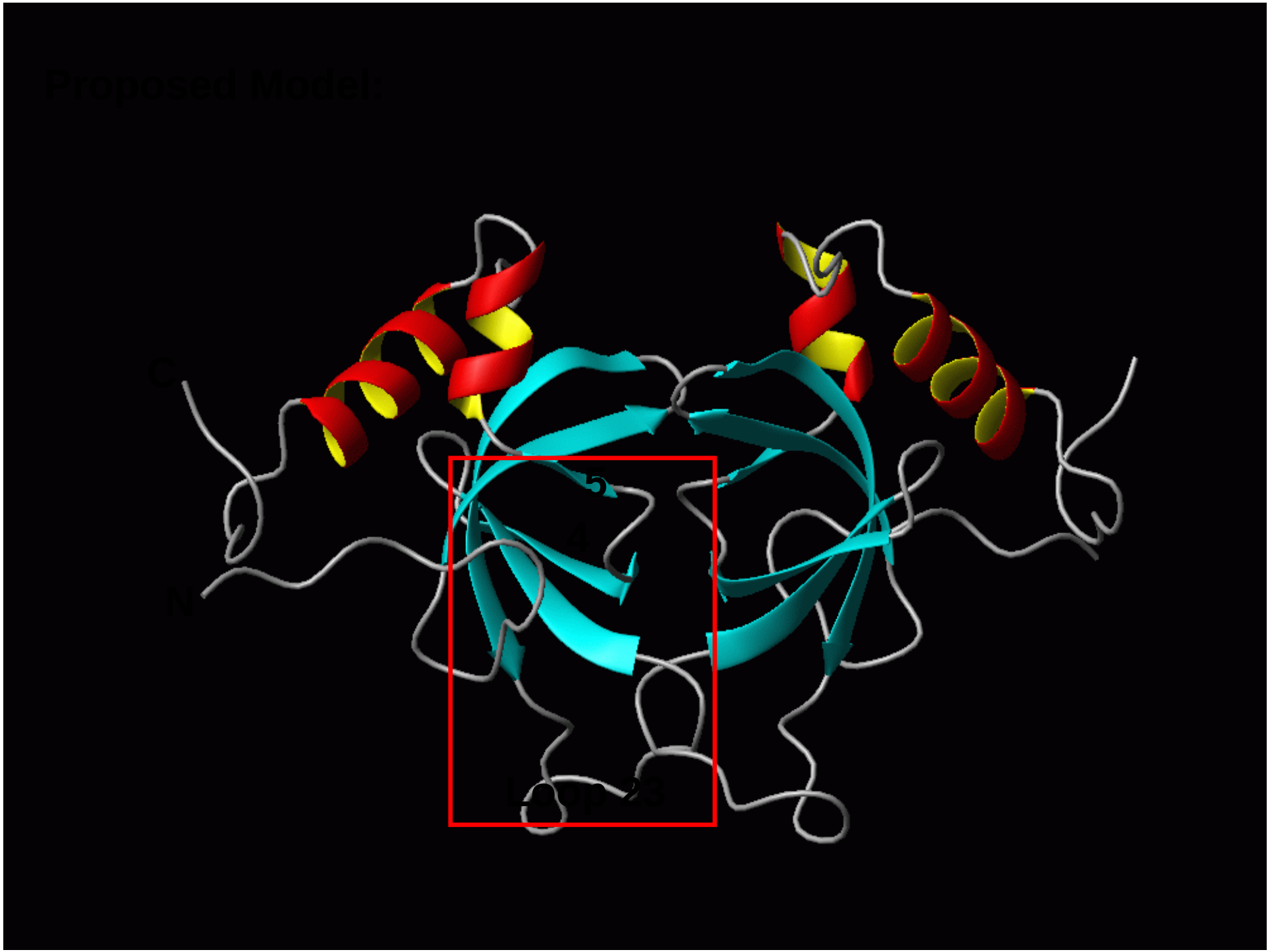

^{15}N-Filtered experiment

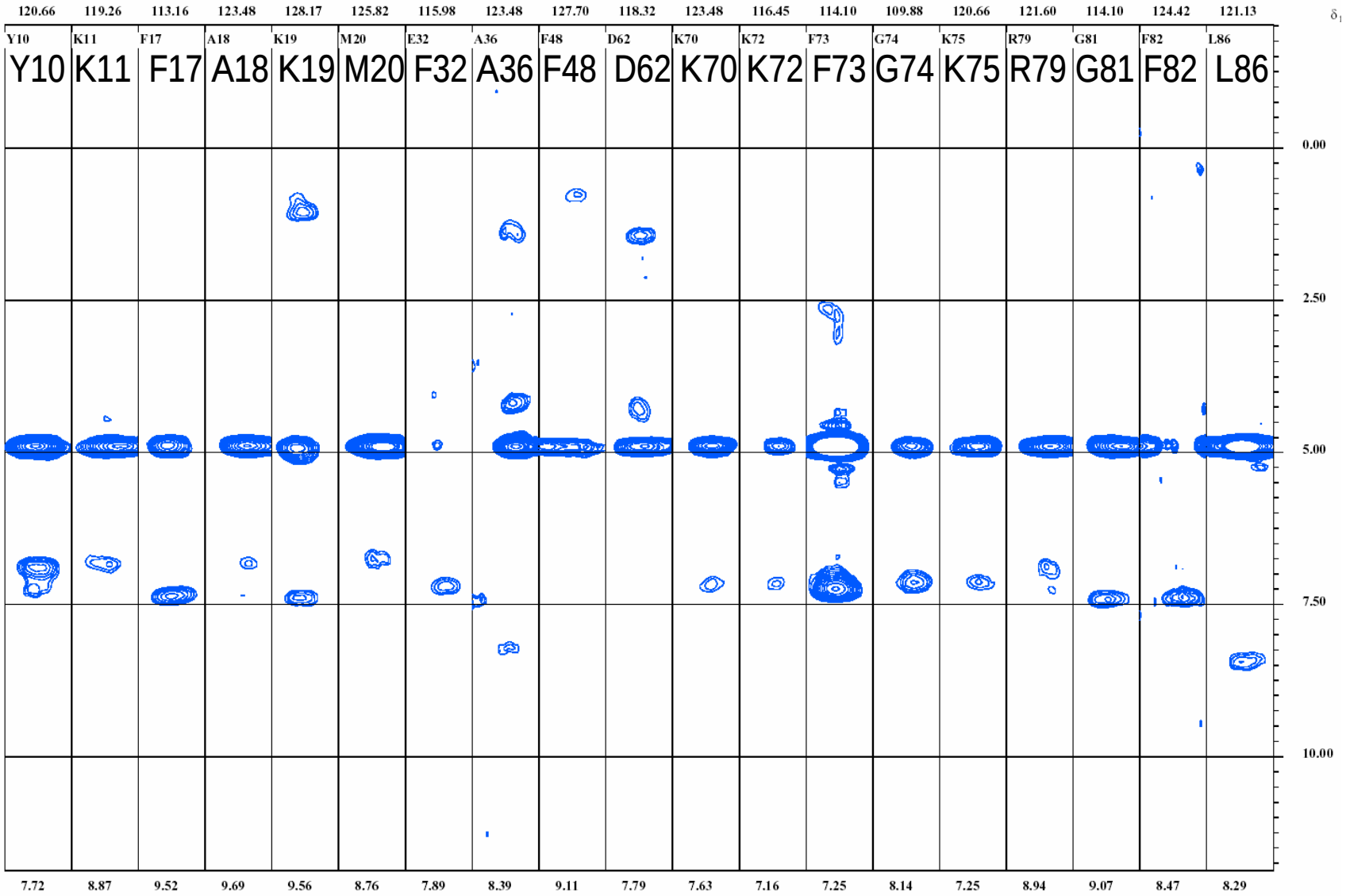

Residues detected by filtered experiments

Time-dependent Conversion of Dimer to Monomer

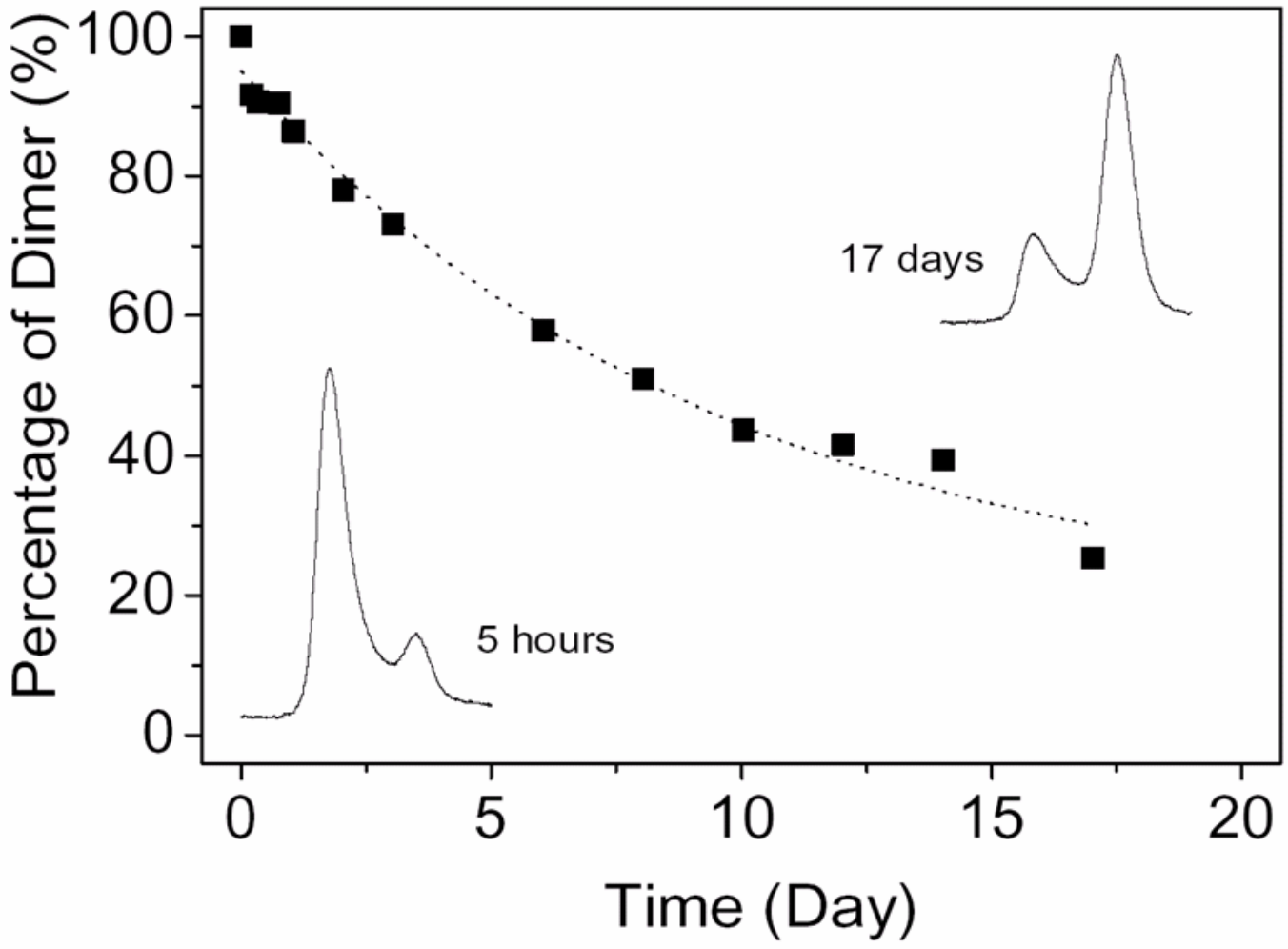

➔ Dimer can dissociates into monomer but monomer cannot form dimer.

➔ Dimer can be re-generated only after refold from denatured

Energy diagram

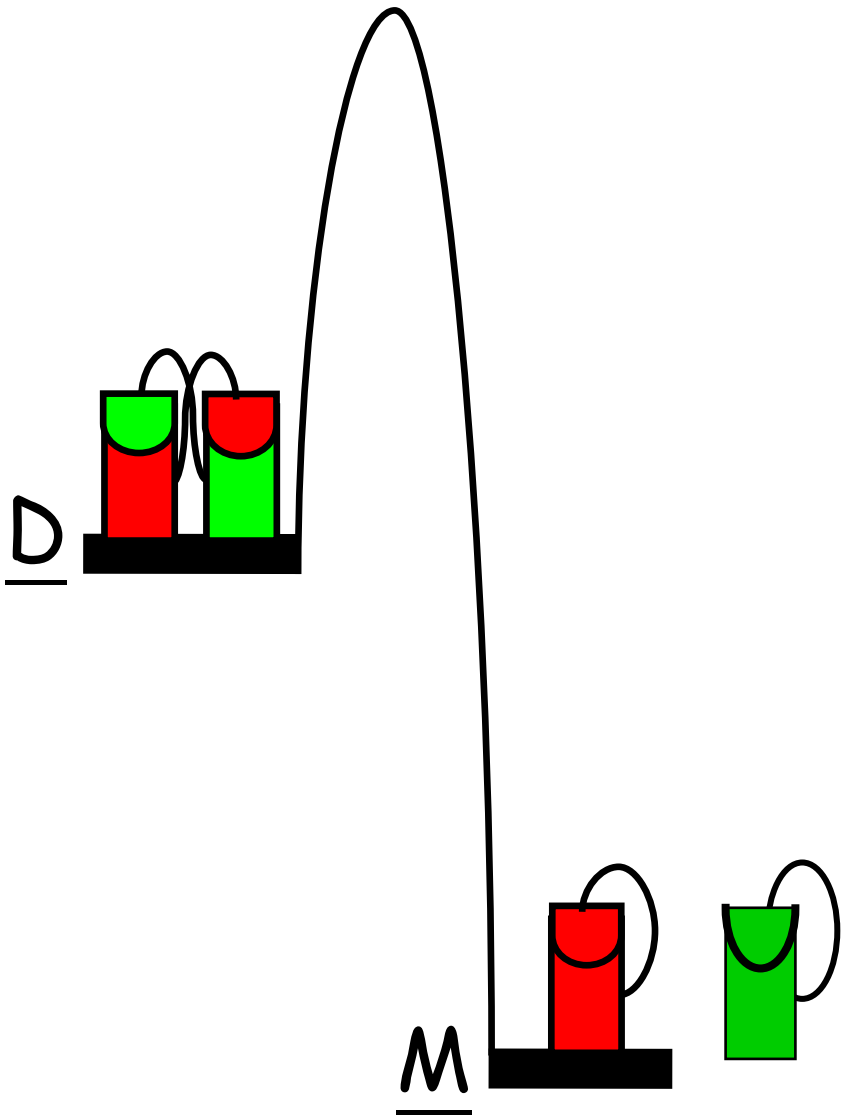

Domain-Swapping mechanism:

Exchange of identical structural element with the corresponding element
in the other subunit of the dimer

Characteristics :

- Separated by a high-energy barrier
- A hinge loop adopting different conformations to help the interchange
- The monomer retains a similar structure except in the hinge loop region.

Proposal: Domain-swapping Model of HATH-dimer

(Strands 1 & 2 of chain 1 pair with strands 2,3 & 4 of chain 2 and vise ver

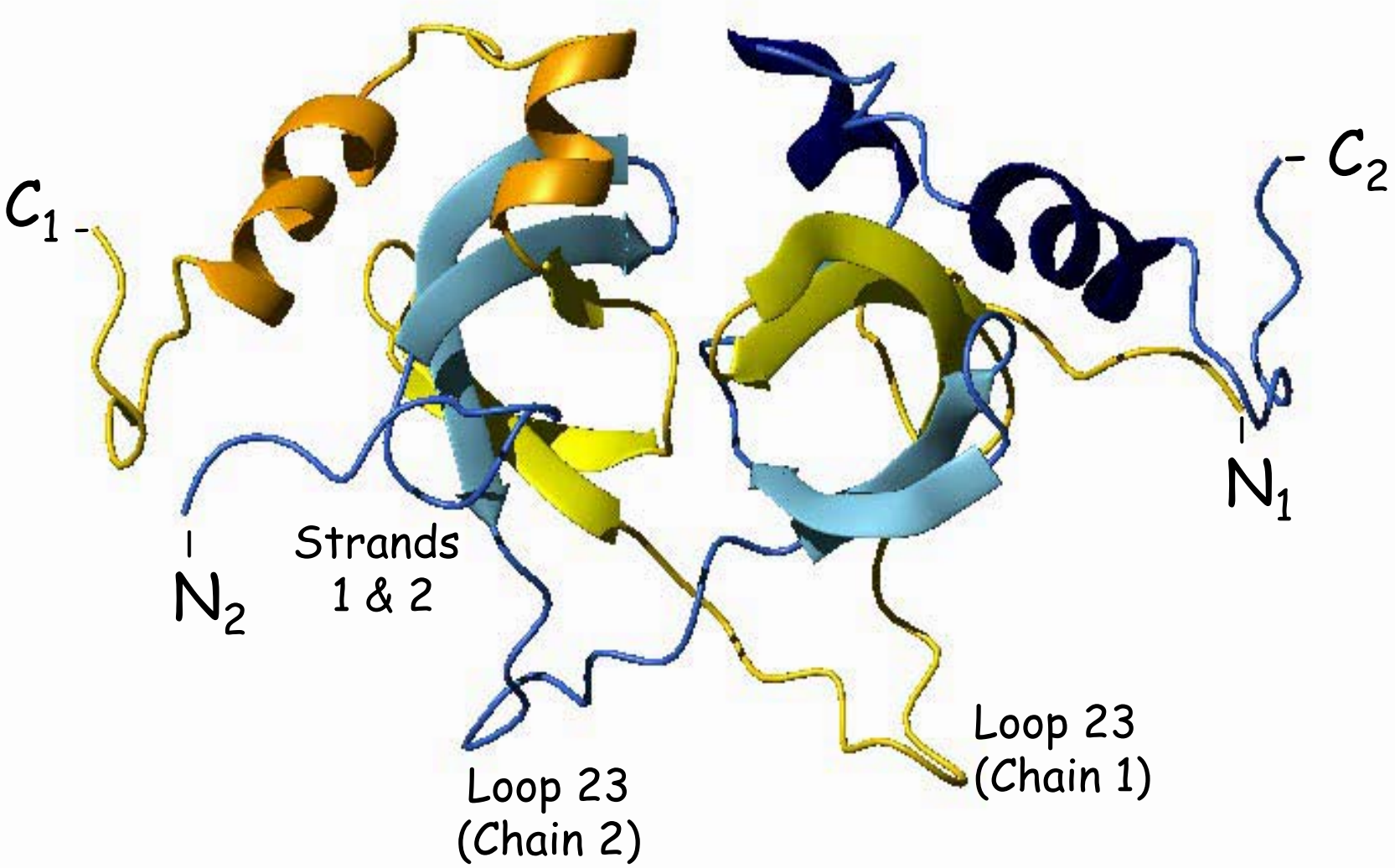

Swapped-dimer formation creates a heparin binding pocket

Electrostatic surface

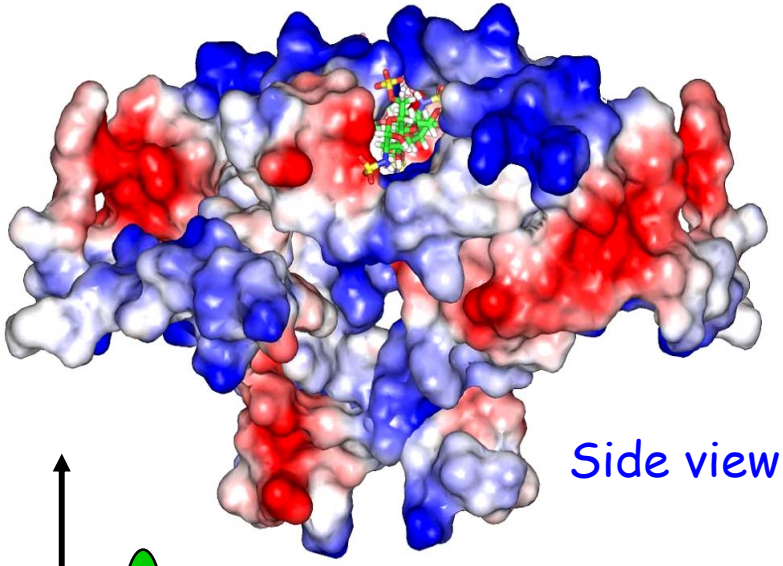

Side view

Heparin

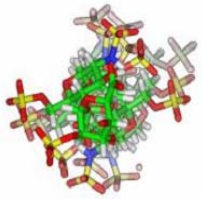

Putative heparin -binding Site

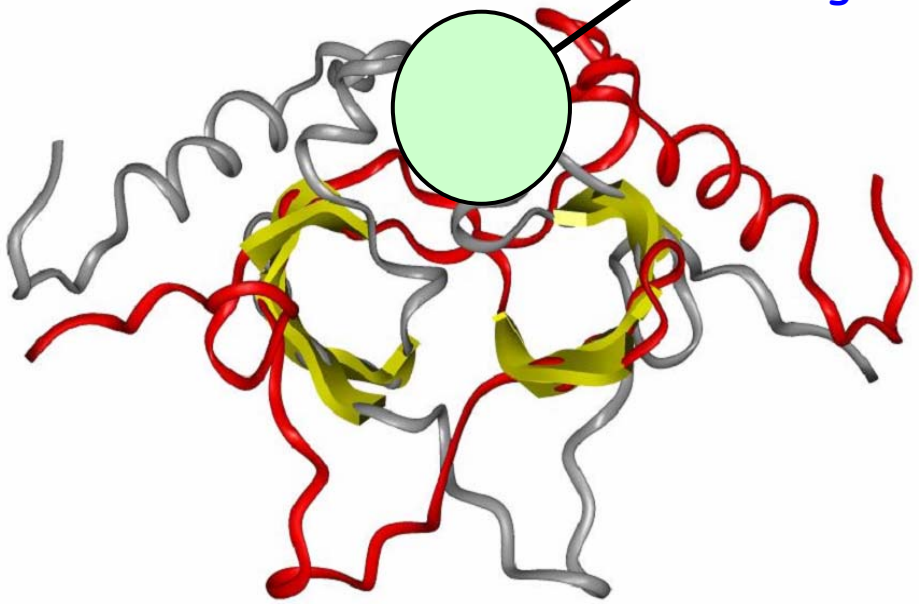

90°

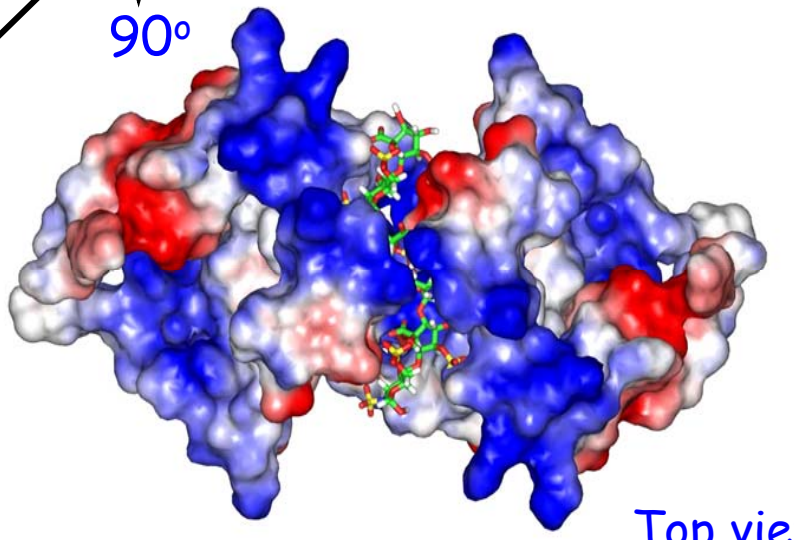

Top view

Summary

- hHDGF is a modular protein with a structured N-terminal "hath" domain and a disordered C-terminal domain. This property is likely to be common among all HRPs.
- The structure of "hath" domain consists of a half β-barrel flanked by two helices, similar to those of the other PWWP domains
- Hath domain is primarily responsible for heparin binding.
- Binding of hath domain to heparin is necessary for protein internalization
- Hath domain forms dimer, possibly involving domain swapping.
- HATH dimer binds to heparin with much stronger affinity than that of the monomer.

National Research Program for Genomic Medicine
High-filed NMR core Facility

Acknowledgements

Huang's lab:

Dr. Shih-Che Sue

Wei-Tin Lee Yu-Jye Lin

Juin-Kuo Yu Szi-Chieh Yu

Carl Yu

Collaborators:

Dr. Joanne Chen (IBMS)

Dr. Wen-Guey Wu (NTHU)

Shao-Chen Lee

National High-field NMR core facility, Taiwan


SCS
SJY
JKY
Carol
Watin